



Delft University of Technology

Faculty of Civil Engineering and Geosciences
MSc Building Engineering

in collaboration with

ARUP

July 1st 2021

Author	N. de Waard
Student nr.	4298659
Project duration	4298659
Gruaduation committee	Dr. Ir. H.R. Schipper Dr. Ir. M.M.E. Pijpers-van Esch Ir. P.H.Ham Ir. V. Heidegger

Abstract

In 2018, the ‘Deltaplan Ruimtelijke Adaptatie’, has been set up by the National Institute of Health and Environment (RIVM) for the purpose of facilitating the transformation to a climate adaptive living environment. As part of the Deltaplan, municipalities have been asked to perform a heat risk assessment through standardised outdoor thermal comfort maps, formulated in terms of the Physiological Equivalent Temperature (PET). The heat risk assessment has increased awareness of urban heat related issues amongst municipalities, and sparked interest in heat-proof (re)development of urban areas. However, appropriate tools for outdoor thermal comfort assessment in the early stage of urban design are currently not available, as established PET simulation tools come at large computational cost. In response to the absence of appropriate outdoor thermal comfort design tools, this thesis proposes a Grasshopper-based PET simulation tool with an adequate balance between time-efficiency and sufficient accuracy for the early design stage. Additionally, a study into the heat mitigation efficiency of varying Height-to-Width ratio (H/W ratio), street orientation and facade albedo for extreme heat events in the Netherlands provides global rules of thumb for heat-proof urban design.

Through literature review, conditions for appropriate determination of four meteorological input parameters for PET calculation (urban air temperature, mean radiant temperature, urban relative humidity and urban wind speed) have been determined, which have been used to construct the PET simulation model. The PET model has been validated to be sufficiently accurate through both literature and sense-checks and shows a considerable improved time-efficiency in comparison with established simulation tools such as ENVI-met. The model is thus considered suitable for application in the early design stage. Application of the model is limited to (1) cities in Western-Europe, (2) situations of low wind speed and (3) the months of April to September.

Because of its rather quick computation time, the Grasshopper PET simulation model has been used to formulate basic rules-of-thumb for heat proof design through a study into the effects of varying H/W ratio, street orientation and facade albedo. The study has been performed for a representative urban canyon in the Netherlands for an analysis period from 12.00 – 18.00 on an above average warm summer day. Study results show decreased spatially and temporally averaged PET in the urban canyon for increasing H/W ratio. Considering street orientation, highest average PET occurs for streets oriented towards the South-East (SE) and lowest average PET occurs for streets oriented towards the North-East (NE). Varying H/W appears to be the most effective strategy for heat mitigation with a heat mitigation potential of up to 5.6 °C, closely followed by varying street orientation with a heat mitigation potential of up to 4.7 °C. Default settings for street orientation affect the effectiveness of varying H/W ratio and vice versa: Varying H/W ratio is considered most effective for SE street orientations (heat mitigation potential of up to 5.6 °C) and least effective for NE street orientations (heat mitigation potential of up to 3.9 °C). Varying street orientation is considered most effective for larger H/W ratios

(heat mitigation potential of up to 4.7 °C for H/W ratio 1.0) and least effective for smaller H/W ratios (heat mitigation potential of up to 3.0 °C for H/W ratio 0.5). From the study results, no firm conclusions can be drawn with regards to the effectiveness of varying between low albedo facades (albedo = 0.3, untreated facades) and high albedo facades (albedo = 0.8, white-painted facades): The results appear to be highly dependent on the number of ambient bounces (ab) of reflected shortwave radiation considered in mean radiant temperature calculation. Depending on the considered number of bounces, either low albedo facades (ab = 2) or high albedo facades (ab = 4) result in lower average PET in the urban canyon. At the time of writing, it is uncertain which number of ambient bounces should be considered realistic for calculation. For both considered number of ambient bounces, however, study results show that the heat mitigation potential of facade albedo is significantly lower than that of H/W ratio and street orientation.

For the considered urban canyon, a combination of H/W ratio 1.0 and SE street orientation results in the lowest average PET (approximately 38 °C), whereas a combination of H/W ratio 0.5 and NE street orientation results in highest average PET (approximately 47 °C). Dependent on the number of ambient bounces considered, either low- or high albedo facades result in highest average PET. However, the contribution of facade albedo on the mentioned PET values is limited (up to ± 1 °C). An exploration into the effects of ground- and facade material on the obtained average PET results suggests that varying ground- and facade material moderately affects average PET results. Further research is needed to quantify the exact effect of varying ground- and facade material on PET.

For future research, it is additionally recommended to perform a more elaborated validation with field measurements. The focus of a validation study should be on calculation of mean radiant temperature, as the calculation method implemented in the PET model is currently a draft version. Other interesting topics for future research are the implementation of vegetation in the PET model, and improvement of the wind speed calculation for more accurate wind speed modelling.

Preface

By submitting this report, eight years of studying at TU Delft will come to an end. Starting in 2013 at the faculty of Industrial Design Engineering, I could not have guessed that eight years later I would graduate from the faculty of Civil Engineering as a Building Engineer. But perhaps it is precisely this background in Industrial Design Engineering that has led to the interest in a topic that explores the interaction between humans and the built environment: The effect of the built environment on experienced outdoor thermal comfort.

Over the past 10 months I've explored the topic of outdoor thermal comfort, which has been completely new to me, with much enthusiasm. Much of this enthusiasm has been stirred up by my graduation committee, who have provided much appreciated positive support throughout the project. First, I'd like to thank Veronika, my company supervisor, who's been very closely involved in my project. I've greatly enjoyed our weekly meetings, which were always very helpful, and most importantly: A lot of fun. Additionally I'd like to thank Marjolein for getting me acquainted with all ins and outs on outdoor thermal comfort and urban microclimates. Our bi-weekly meetings have significantly helped me maintain focus and have prevented me from straying to far from the core concept of the project. I'd like to thank Roel who has supported me from the beginning of the project and who's critical insights have helped me to critically reflect on my own work. Finally, I'd like to thank Pieter, who's joined the project at a later stage, but nevertheless has provided great insight into the report structure and who's tips have helped me to significantly improve the report.

In addition to my committee I'd like to thank the many experts in the field of outdoor thermal comfort and computational modelling who've greatly helped me by answering many of my questions. I'd like to thank Sytse Koopmans and Laura Kleerekoper for discussing heat mitigation development in the Netherlands with me, and Emanuele Naboni, Nathaniel Jones, Viktor de Lucas, Jake Haskell, Jonathan Natanian and Chris Mackey for their guidance in computational modelling. Throughout the project I've been very pleasantly surprised by the willingness of all of you to invest time in my personal project.

Nynke de Waard

Rotterdam, July 2021

Contents

I	Research framework	2
1	Introduction	3
1.1	Problem Context	3
1.1.1	Urban Climates	3
1.1.2	A growing concern for (urban) heat	4
1.1.3	The urban heat issue	6
1.2	State of the Art	7
1.2.1	Identifying heat-risk areas through standardized heat maps	7
1.3	Knowledge gaps	8
1.4	Research aim	10
1.4.1	Research objectives	10
1.4.2	Research questions	11
1.4.3	Scope	12
1.5	Scientific and societal Relevance	12
1.6	Report outline	12
2	Research approach	14
2.1	Literature review	14
2.2	Model development	15
2.3	Parametric study	15
II	Literature review	16
3	Human biometeorology and thermal comfort	17
3.1	Human bioclimates	17
3.2	Outdoor thermal comfort	21
3.2.1	Relative importance of meteorological thermal comfort parameters	23
3.2.2	Thermal comfort index PET	24
3.2.3	Heat stress	25
3.3	How urban characteristics affect thermal comfort	26
4	The introduction of standardized PET heat maps as a control tool	27
5	Existing computation tools for PET calculation	29
III	Model development	30
6	A parametric model for quick PET assessment in the early design stage	31

6.1	Model setup	32
6.2	Urban air temperature calculation	33
6.2.1	Translation of the UHI_{max} equation for hourly transformation of rural- to urban air temperature	35
6.2.2	Implementation of air temperature calculation in PET model Grasshopper	36
6.2.3	Validation urban air temperature calculation	39
6.3	Urban MRT calculation	39
6.3.1	Honeybee Legacy Microclimate Map MRT calculation	40
6.3.2	Limitations Honeybee Legacy Microclimate Map MRT calculation	41
6.3.3	Application of Radiance for improved MRT calculation	41
6.3.4	Comparison of both calculation methods	45
6.3.5	Validation of MRT calculation	46
6.4	Urban relative humidity calculation	49
6.5	Urban wind speed calculation	49
6.5.1	Implementation of wind speed calculation in PET model Grasshopper	53
6.5.2	Validation wind speed calculation	56
6.6	Calculation efficiency optimisation	56
6.7	Validation	57

IV A parametric study into building-related heat mitigation strategies 59

7 Research description 60

7.1	Research questions	60
7.2	Methods	61
7.2.1	Data collection	61
7.2.2	Data analysis	64
7.3	Hypotheses	65
7.3.1	Hypotheses corresponding to sub-question 2.a	65
7.3.2	Hypotheses corresponding to sub-question 2.b	66
7.3.3	Hypotheses corresponding to sub-question 2.c	67

8 Results 68

9 Interim exploration and discussion of study results 70

9.1	A comparison of PET evaluation methods for heat mitigation assessment	70
9.2	Assessment of individual heat mitigation strategies and identification of interdependencies	72
9.2.1	H/W ratio heat mitigation performance	72
9.2.2	Street orientation heat mitigation performance	73
9.2.3	Facade albedo heat mitigation performance	75
9.3	Interpretation of numerical average PET results	80
9.3.1	Effect of surrounding environment on PET results	82
9.3.2	Effect of facade material on PET results	82
9.3.3	Effect of ground material on PET results	84

V	Discussion, conclusion and future studies	86
10	Discussion	87
11	Conclusion	90
11.1	Conclusions to the first research question	90
11.2	Conclusions to the second research question	92
11.3	Conclusion to sub-questions 2.a and 2.b	93
11.4	Conclusion sub-questions 2.c	94
12	Recommendations	96
12.1	Recommendations for future research	96
12.2	Recommendations for practice	97
A	Heat mitigation strategies review	107
B	SVF and SEF comparison	111
C	Diurnal Cycle	112
D	Python code PET simulation model	114
D.1	Transform datetime information	114
D.2	Air temperature calculation: Find fastest calculation path	115
D.3	Air temperature calculation: Calculate max, min and average weather values over deconstructed days	116
D.4	Air temperature calculation: Calculate urban air temperature	117
D.5	Wind speed calculation: Find fastest calculation path	122
D.6	Wind speed calculation: Add up to frontal facade orientation per wind direction	122
D.7	Wind speed calculation: Calculate urban wind speed	123
D.8	Wind speed calculation: Transform to correct data structure	126
E	Exploration into the effects of varying the surrounding environment and facade- and ground material	128
E.1	Results exploration	128
E.1.1	Surrounding environment of the urban canyon	128
E.1.2	Facade material	129
E.1.3	Ground material	129
E.2	Discussion of exploration	130
E.2.1	Surrounding environment of the urban block	130
E.2.2	Facade material	137
E.2.3	Ground material	138

List of abbreviations

CFD	Computational Fluid Dynamics
FFD	Fast Fluid Dynamics
H/W ratio	Height-to-Width Ratio
IPCC	Intergovernmental Panel on Climate Change
MRT	Mean Radiant Temperature
N	North
NE	North-East
PET	Physiological Equivalent Temperature
RIVM	Rijksinstituut voor Volksgezondheid en Milieu
S	South
SE	South-East
SEF	Sky Exposure Factor
SVF	Sky View Factor
UHI	Urban Heat Island
UWG	Urban Weather Generator



Figure 1: The vast impact of urbanisation on change of natural landscape is well exemplified by the urban sprawl of Mexico city, altering the characteristics of surrounding hills (Barcroft Media, 2013)

Part I

Research framework

Chapter 1

Introduction

1.1 Problem Context

1.1.1 Urban Climates

Approximately 4.5 billion years ago, planet earth was formed. Our species, homo sapiens, have only inhabited the earth for a small fraction of these 4.5 billion years [84]. Nonetheless, our impact on the planet is enormous. This is well exemplified by landscape changes resulting from urbanisation and urban sprawl of modern settlements in figure 1.

During the agricultural revolution some 12,000 years ago, our forefathers started domesticating flora and fauna and formed the first permanent settlements [88]. These settlements have grown substantially: Nowadays over half of earth's population resides in urban settlements, of which some have more than 10 million inhabitants [98]. Zooming in on the more recent history of urban settlements: Within the timeframe of the last 200 years, the earth's population has increased tremendously from an approximate 1 billion to an estimated 7.7 billion people in 2019. Simultaneously, the percentage of people residing in European urban settlements has increased from 3% in 1800 to 74.5% in 2018. And even though population growth is expected to stabilize in European countries this century, the United Nations have estimated European urban resident fractions to grow up to 83.7% by 2050 [99, 100]. In the Netherlands, the cities of Amsterdam and Rotterdam will grow up to an estimated population of 1.22 and 1.05 million people respectively [98]. These predictions, which are subject to a certain level of uncertainty, may be influenced by technological progress, economic fluctuations and urban policy: Advancement of more efficient public transit systems or an increase in remote working, facilitated by digital communication, may potentially reduce the urbanization rate or impact urban form in other ways. Still, it is evident that urban areas will house the greater number of people in the future [75].

From figure 1 it is apparent that urbanisation is accompanied by an extensive change of former rural, vegetation dominated landscape, which affects the local atmosphere in urban areas. Changes in urban fabric, land cover and urban structure as well as increased human activity cause distinct differences between urban (micro)climates and rural climates. These urban climates are characterized by e.g. increased air pollution, increased air temperature and increased flooding. And with the prospected growth of cities, (unwanted) urban climate effects will most likely intensify in the

near future. Additionally, the background climate in which urban areas are nested, is subject to a drastic change due to anthropogenic greenhouse gas emissions, intensifying potentials hazards such as overheating of cities, flooding or extreme air pollution. These future prospects emphasize the need to understand global climate change, urban climates and how the built environment may affect the manifestation of distinct urban climates [75].

1.1.2 A growing concern for (urban) heat

Since halfway through last century, global air temperatures have risen. Human activities, including emissions of anthropogenic greenhouse gasses, have proven to be responsible for the observed global warming. The increase of greenhouse gasses in the atmosphere and subsequent global warming have resulted in climate change effects such as warming of the oceans, melting of large quantities of snow and ice, as well as sea level rise. Additionally, climate change has disrupted precipitation patterns across the globe [42].

Both in rural and urban environments, the above-mentioned climate change effects are causes of nuisance. However, the distinctive geometric character, fabric and increased land cover of cities make urban areas even more vulnerable to environmental hazards [75]. Increased overheating and decreased drainage of rainwater in the paved urban setting compromises health and safety of urban dwellers, especially during extreme weather events such as heatwaves and heavy precipitation events (figure 1.1a and 1.1b). Evidently, the Netherlands has to adapt to an ever changing climate. The ‘Deltaplan Ruimtelijke Adaptatie’ [73], set up in 2014, states that the state, provinces, water authorities and municipalities should together ensure the Netherlands to be climate resilient and water-robust in 2050. For this purpose, all governments have to ensure spatial (re)design of streets and neighbourhoods to be climate resilient from 2020 onwards: Damage and nuisance due to excessive heat, drought and flooding should be reduced to a minimum. Considering flooding, the Netherlands has a lot of knowledge and expertise in the field of climate adaptive measures to improve the resilience of the living environment. This is partly a result of the large economic impact that is often associated with water damage. Regarding heat, however, it has been insufficiently clear which measures are effective in creating heat resilient cities, leaving the subject often unaddressed in spatial planning [67, 77].

Inadequate knowledge about heat-resilient city planning is considered worrisome, given the predicted air temperature increase next decades. Weather data from 1920 to 2020 shows a trend of increasing occurrence, intensity and duration of extreme heat episodes in the Netherlands (figure 1.2) [5] and research has shown that this trend is not likely to change in the near future. The Intergovernmental Panel on Climate Change [42] has outlined potential future scenarios regarding the global increase in air temperature next decades, based on various predictions for future greenhouse gas emission levels. From these future scenarios it is clear that even in the most favourable scenario, global air temperatures will rise [32, 29]. From the IPCC future scenarios, the dutch meteorological institute, the KNMI, has predicted an air temperature increase between now and 2050 of approximately 1 °C in the most favourable situation as opposed to approximately 2 °C in the most unfavourable situation [48].



(a) A man protecting himself from the sun during a heatwave in NYC



(b) A bike-rider riding through flooded city streets

Figure 1.1: Extreme weather events such as heatwaves or excessive precipitation compromise comfort, health and safety of urban dwellers

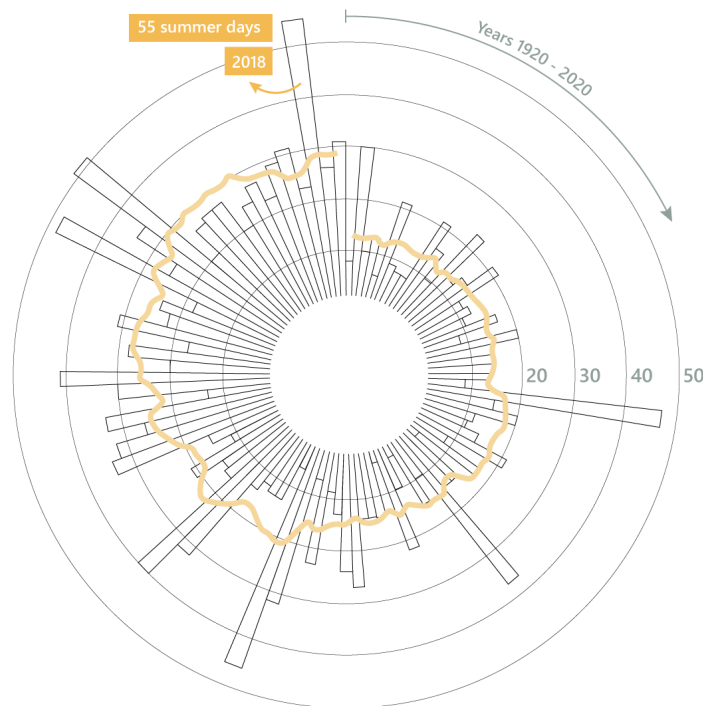


Figure 1.2: A trend of increased number of summer days (air temperature $> 25\text{ }^{\circ}\text{C}$) in the Netherlands from 1920 - 2020. Retrieved from [5]

1.1.3 The urban heat issue

From the previous paragraphs, it is clear that both the predicted increase and intensity of warm summer days and the increasing amount of urban dwellers, will result in heat becoming a bigger issue in urban areas. To fully grasp the urban heat issue, it is important to understand how increased heat manifests itself in urban areas.

In the late 19th century, Luke Howard was the first climatologist to observe local warming effects of urban regions. From climate data of the city of London, Howard observed increased urban air temperatures compared to rural air temperatures: the Urban Heat Island (UHI) phenomenon [66]. Global warming and rapidly growing cities have sparked the scientific interest in this phenomenon over the last century. And especially in the last two to three decades, many scientists have devoted their time to UHI mitigation research [3]. In the Netherlands, where heat is becoming increasingly problematic, research into the UHI concept has been conducted too. Research confirms urban air temperatures in the Netherlands to be some degrees higher than corresponding rural air temperatures [89, 105, 104, 10, 106]. Urban Heat Islands form as a result of reduced vegetation, an increased amount of paved and impervious material use, distinct urban geometry and anthropogenic heat. They present themselves most vividly at night, when urban infrastructure causes urban areas to cool down more slowly compared to their rural surroundings [103].

The UHI effect as described above has generally been regarded as the main concern considering urban heat. However, by reducing urban heat issues to the increase of urban air temperatures only, would be neglecting part of the urban heat problem [61]: A more elaborated take on urban heat issues would be the following: Heat issues in urban areas in the Netherlands occur as a result of warm weather. Due to

global climate change, warm weather extremes will occur more frequently and maximum air temperatures are expected to increase. Urban areas, characterised by their increased land cover and complex urban structure, function as amplifiers of heat. The heat amplifying characteristics of urban areas manifest themselves in twofold: Both an increase in urban air temperature (relative to rural air temperature), which is pronounced most vividly at night-time (Urban Heat Island phenomenon) and a decrease in urban outdoor thermal comfort experienced predominantly during the day (figure 1.3) [49]. Regarding the mitigation of urban heat issues, one should thus not solely focus on air temperature, but also on additional variables that constitute thermal comfort: wind speed, radiation and relative humidity.

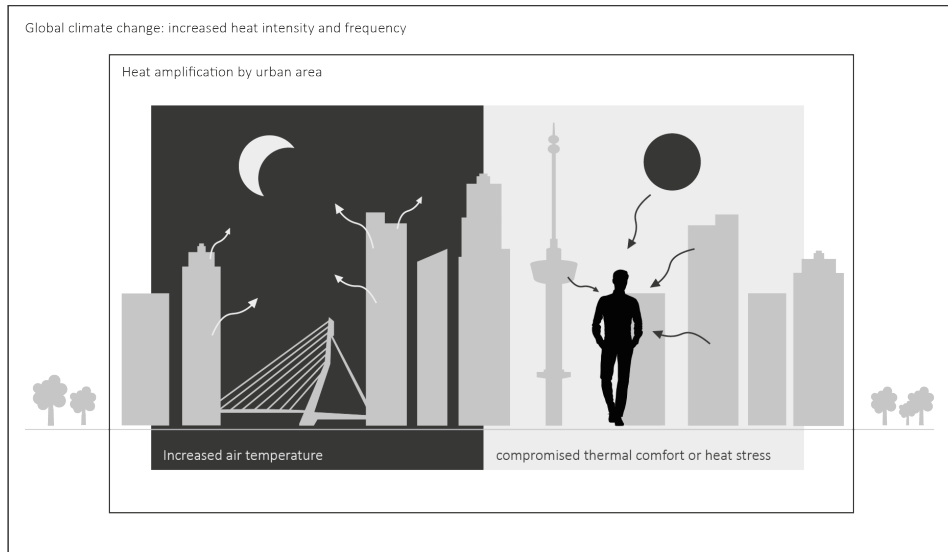


Figure 1.3: The urban heat issue

The built-environment has the potential to play a significant role in mitigation of thermal comfort related urban heat issues by altering the meteorological variables that constitute thermal comfort. Through careful management of urban form, vegetation and material usage, local urban climates have the potential to become even more thermally comfortable than neighbouring rural climates [61]. However, existing buildings and outdoor space in the Netherlands, which have been designed for a cooler climate, have often not been adapted to increased heat yet [49]. Which makes that, in the current situation, city life phases a problematic future. To create cities that are more resilient to future climate scenarios, the compromised safety and health should be an incentive to re-evaluate urban form and function and eventually reshape cities.

1.2 State of the Art

1.2.1 Identifying heat-risk areas through standardized heat maps

The ‘Deltaplan Ruimtelijke Adaptatie’, formed to facilitate the creation of a climate resilient environment in the Netherlands in 2050 (paragraph 1.1.2), comprises three steps to steer climate adaptation: knowing, wanting, working (weten, willen, werken): Governments should map drought-, flooding-, and heat-related vulnerabilities within the regions they are responsible for, through carrying out so-called

stress-tests (knowing) [45]. Subsequently, concrete adaptation goals are formulated (wanting). These adaptation strategies will be secured by drafting an implementation agenda and potential alteration of laws and regulations (working) [80].

To date, municipalities, water authorities and provinces are the least advanced in exploring the theme heat [77]. Only recently (2020), strategies for the analysis of heat-related issues through standardised heat maps (stress-tests) have been formulated by a consortium of municipalities and research organisations [49]. Commissioned by the consortium, methods for drafting two standardised heat maps have been developed at Wageningen University (WUR): The first method allows for mapping of the number of warm nights (air temperature > 20 degrees Celsius). The second provides a detailed representation of outdoor thermal comfort during the day [46]. Both maps are available in the ‘klimaat effect atlas’ [1]. The latter map is particularly informative for liveability in outdoor space during extreme heat events. This map uses the Physiological Equivalent Temperature (PET) index as indicator for outdoor thermal comfort and is drafted through a simplified PET calculation method which uses spatial information and rural weather data as input [50, 80].

The stress-test described above constitutes the ‘knowing’ part of the ‘Deltaplan Ruimtelijke Adaptatie’. To facilitate the formulation of concrete adaptation goals (the ‘wanting’ part of the Deltaplan), Kluck et al [49] have consulted municipalities through workshops. In cooperation with the municipalities, a set of outdoor thermal comfort oriented heat mitigation guidelines for urban designers is drafted (table 1.1).

Table 1.1: Heat mitigation design guidelines [49]

What?	How?
Distance to a cool area.	Every building with a residential function should be sufficiently close to a cool area (pleasant on warm days). The proposed maximum distance is 300 [m].
Percentage of shade on important walking routes.	At the warmest moment during the day. Important areas should be shaded for at least 40% of their total area. On other routes the shade percentage is recommended to be 30%.

1.3 Knowledge gaps

In response to the state of the art research, two knowledge gaps have been identified.

(1) A computationally efficient model for outdoor thermal comfort in the preliminary design stage.

The introduced heat stress-test according to the ‘Deltaplan Ruimtelijke Adaptatie’ provides an instruction for the heat mitigation approach in the Netherlands in the next few years. This has raised awareness of the importance of heat-related climate adaptation measures amongst municipalities. Consequently, municipalities are increasingly interested in redevelopment of existing urban areas to make them heat

resilient, or the development of new heat resilient urban areas. For this purpose, an initial set of heat design guidelines (table 1.1) has been developed. However, these design guidelines are formulated quite broadly, and are not formulated in terms of PET. As heat-performance of urban areas is assessed through the index PET in the heat maps, it is preferred to evaluate urban design in terms of PET directly from the start of a design project. Whilst some tools for simulation of PET are available to urban designers, these tools generally simulate PET at large computational cost: Most established models for PET simulation rely on Computational Fluid Dynamics (CFD) and Energy simulations, which causes PET calculation to take up to multiple hours or even days [90, 31]. These complex tools are very useful when a detailed picture is required for a final design. However, in the early design stage, when rapid assessment of different design options is desirable, the established tools are not quite useful. At present, urban designers are still dependent on the design guidelines in the early design stage: Adequate tools for rapid PET assessment in the early design stage are not widely available (figure 1.4).

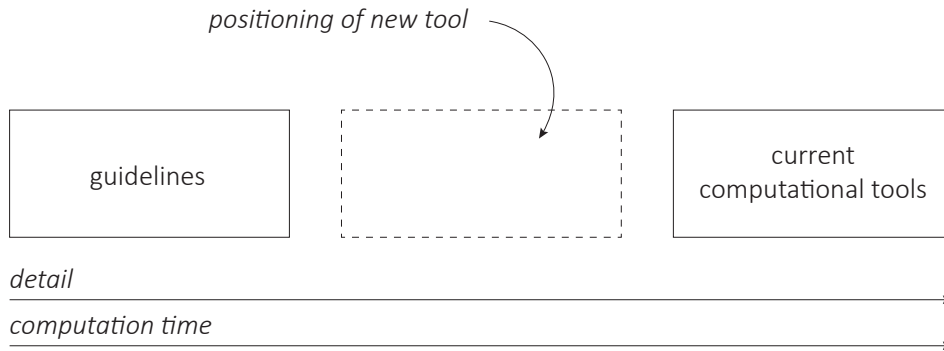


Figure 1.4: Positioning of the new tool

(2) The effect of heat mitigation measures in the temperate climate of the Netherlands.

In addition to an adequate simulation tool for rapid PET assessment, urban designers would benefit from rules-of-thumb for the PET heat mitigation potential of various design measures. In warm climates such as arid and hot humid climates, the effect of heat mitigation measures on outdoor thermal comfort has been studied over the years. However, in temperate climates such as that of the Netherlands, outdoor thermal comfort heat mitigation measures have been studied less extensively. From an extensive literature review, Kluck et al. [49] have drafted an overview of design measures for heat mitigation and their corresponding cooling potential as described in literature (appendix A). From this review, it appears that the effects of 'green' (vegetation-related) and 'blue' (water-related) design measures are broadly known. The effect of 'grey' design measures on outdoor thermal comfort, however, is less defined (table 1.2). For many design measures, the potential heat reduction in terms of PET is currently unknown.

Table 1.2: Grey heat mitigation as identified by Kluck et al. [49]. [??] means effects are yet unknown. [-] means effects are negligible.

Design Measure	Scale	Cooling effect [$^{\circ}\text{C}$ PET]
Dynamic shading	Local	2.0 - 17.0
Wind corridors	Cold	??
Large open areas	Cool	??
H/W ratio street	Local	??
Street orientation	Local	Max 10.2
High albedo facades	Local	??
High albedo pavement	Local	??
White-painted roofs	Urban	-

1.4 Research aim

1.4.1 Research objectives

This thesis aims to fill the knowledge gaps as identified in paragraph x. The following research objectives have been formulated in response to these knowledge gaps:

(1) The first objective of this research is to create a computationally efficient parametric model for PET calculation to be used by urban designers in the early design stage.

This tool will fill the gap between the design guidelines as established by Kluck et al. [49] and existing computational tools that are computationally heavy (figure 1.4). Through its rapid PET simulation, the tool should provide urban designers with a means to incorporate PET simulation in early design.

(2) The second objective of this research is to quantify how building-related grey heat mitigation strategies on the urban block scale impact outdoor PET values in the Netherlands.

To provide urban designers with rules-of-thumb for the heat mitigation potential of design measures in terms of PET, the effectiveness of varying selected heat mitigation measures will be assessed. From table 1.2, building-related heat mitigation measures on urban block scale (table 1.3) have been selected for analysis, as these design measures are of specific interest for urban designers: Implementation of design measures at a large scale (f.e. implementation of large open spaces) is often limited due to constraints of available space in dense urban areas, whereas smart varying of street orientation or H/W ratio at urban block scale for the purpose of heat mitigation may potentially be applied to many urban design projects. Note that from table 1.2, any dynamic design measures such as dynamic sunshades or canopies have been neglected, as these measures are in general not considered in urban design. Even though heat mitigation potential of street orientation has been assessed for the Netherlands before, (re)evaluation of this design measure remains interesting as any interdependencies between the selected design measures have not been addressed in literature.

Table 1.3: Grey heat mitigation design measures on the urban block scale selected for further analysis

Design Measure	Scale	Cooling effect [deg C PET]
H/W ratio street	Local	??
Street orientation	Local	Max 10.2
Facade albedo	Local	??

1.4.2 Research questions

The presented research objectives lead to two main research questions, which are both subdivided into multiple sub-questions. The first research question relates to research objective (1) and the second research question to research objective (2).

(1) How can a parametric computational model be set up for outdoor PET calculation with an adequate balance between time-efficiency and sufficient accuracy for the early design stage?

1.a] How is thermal comfort determined and affected by surrounding environment?

- Which parameters related to human biometeorology and to the external environment affect thermal comfort?
- How is the thermal comfort index PET calculated?
- How does the urban environment affect thermal comfort?

1.b] How is sufficient accuracy of the computation model ensured?

- What is the relative importance of different thermal-comfort related input parameters?
- How has the Deltaplan Ruimtelijke Adaptatie PET-calculation method, used as a heat performance control tool in the Netherlands, simplified PET calculation?

1.c] How can the PET calculation method be modified for improved time-efficiency?

- Which aspects of the PET calculation cause current tools to be computationally heavy?
- Which constraints for sufficient accuracy (following from sub-question 1.2) limit the alteration of PET calculation?
- How can sub-calculations of the Deltaplan Ruimtelijke Adaptatie PET calculation method be applied to improve calculation efficiency?

(2) How effective are the building-related heat mitigation measures identified by Kluck et al. [49] (H/W ratio, street orientation and facade albedo) in providing outdoor thermal comfort during extreme heat events in the Netherlands?

2.a] What is the individual heat mitigation effectiveness for varying the selected heat mitigation measures?

- 2.b]** How is the individual heat mitigation effectiveness of each selected heat mitigation measure affected by varying the other two heat mitigation measures? (i.e. does a dependency between the heat mitigation measures occur?)
- 2.c]** Which combination of input values for the selected heat mitigation measures results in minimum- and maximum outdoor thermal comfort?

1.4.3 Scope

This thesis considers urban outdoor thermal comfort in the temperate climate of the Netherlands. The research is confined to extreme heat events and considers Dutch weather data and geographic information only. As this thesis focuses on outdoor thermal comfort, the term 'heat mitigation measures' refers to outdoor thermal comfort related heat mitigation in the context of this research. Mitigation measures are assessed at the urban block scale only.

1.5 Scientific and societal Relevance

Increased understanding of outdoor thermal comfort and the implications of heat mitigation measures for urban design has a clear societal relevance: Ignorance of urban heat issues may result in reduced comfort and compromised safety for urban dwellers. European mortality rates as a consequence of extreme heat are considerably larger than mortality rates as a consequence of other natural hazards such as for example floods. And with an ageing population, the amount of people vulnerable to heat related health issues is ever increasing [67].

Scientifically, this research is relevant by contributing to the limited knowledge of outdoor thermal comfort in temperate climates and the effect of relevant mitigation strategies. The accumulation of scientific knowledge through this research will in turn contribute to reducing the societal impact as discussed above.

1.6 Report outline

This thesis is subdivided into five sections (figure 1.5). The research framework (section I) is composed of the first two chapters and forms the foundation of the research and report. In section II, a literature review is presented, which forms the scientific base for research. From the literature review, appropriate calculation methods are selected for model development (section III) and hypotheses are drafted as input for the Parametric study (Section IV). Major findings of the thesis are presented and discussed in section V: Conclusion, Discussion and Future studies.

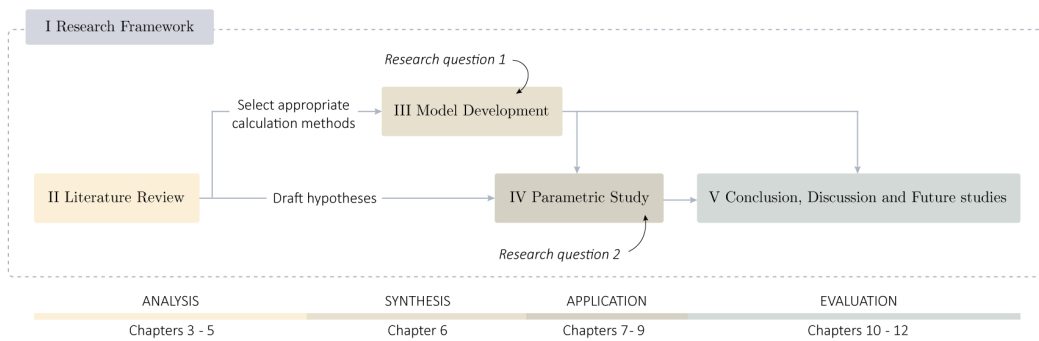


Figure 1.5: Report outline

Chapter 2

Research approach

The objective of this research is twofold:

- To develop a model for PET simulation in the early design stage with an adequate balance between calculation accuracy and time-efficiency.
- To generate rules-of-thumb for heat proof design through quantification of the heat mitigation effectiveness of H/W ratio, street orientation and facade albedo.

These research objectives and corresponding research questions are addressed through a mixed research approach: While the research is largely based on numerical data (validation of PET input calculation methods and assessment of numerical PET data) and thus largely quantitative, some qualitative aspects are embedded in the research as well. Design decisions are based on both insights obtained from literature and interviews with experts in the field of outdoor thermal comfort and computational modelling. In this chapter, the research approach of the three sections that form the body of this thesis: Literature review, Model development and the Parametric study is described.

2.1 Literature review

The main purpose of the literature review is to form a sufficient scientific base for development of the parametric model and subsequent analysis of heat mitigation efficiency of selected design measures through the parametric study. The literature review is structured according to research questions 1.a - 1.c. Interviews with Sytse Koopmans (developer standardised PET-map calculation method) have been conducted for better interpretation of the limitations of the standardised calculation method. Additionally, an interview with Laura Kleerekoper (developer heat design guidelines) has been set up to increase insight into future developments of the 'Deltaplan Ruimtelijke Adaptatie' and potential future urban heat-legislation.

2.2 Model development

The model is developed through both insights obtained from literature and consultation of experts in the field of outdoor thermal comfort and computational modelling. Interviews with Emanuele Naboni (associate professor KADK and University of Parma), Nathaniel Jones (building physicist Arup), Viktor de Lucas (engineer Arup), Jake Haskell (Senior Engineer Computational and Digital Engineering), Jonathan Nathaniel (research associate TUM) and Chris Mackey (developer Ladybug Tools) have been conducted for design decision support.

2.3 Parametric study

The parametric study aims to answer the second research question into the heat mitigation effectiveness of varying H/W ratio, street orientation and facade albedo. The study is performed for an urban canyon in a theoretic urban environment (chapter 7). In addition to an extensive study into the effectiveness of H/W ratio, street orientation and facade albedo, an exploration into the effects of varying the urban surrounding environment, ground material and facade material on outdoor thermal comfort is performed. These results are discussed in chapter 9: 'Interim exploration and discussion of study results'.

Part II

Literature review

Chapter 3

Human biometeorology and thermal comfort

3.1 Human bioclimates

Humans are homeothermic organisms: their thermoregulatory system maintains a core body temperature between 36.1 and 37.8 degrees Celsius under exposure to a large range of environmental conditions. Humans are able to internally generate heat through metabolism and muscle contraction and exchange heat with their external environment through conduction, convection, radiation and evaporation [15]. They regulate thermal processes to ensure the net heat gain or loss with the external environment approaches zero: heat is conserved in cold ambient conditions and released in a warm ambient environment [75]. Thermoregulation can be both an automatic response of the body and be driven by voluntarily actions. In cold conditions, blood flow to the limbs is constricted (vasoconstriction) to reduce heat loss to the ambient environment. Additionally, the body may start shivering to generate more heat. Both processes are automatic processes. Voluntarily thermoregulatory actions to reduce heat loss in cold conditions rely on human decision-making: one can for example decide to wear more clothes or stay indoors. In warm conditions, automatic processes to maintain a stable core body temperature are vasodilation or sweating. Additionally, humans may perform voluntarily heat regulation actions such as wearing less clothes or turn on a fan [15, 35].

According to the law of energy conservation, heat exchange with the external environment and internal heat generation can be written in the form of an energy balance: Heat storage is equal to heat production within the body minus the heat loss (equation 3.1). The left term in equation 3.1 (ΔQ_S) presents heat storage in the human body. To maintain a stable core temperature of approximately 37 degrees Celsius, ΔQ_S should approach zero [75, 26]. Q_M presents the heat production and the sum of Q^* , Q_H , Q_E and Q_G forms the net heat gain from- or net heat loss to the external environment (depending on the sign of the individual elements) [34]. In this equation Q^* refers to radiative heat exchange, Q_H to sensible heat exchange (convection), Q_E to latent heat exchange (evaporation) and Q_G to heat exchange through conduction (figure 3.1). For all fluxes, the quantity of heat transfer to the external environment is dependent on either a temperature- or a vapour pressure gradient, resistance of the clothing layer and the area of the skin surface [35, 26].

$$\Delta Q_S = Q_M - (\pm Q^* \pm Q_H + Q_E \pm Q_G) \quad (3.1)$$

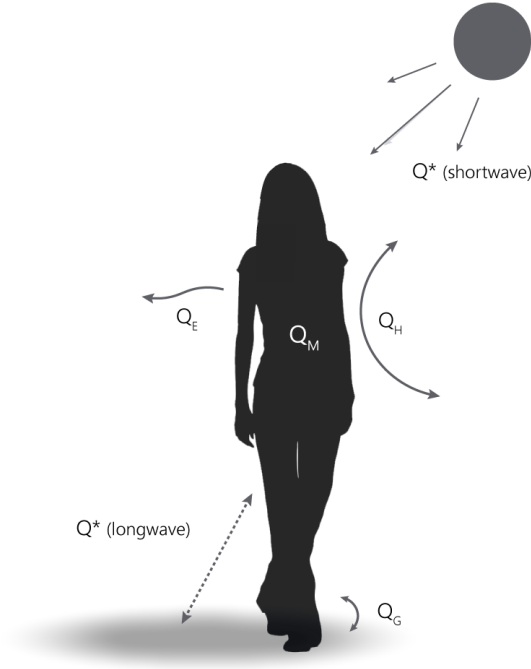


Figure 3.1: Heat fluxes of the human energy balance. Adapted from [34]

Internal heat production Q_M

Internal heat production (Q_M) is determined by metabolic activity. The body at rest generates the quantity of heat needed for the body's primary functions (respiratory and circulatory systems) to function properly. In situations where the body is not at rest, muscle activity increases. Accordingly, metabolic activity increases to provide the muscles with sufficient oxygen and nutrients. While part of the energy generated by the active muscles is released as external work, the largest share is released as internal heat (equation 3.2) [34].

$$\text{heat production } (Q_M) = \text{metabolic rate} - \text{external work} \quad (3.2)$$

Radiation Q^*

Heat can be transferred from hot to cold bodies via thermal radiation [76]. Thermal radiation covers part of the electromagnetic spectrum with wavelengths ranging from $0.1 \mu\text{m}$ to $100 \mu\text{m}$. Waves in this part of the electromagnetic spectrum have the ability to affect the thermal state of matter [65].

According to Planck's law, objects at higher temperatures emit radiation at shorter wavelengths [78]. Planck's law can be visualised using characteristic Planck curves for an idealised emitter, or blackbody: A theoretical concept that describes an object that has zero reflectance and thus absorbs all incident irradiation. From

Kirchoff's law (absorptivity of an object at a certain wavelength equals the emissivity at that wavelength) it then follows that blackbodies are also perfect emitters [65, 108]. In figure 3.2, normalized Planck curves of blackbody emitters at temperatures of the sun and the earth-atmosphere system are given. Due to their differences in temperature, the sun and the earth-atmosphere system emit radiation at distinctively different wavelengths. With its significantly higher temperature, the sun emits thermal radiation in wavelengths ranging from 0.1 to 3 μm . Oppositely, the earth-atmosphere system emits thermal radiation with larger wavelengths (3 to 100 μm) due to lower temperatures within this system. Because of these significant differences, thermal radiation from the sun (ultraviolet radiation, radiation in the visible spectrum and near-infrared radiation) is in practice often categorized as shortwave radiation, whereas thermal radiation emitted within and from the sun- and earth atmosphere system (thermal infrared radiation) is categorized as longwave radiation [75].

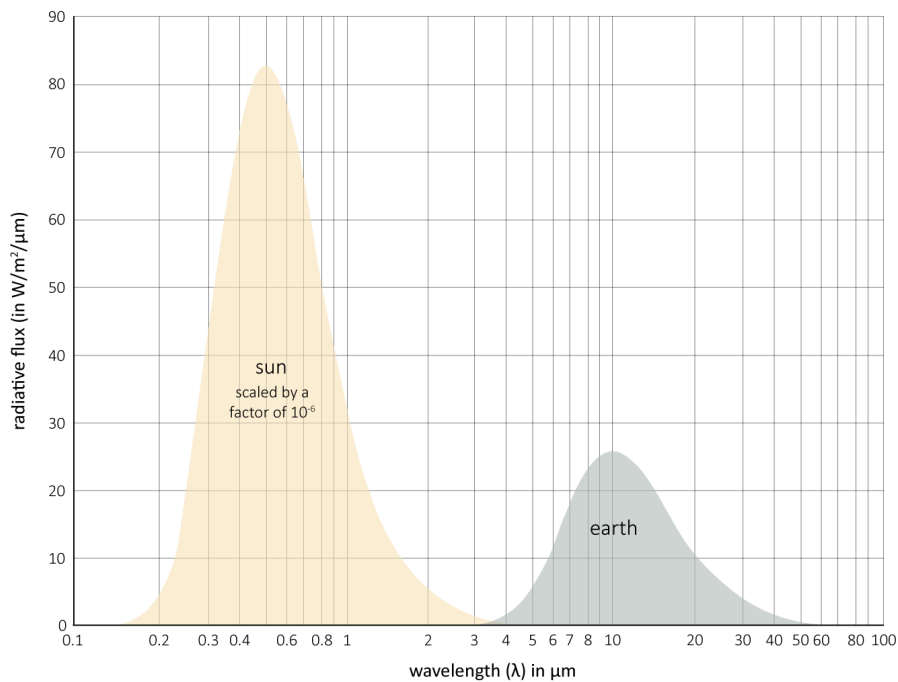


Figure 3.2: Planck curves of blackbody emitters at temperatures of the sun and the earth-atmosphere system. Adapted from [75]

In outdoor situations, humans exchange radiant energy with their surroundings through both short- and longwave radiation. The amount of received shortwave irradiance (K_{in}) (radiant energy per unit time) is determined by the location of the sun with respect to the location on earth, the transmittance of the atmosphere and the reflectivity of clouds, sky and objects in the direct environment. The shortwave irradiance is subdivided into two components depending on the radiation path: Shortwave irradiance received directly from the sun (direct irradiance S) and incoming shortwave irradiance from all surrounding directions due to scattering within the sky or by reflection of surrounding objects (diffuse irradiance D) (equation 3.3).

$$K_{in} = S + D \quad (3.3)$$

The net shortwave irradiance (K^*) depends on the reflectivity (albedo α) of the

human body surface (equation 3.4). The degree of reflectivity is determined by both skin pigmentation and clothing and ranges from zero to one, increasing with reflectivity.

$$K^* = K_{in}(1 - \alpha) \quad (3.4)$$

The net (all-wave) irradiance (Q^*), that describes radiant heat transfer between the human body and its environment (equation 3.6), is the sum of the net shortwave (K^*) and net longwave (L^*) (equation 3.5) irradiance [75].

$$L^* = L_{in} - L_{out} \quad (3.5)$$

$$Q^* = (S + D)(1 - \alpha) + L_{in} - L_{out} \quad (3.6)$$

Sensible heat flux Q_H (convection)

Sensible heat transfer occurs through convection. Convective losses may occur either through breathing or occur at the skin surface. Breathing accounts for only a small fraction of all convective losses from the human body. Accordingly, the largest share of sensible heat transfer is a result of convective heat losses from the skin to the ambient environment [97]. The rate of convection at the skin surface is a function of the temperature difference between the clothed body (T_{cl}) and ambient environment (T_a), the convective heat transfer coefficient (h_c) and the clothing area factor (f_{cl}), which presents the ratio of the clothed surface area to the nude body surface area (A_{cl} / A_D) (equation 3.7) [8]. The convective heat transfer coefficient (h_c) is positively related to wind speed: Larger wind speeds increase the rate of convective heat transfer with the ambient environment [87].

$$Q_H = f_{cl}h_c(t_{cl} - t_a) \quad (3.7)$$

Latent heat flux Q_E (evaporation)

Latent heat transfer includes all heat loss through evaporation. Similar to sensible heat transfer, evaporative losses may occur either through breathing or at the skin surface, with evaporative losses through the skin surface representing the largest share of the sum of both evaporative losses. At large ambient temperatures, the human body is triggered to excrete moisture through sweat glands at the skin surface to increase the rate of evaporative heat loss. Evaporative heat loss through the skin surface is a function of the skin wettedness (w), the vapour pressure difference between the skin and ambient air ($p_{sk,s} - p_a$) (which is dependent on air temperature [35]), evaporative heat transfer resistance of clothing (R, cl), the clothing area factor (f_{cl}) and the evaporative heat transfer coefficient (h_e) [8] (equation 3.8). The evaporative heat transfer coefficient (h_e) is comparable with the coefficient for convective heat transfer (h_c): its relationship with wind speed is positive. Increased wind speeds will thus lead to a larger evaporative heat flux [57].

$$Q_E = \frac{w(p_{sk,s} - p_a)}{R_{e,cl} + 1/(f_{cl}h_e)} \quad (3.8)$$

Conduction Q_G

Heat transfer through conduction is usually insignificant due to its small effect on thermal comfort [44], and therefore often neglected in human thermal balances [26, 8]. An exception to this is when people are fully or partly immersed in liquid substances, or in direct contact with either hot or cold objects over a large area of their body surface [35]. Since these situations do not apply to general outdoor thermal comfort calculations, conductive heat transfer is not further considered in this report.

3.2 Outdoor thermal comfort

Thermal comfort is often defined as *"the condition of mind in which satisfaction is expressed with the thermal environment"* [9]. Important to note in this definition is the psychological aspect of one's thermal state: Despite the development of measures for expressing thermal comfort in a numerical form, no two individuals are likely to experience thermal comfort precisely the same. Differences in perception of thermal comfort by individuals are the result of various factors, amongst which are cultural environment, thermal expectations, acclimation and many more individual or social factors [75, 20].

For general calculation of thermal comfort, however, individual perception of thermal comfort, modified by a range of psychological aspects cannot reasonably be considered. A more objective assessment of thermal comfort therefore considers physiological aspects only. In accordance with this approach, the human body is in a state of thermal comfort when the physiological effort of core body temperature regulation is minimal (ΔQ_S approaches zero).

ΔQ_S , and consequently thermal comfort, is determined by the balance of internal heat production, radiative heat transfer, convective heat transfer and evaporative heat transfer (heat transfer by conduction is omitted due to its negligible impact). From equations 3.3 - 3.8, it follows that individual heat flows, and therefore thermal comfort, are instantly affected by four meteorological variables (table 3.1) [20, 37]:

Table 3.1: Meteorological variables and the corresponding heat transfer mechanism they affect

Meteorological variable	Heat transfer mechanism
Air temperature	Convection and evaporation
Mean radiant temperature	Radiation
Relative humidity	Evaporation
Wind speed	Convection and evaporation

Air temperature regulates the extent of convective heat transfer: The temperature gradient between skin- and air temperatures determines the rate of convective heat

transfer (equation 3.7). When ambient air temperature exceeds skin temperature, the human body will experience convective heat gain. Conversely, when ambient air temperature is lower than the skin temperature, the human body will lose heat to its external environment through convection [34].

Indirectly, air temperature affects evaporation as it affects maximum moisture content of the air, which in turn affects evaporative heat loss (equation 3.8). Below, in the section on relative humidity, evaporative heat loss is explained in more detail.

Due to complexity of the radiation field, shortwave- and longwave irradiance are often summarised in a single parameter: the **mean radiant temperature** (MRT). MRT is defined as “the uniform temperature of a fictive black-body radiation enclosure (emission coefficient = 1) which would result in the same net radiation energy exchange with the subject as the actual, more complex radiation environment” [44] (figure 3.3). Three shortwave radiation fluxes are considered in MRT calculation: irradiance received directly from the sun (I), diffusely reflected from particles in the sky (D) and diffusely reflected by surrounding geometry (R). In the longwave spectrum, two radiation fluxes are considered: thermal radiation received from the sky (A) and from the surrounding geometry (E). MRT is expressed in °C and can be calculated from the radiation fluxes mentioned above through equation 3.9. In this equation, σ is the Stefan-Boltzman constant and is equal to $5.67 \cdot 10^{-8}$, ϵ_p is the human body emission coefficient (0.97) and a_k presents the shortwave radiation absorption coefficient of the clothed human body for which an average value of 0.7 is often used. The surface projection factor (f_p) is dependent on the solar altitude and can be determined from table 3.2.

The amount of received longwave irradiance (E_i) and reflected shortwave irradiance (D_i) from surrounding geometry is determined by dividing one’s surroundings into n surfaces with equal temperature over its surface (isothermal surfaces). For these surfaces, longwave irradiance E_i is determined from the surface temperature to the power four (T_i) and its emission coefficient (ϵ_i) through equation 3.10. The reflected shortwave radiation from each surface (D_i) and the longwave radiation emitted by each surface (E_i) are multiplied by their corresponding view factors to determine their relative impact [41, 44].

$$T_{mrt} = \sqrt[4]{\frac{1}{\sigma} \cdot \sum_{i=1}^n \left(E_i + a_k \cdot \frac{D_i}{\epsilon_p} \right) \cdot F_i + \frac{f_p \cdot a_k \cdot I^*}{\epsilon_p \cdot \sigma}} \quad (3.9)$$

$$E_i = \epsilon_i \cdot \sigma \cdot T_i^4 \quad (3.10)$$

Table 3.2: Surface projection factors f_p for varying solar altitude γ

γ	0°	10°	20°	30°	40°	50°	60°	70°	80°	90°
f_p	0.308	0.304	0.292	0.271	0.237	0.205	0.174	0.140	0.108	0.082

Relative humidity affects evaporative heat loss from the human body. Evaporative heat loss is determined by the moisture content in the air, which is in turn (partly) determined by relative humidity. It must be stressed that moisture content is the determining factor here: As relative humidity describes the ratio between the amount of water vapour in the air and the moisture saturation level of the air, and the

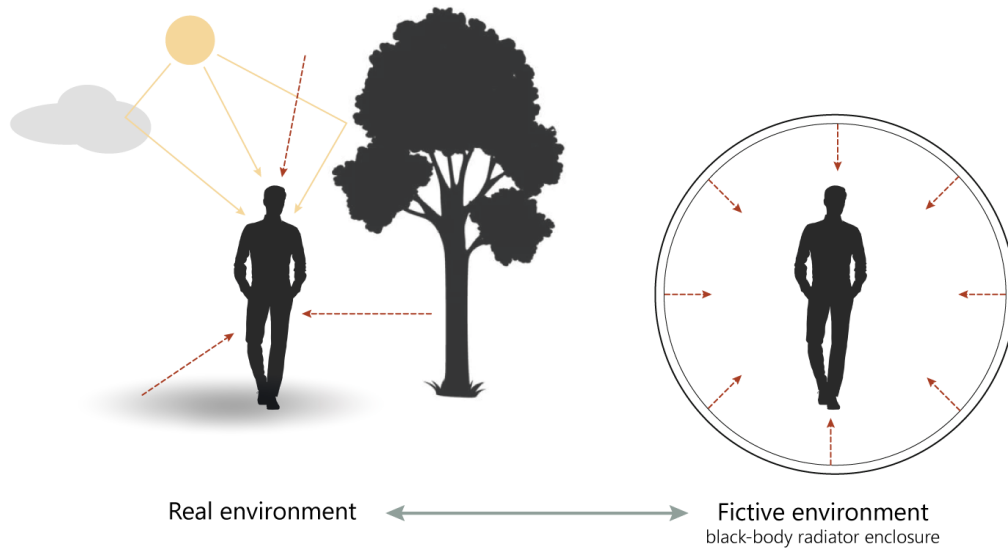


Figure 3.3: title here

maximum moisture concentration in the air is dependent on air temperature, the combination of relative humidity and air temperature is what determines evaporative heat loss. Therefore, environments with the same relative humidity, but differing air temperatures, will result in different rates of evaporative heat loss [34].

Wind speed affects both convective and evaporative heat transfer through mixing of the local air layer around the body [75]. With increased wind speeds, both convective and evaporative heat transfer is increased. As a result, in cool conditions, when heat is transferred from the human body to the ambient environment, larger wind speeds will lead to increased cooling rate of the human body. Vice versa, for extremely hot (and humid) conditions, when heat is transferred from the external environment to the human body, larger wind speeds will cause the body to heat up at an increased rate [34].

In 1962, Macpherson described two additional variables that, besides the four meteorological variables, affect thermal comfort. These two variables are metabolic rate (which is dependent on one's activity) and clothing insulation [20]. Activity levels determine internal heat production, whereas clothing insulation affects one's thermal state by limiting heat and vapour transfer to and from the external environment [34]. As both variables are related to humans and their behaviour, these variables are referred to as **personal variables**. Figure 3.4 summarises all variables (both meteorological and personal) affecting thermal comfort.

3.2.1 Relative importance of meteorological thermal comfort parameters

The thermal state of the human body is determined from the balance between internal heat production and net heat gain or release through radiation, convection and evaporation. These processes are affected by the combined effect of all meteorological parameters. Due to the interrelation between the meteorological parameters, the relative importance of the parameters is not fixed. To illustrate this, the relative

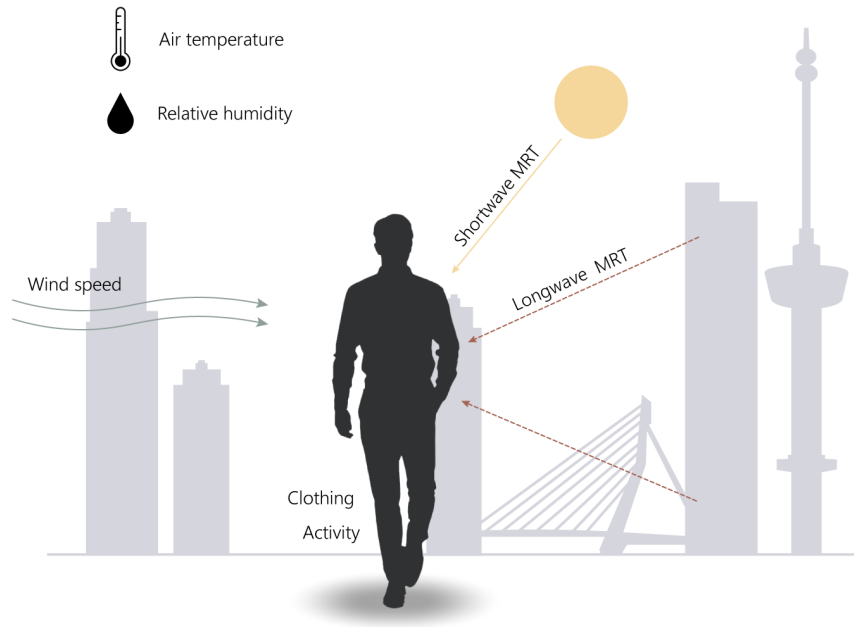


Figure 3.4: title here

importance between mean radiant temperature and air temperature are compared for low- and high wind situations: When wind speeds are low, MRT is of equal importance as air temperature in thermal comfort determination. However, for higher wind speeds, air temperatures are of larger importance than MRT because convective heat losses are now the dominating heat transfer mechanism [37].

Additionally, the relative importance of the meteorological parameters is complicated as it varies with the body's thermoregulatory responses. Wind speed, for example, has a larger effect on thermal comfort when one is sweating [37].

However, research has shown that, in situations of extreme heat when wind speeds are usually low and skies are clear, MRT is the most important parameter affecting thermal comfort. In sunlit areas, differences between MRT and air temperature can become larger than 30 °C. Consequently, MRT greatly affects PET. The relative importance of the longwave- and shortwave share of MRT is dependent on time of day and date of analysis, geographic location and surrounding environment. During the night, when sunlight is absent, MRT is determined by longwave radiation only. Throughout the day, the impact of shortwave MRT increases with increasing sun altitude. Depending on urban geometry, either shortwave- or longwave radiation is governing in MRT determination [44].

3.2.2 Thermal comfort index PET

Various models for thermal comfort calculation based on the human heat balance have been developed. Amongst the most well known and most widely used methods is the 'physiological equivalent temperature' (PET). PET is defined as *'the air temperature at which, in a typical indoor setting (without wind and solar radiation), the energy budget of the human body is balanced with the same core and skin tem-*

Table 3.3: Assumed values for the four meteorological variables for the reference indoor situation

Indoor meteorological variable	Value
Air temperature	20 [°C]
MRT	20 [°C]
Relative humidity	50 [%]
Wind speed	0.1 [m/s]

perature as under the complex outdoor conditions to be assessed' [63]. PET shows good agreement with biometeorological assessment of the thermal environment for different climates [62], and due to this accuracy and applicability in different climates, PET is the most commonly used thermal comfort index in Europe: The German standard for biometeorological evaluation of urban and regional planning (VDI 2787-2) has standardized the use of PET in outdoor thermal comfort evaluation, and recently also the Netherlands has introduced a standardized heat assessment method expressed in PET [49, 36]. Another argument for the widespread use of PET in urban design is its comprehensibility: As PET is expressed in degrees Celsius and represents the temperature one would experience in indoor situations where one is sheltered from wind and shortwave radiation, PET enables simple comparison of the complex outdoor environment with one's own experience of thermal comfort conditions indoors [37, 62].

At the basis of the PET calculation is the Munich Energy-balance Model for Individuals (MEMI), which uses the human heat balance (equation 3.1) for its energy transfer calculation. For these calculations, values for clothing and activity are assumed constant to liberate the calculation from any personal-behaviour related variables. Standardly, activity levels are assumed to be moderately low (generating an additional 80 [W] next to the energy generated by metabolism for the body at rest) and the resistance of clothing is assumed to be 0.9 [clo]. These values are standardized for a 1.80 [m] male of 75 [kg]. Assumed values for the meteorological variables for the reference indoor situation are presented in table 3.3 [37]. With personal thermal comfort variables and reference indoor meteorological variables set, PET can be calculated from the four meteorological variables (air temperature, MRT, relative humidity and wind speed) as experienced at 1.2 [m] height (average centre of gravity Dutch standing person).

3.2.3 Heat stress

PET values are related to the thermal state of the body. Between 18 and 23 °C, the thermal environment is experienced as neutral and limited effort of the body is required to maintain a stable core body temperature of 37 °C. However, as PET values rise, thermoregulation will become increasingly difficult: exposure to PET values larger than 41 °Celsius will result in experience of extreme heat stress (table 3.4). Depending on an individual's age and health conditions, continued exposure to extreme heat stress may lead to hypothermia: A situation in which an individual is unable to maintain stable core body temperature [75, 49] resulting in potential heat disorders.

Note that, as thermal sensation is dependent on climate, the neutral zone in table

Table 3.4: Thermal perception and experienced heat stress and corresponding PET. Adapted from [11]

PET [°C]	Thermal perception	Grade of physiological stress
<4.1	Very cold	Extreme cold stress
4.1 - 8.0	Cold	Strong cold stress
8.1 - 13.0	Cool	Moderate cold stress
13.1 - 18.0	Slightly cool	Slight cold stress
18.1 - 23.0	Comfortable	No thermal stress
23.1 - 29.0	Slightly warm	Slight heat stress
29.1 - 35.0	Warm	Moderate heat stress
35.1 - 41.0	Hot	Strong heat stress
>41.0	Very hot	Extreme heat stress

3.4 shifts to 20 - 25 °C for Mediterranean climates and to 26 - 30 °C for humid climates [18].

3.3 How urban characteristics affect thermal comfort

Urban areas affect outdoor thermal comfort as they affect the meteorological input parameters for outdoor thermal comfort calculation. Air temperatures are increased within urban areas as a result of increased heat retaining capacity of common urban materials, decrease in vegetated cover and increased anthropogenic heat release [103]. Urban morphology affects wind patterns and generally leads to reduced average wind speeds in urban areas. Additionally, the radiative environment is altered by urban morphology in both the longwave- and shortwave spectrum. On the one hand, urban morphology may reduce PET through providing larger areas of shade (reducing received shortwave irradiance). On the other hand pedestrians may experience increased PET in urban areas through increased received longwave MRT, as pedestrians are more likely to be surrounded by objects with larger surface temperatures. Relative humidity is affected by urban characteristics to a limited extent [54].

Chapter 4

The introduction of standardized PET heat maps as a control tool

In response to global air temperature rise as a consequence of climate change, interest in heat issues has increased in the Netherlands in recent years. On behalf of the RIVM (National Institute of Public Health, Well-being and Sport), a standardized method for mapping areas vulnerable to heat issues in the Netherlands has been developed by Wageningen University [50]. The standardized method allows for rapid calculation of PET on a 1-m scale through the equations below (figure 4.1). The first equation is valid for sunlit areas, whereas the second equation is valid for night-time and shaded areas.

$$PET_{sun} = -13.26 + 1.25T_a + 0.011Q_s - 3.37\ln(u_{1.2}) + 0.078T_w + 0.0055Q_s\ln(u_{1.2}) + 5.56\sin(\phi) - 0.0103Q_s\ln(u_{1.2})\sin(\phi) + 0.0546B_b + 1.94S_{vf}$$

$$PET_{shade,night} = -12.14 + 1.25T_a - 1.47\ln(u_{1.2}) + 0.060T_w + 0.015S_{vf}Q_d + 0.0060(1 - S_{vf})\sigma(T_a + 273.15)^4$$

In these equations T_a is the urban air temperature [K], Q_s the solar radiation [W/m^2], $u_{1.2}$ the urban wind speed at 1.2 [m] height [m/s], T_w the wet-bulb temperature [K], ϕ the solar altitude angle [°], B_b the Bowen ratio [-], S_{vf} the sky view factor [-], σ the Stefan Boltzmann constant [W/m^2K^4] and Q_d the diffuse radiation [W/m^2] [51].

These equations have been determined empirically from PET results for different urban configurations. It should be noted that the urban configurations for which the PET equations have been trained have been varied geometrically only. Impact of varying facade materials or solar reflectance of objects (albedo) has thus not been incorporated in the Rayman PET calculation, and is consequently not considered in the standardized PET equations. Since material characteristics and albedo are not considered in calculation, the contribution of radiation to PET calculation is fairly simplified in the standardized method: Direct- and diffuse irradiance values are obtained from a rural weather file and applied directly in the PET_{sun} and $PET_{shade,night}$ equations. Accordingly, the amount of irradiance received is dependent on rural weather data and urban configuration (shading patterns) only [50].



Figure 4.1: An example PET map of Wageningen, created using the Dutch standardized PET calculation method

In addition to radiation, the relative humidity input for thermal comfort calculation is obtained from rural weather data as well: wet bulb temperatures as measured at rural reference weather stations are included in the PET equations. In contrast to the meteorological variables radiation and relative humidity, wind speed and air temperature are not directly obtained from rural weather data: representative urban values are calculated from rural weather data through established methods (explained in further detail in section III) [58, 95] for improved accuracy of the PET calculation.

With the development of a calculation method for standardized PET maps, municipalities in the Netherlands are able to map potential heat-risk areas. In this way, heat maps are applied as a control tool on city-scale. Urban planning projects, however, are often at a smaller scale: (re)design of an urban area often happens at the urban block scale. It is therefore important to emphasise the applicability of this calculation method for different scales: due to inaccuracies of MRT calculation (material characteristics and albedo not considered) this method is considered insufficient at a smaller scale. Currently a small number of accurate (and computationally heavy) MRT and PET simulation software packages exist for urban designer to use in urban planning. These computation models will be discussed in further detail in the next chapter.

Chapter 5

Existing computation tools for PET calculation

Amongst the most widely used software packages for PET calculation are ENVI-met [13] and RayMan [64]. ENVI-met is a computational fluid dynamics (CFD) and thermodynamics based model for holistic simulation of the urban environment, whereas RayMan is a three-dimensional Radiation model.

Especially ENVI-met is remarkably computationally heavy. Simulation of complex interactions between urban surfaces, plants and air allow for detailed microclimate simulations, however at high computational cost: Simulations that take up multiple hours or days for a simple urban configuration are not uncommon [13]. While Rayman is considerably faster than ENVI-met, the software is also considerably less complete in its simulations. As a three-dimensional radiation model, RayMan can be used for calculation of MRT for urban-specific configurations. However, for calculation of PET, values for air temperature, relative humidity and wind speed have to be entered manually: RayMan is not capable of calculating urban values for air temperature and wind speed from urban geometry. Additionally, the MRT calculation of RayMan is simplified quite heavily compared to ENVI-met MRT calculation.

Both methods are thus considered unsuitable for PET simulation in the early design stage. In the next chapter, development of a more suitable tool for PET assessment in the early design stage is presented.

Part III

Model development

Chapter 6

A parametric model for quick PET assessment in the early design stage

At present, urban designers rely on either very broadly formulated design rules or heavy computational models (figure 1.4) for the design of heat-proof urban areas. Adequate tools for quick PET assessment in the early design stage are not widely available. In this chapter, a parametric model for quick PET assessment in the early design stage, with an acceptable balance between accuracy and computational efficiency, is proposed.

The proposed model has been drafted in Grasshopper3D [2], a graphical programming language that comes with the 3D modelling software Rhinoceros by McNeel&Associates. The decision to create the PET calculation model in Grasshopper is based on a number of reasons:

- Grasshopper is widely used by designers, as the visually oriented programme eliminates the well known entry barrier to traditional text-based programming languages: learning the textual language. As many designers use Grasshopper in daily practice, they are familiar with the interface, and thus considered more likely to adopt the model.
- Grasshopper has a large availability of plugins with pre-programmed (environmental) calculations. These pre-programmed calculations are valuable as a basis for PET calculation [82]. Through these plugins, inter-operability with external simulation engines such as EnergyPlus [102] and Radiance [30] is possible.
- Pre-programmed calculations are free and open source. Consequently, users are able to see what's under the hood of the calculations, and even more important: Able to adapt any calculations to their personal preferences.
- A final reason for choosing Grasshopper as design interface is the ability of Grasshopper to perform coupled calculations based on different scientific foundations: The largest share of current simulation tools has been developed to assess one separated environmental issue only. Grasshopper, however, offers

an interface for coupling different external simulation engines as well as plugins related to various scientific disciplines. The interface is therefore highly suitable for the integration of multiple scientific disciplines, which is advantageous for overall design, as it allows for assessment of multiple key performance indicators (KPI) at once [69].

In the first paragraph of this chapter, the structure of the developed PET calculation model in Grasshopper is presented. Paragraphs two to five show the calculation procedure for each urban meteorological PET input parameter from rural weather data. Subsequently, implemented optimisations for calculation efficiency are explained shown. The final paragraph of this chapter discusses validation of the overall model.

6.1 Model setup

PET can be calculated from four meteorological parameters: air temperature, MRT, relative humidity and wind speed. The Ladybug Tools plugin of Grasshopper comes with a component for PET calculation based on the original Fortran code by Höppe [17]: “Ladybug Thermal Comfort Indices”. With air temperature, MRT, relative humidity and wind speed input data supplied, this component calculates PET conform the method as established by Höppe [37].

With PET calculation integrated in Ladybug Tools, the challenge of generating a PET simulation model for the urban environment is thus not the eventual PET calculation itself, but understanding and calculating how the urban environment modifies the four meteorological input parameters. Different methods for modification of the the four meteorological input parameters from rural weather data to urban values have been implemented (figure 6.1) in the PET simulation model. Some of these methods have been simplified to a larger extent than others, in correspondence with both relative importance of the meteorological variable as well as potential calculation expenses.

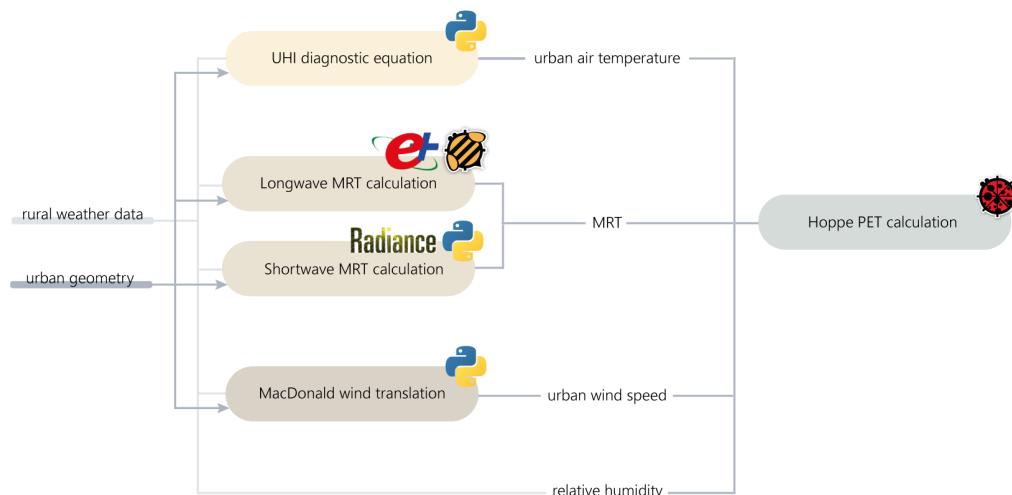


Figure 6.1: Structure of the PET calculation model in Grasshopper

Figure 6.2 shows an example configuration of an urban block for which the model

could calculate PET from urban meteorological input parameters. For each individual hour of the year, the model is able to calculate PET for all analysis points on a grid which is variable in size.

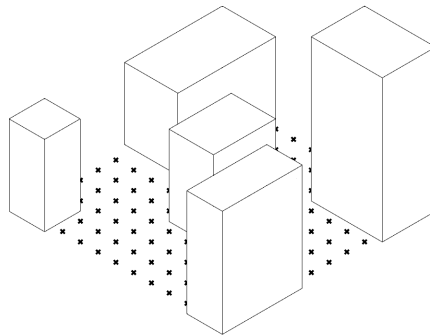


Figure 6.2: Example configuration of an urban block with corresponding analysis points

Below, the calculation of urban air temperature, MRT, relative humidity and wind speed as applied in the PET model, as well as considerations for simplification are explained in further detail. For each individual calculation, a validation is presented.

6.2 Urban air temperature calculation

In practice, difference between urban- and rural air temperature (UHI) is often determined through complex computer models, connecting large-scale atmospheric models to smaller scale urban (energy) models [16, 95]. For Grasshopper specifically, Urban Weather Generator (UWG) that comes with the Dragonfly plugin, has been developed for quantification of UHI [14, 72]. UWG morphs rural weather files to urban weather files through urban block scale energy balances. Despite being more computationally efficient than most established UHI calculation models, UWG computation can still be considered somewhat heavy as it relies on energy modelling. Another disadvantage of UWG (as well as other complex UHI computation models), is the reliance of the computation on relatively detailed input information, which in the early design stage is not yet known.

A more holistic approach of UHI determination, that requires less detailed input information, is therefore preferred. As alternative to complex computation models, Theeuwes et al. [95] have developed a diagnostic equation (equation 6.1, table 6.3) for UHI determination through dimensional analysis. The quantity of input information needed for calculation according to this method is limited: Two urban-related parameters, vegetation fraction (F_{veg}) and sky view factor (SVF), are required and four meteorological parameters, mean downward shortwave radiation (S_{in}), daily maximum- and minimum air temperature (T_{max} and T_{min}) and daily mean wind speed (U) should be gathered from rural weather data. As the equation shows good agreement with measured rural- and urban air temperature data for cities in North-Western Europe, the equation appears to be adequate for application in the PET calculation model.

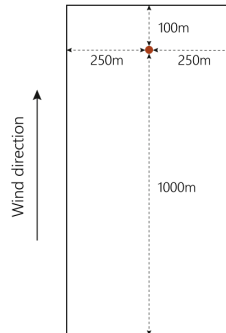
$$UHI_{max} = (2 - SVF - F_{veg}) \sqrt[4]{\frac{S_{in}(T_{max} - T_{min})^3}{U}} \quad (6.1)$$

Table 6.1: Input parameters for diagnostic UHI-equation Theeuwes et al. [95]

Symbol	Parameter	Unit
SVF	Sky view factor averaged over source area	
F_{veg}	Vegetation fraction averaged over source area	
S_{in}	Mean downward shortwave radiation over the current day	Km/s
T_{max}	Maximum (hourly) air temperature between 08.00 current day - 07.00 subsequent day	K
T_{min}	Minimum (hourly) air temperature between 08.00 current day - 07.00 subsequent day	K
U	Mean wind speed between 08.00 current day - 07.00 subsequent day	m/s

Before explaining into further detail how equation 6.1 can be applied for hourly urban air temperature calculation, some notes on how to obtain the parameters listed in table 6.3 are presented:

When wind speed measured at the rural reference station at 10 [m] height is larger than/equal to 1.5 [m/s], the average **sky view factor**¹ should be determined over a 500x1100 [m] source area around the grid point for which one wants to calculate urban air temperature (figure 6.3). In case of low wind situations (rural wind speed at 10 [m] height < 1.5 [m/s]), a source area of 700x700 [m] should be used [51]. The average SVF over the appropriate source area is determined by calculating the SVF in test points on a 25 [m] grid within the source area, after which the average SVF over all points is determined. The grid is set to 25 [m], as this dramatically reduces calculation time: For a 25 [m] grid, 880 independent SVF calculations have to be performed (when considering the source area in figure 6.3), in comparison to 550,000 independent SVF calculations for a 1 [m] grid. The effect of a large grid size on calculation accuracy is assumed negligible for final average SVF calculation over the source area.

**Figure 6.3:** Source area for calculation of spatially averaged SVF and F_{veg} . Adapted from [51]

Similar to calculation of the SVF, the **vegetation fraction** is determined over the rectangular source area (figure 6.3 when rural wind speeds are greater than, or equal

¹Note that SVF should not be confused with sky exposure factor (SEF), something that regularly occurs in practice (appendix B).

to 1.5 [m/s]. For lower wind speeds, the 700x700 [m] square source area is used. The vegetation fraction over the source area is determined through division of vegetated surface area by the total source area.

The **mean downward shortwave** radiation (S_{in}) over the current day can be calculated through equation 6.2 [12], where S_{global} refers to the global horizontal shortwave radiation, ρ_{air} to the air density and c_{air} to the specific heat capacity of air. For common air temperatures, c_{air} is equal to 1006 [J/kg · K] [25]. As air density is dependent on air temperature, the value for ρ_{air} is obtained by selecting the air density value corresponding to the mean daily temperature by linear interpolation of the values in table 6.2 [24].

$$S_{in} = \frac{S_{global}}{\rho_{air} \cdot c_{air}} \quad (6.2)$$

Table 6.2: Air density corresponding to air temperature

Air temperature in [degrees C]	Air density in [kg/m3]
-20	1.445
0	1.382
10	1.352
20	1.324
30	1.297
40	1.271

The determination of **daily maximum air temperature**, **daily minimum air temperature** and **daily mean wind speed** is relatively straightforward. For a time-span between 08.00 of the current day and 07.00 the subsequent day, either minimum, maximum or mean values of meteorological data is subtracted from rural weather data.

6.2.1 Translation of the UHI_{max} equation for hourly transformation of rural- to urban air temperature

The UHI calculation method proposed by Theeuwes et al. [95], calculates the daily maximum difference between urban- and rural air temperature ($UHI_{max} = \max[T_{urban} - T_{rural}]$). However, for PET calculation, hourly values of urban air temperature should be calculated. From observations of rural- and urban air temperature data, UHI is known to peak (reach UHI_{max}) after sundown, in the evening or night [89]. Throughout the day, smaller differences between rural- and urban air temperatures are observed, and only part of UHI_{max} contributes to increased urban air temperatures.

Oke [74] has captured the diurnal evolution of UHI in a characteristic curve (figure 6.4). This characteristic curve shifts depending on day length, as the peak UHI depends on time of sunrise and sundown. Koopmans et al. [51] have translated the diurnal cycle by Oke to a table of (hourly) correction factors (diurnal_cycle[h]), dependent on hour of the day and time of the year (as time of the year affects day length). The correction factors are presented in appendix C. Using the correction factors, the difference between rural- and air temperature at a specific hour of the

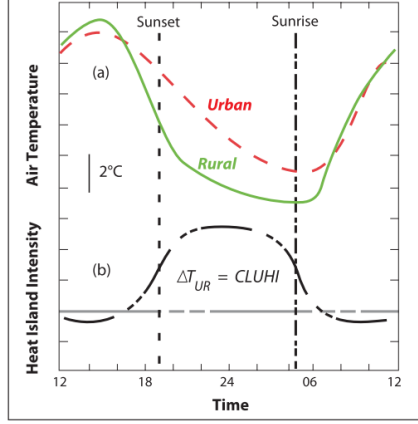


Figure 6.4: Diurnal Cycle by Oke

day ($T_{add}[h]$) can be determined by multiplying the hourly correction factors with the calculated value of UHI_{max} (equation 6.3). Subsequently, the hourly urban air temperature ($T_{a,urban}[h]$) is determined through adding the temperature increase (T_{add}) to the hourly rural air temperature ($T_{a,rural}[h]$) (equation 6.4).

$$T_{add}[h] = diurnal_cycle[h] \cdot UHI_{max} \quad (6.3)$$

$$T_{a,urban} = T_{a,rural} + T_{add} \quad (6.4)$$

6.2.2 Implementation of air temperature calculation in PET model Grasshopper

The described calculation procedure for urban air temperatures has been implemented in the Grasshopper script through a component written in Python (figure 6.5). An elaboration on all Python code is provided in appendix D. Figure 6.5 presents an example calculation for a fictive urban area in which the urban air temperature is calculate in one calculation grid point. The analysis period of the example calculation spans two days and three hours per day (12.00-15.00), so six hours in total. The urban air temperature output is structured as discussed in paragraph x (dayhour list of grid points). Since the considered hours are in the middle of the day, rural-urban air temperature differences are relatively small.

Table 6.3 provides an overview of the input parameters for the Python air temperature calculation component. The meteorological parameters ruralTemp, ruralU, windDir, Tmax, Tmin, AvgU, avgTemp and Rad are received from an imported .epw weather file. As Tmax, Tmin and avgU are values related to a time-span between 08.00 of the current day and 07.00 of the subsequent day, these value's can not directly be taken from the .epw file. To take maximum, minimum and average values in this time-span, a two-step approach is implemented: (1) using the Python datetime library, all successive dates for the selected current dates are determined (consult appendix D for Python script). Using the datetime Python library, this script is automated to correctly present successive dates (figure 6.6a). (2) Lists of combined hourly data from 08.00 - 24.00 the current day, and hourly data from 0.00 - 07.00 the subsequent day are created, from which Tmax, Tmin and avgU can be

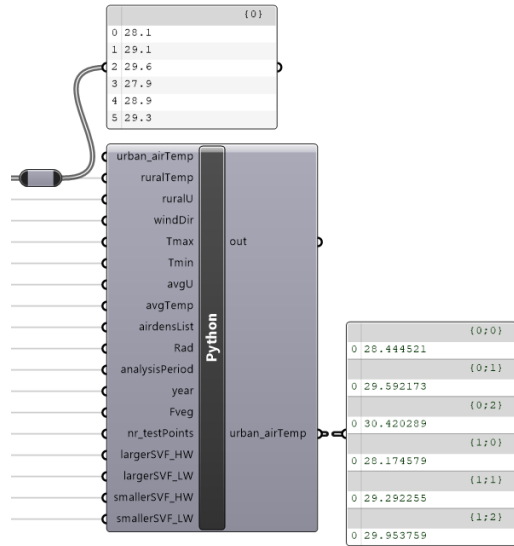
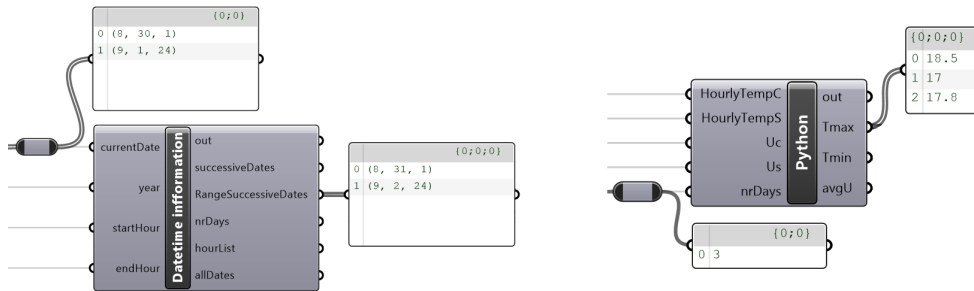


Figure 6.5: Airmtemp calculation



(a) Python datetime calculation for finding successive dates (b) Calculation of Tmax, Tmin and avgU for lists of combined hourly weather data

Figure 6.6: Two-step calculation approach for Tmax, Tmin and avgU calculation

determined. Through a loop function, this calculation can be performed for multiple days at once (figure 6.6b).

SVF is calculated through the "Ladybug View Analysis" component (figure 6.7). The appropriate source area surface is fed to the `_geometry` input. The `_gridSize_` input is set to 25, to calculate SVF over the source area on a 25-m grid. The `ViewStudyResult` output prints a list of SVF values calculated for each test point in the 25-m grid. To calculate the average outdoor SVF, grid points located within buildings (SVF = 0) are removed from the list using a "Cull Pattern" component. The average SVF is subsequently determined from the residual values.

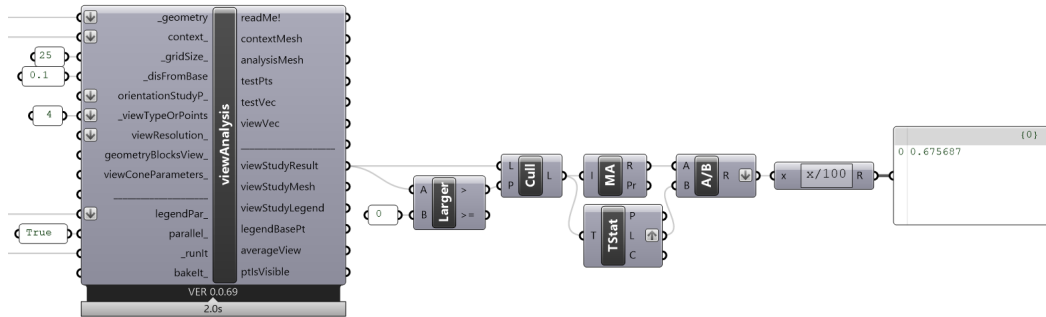


Figure 6.7: Average SVF calculation for a single source area

Table 6.3: Input parameters for diagnostic UHI-equation Theeuwes et al. [95]

Parameter	Required input	Unit
ruralTemp	Hourly rural air temperatures	°C
ruralU	Hourly rural wind speed	m/s
windDir	Hourly wind direction	
Tmax	Maximum (hourly) air temperature between 08.00 current day - 07.00 subsequent day	°C
Tmin	Minimum (hourly) air temperature between 08.00 current day - 07.00 subsequent day	°C
avgU	Mean wind speed between 08.00 current day - 07.00 subsequent day	m/s
avgTemp	Average daily air temperature	°C
airdensList	List of linear interpolated air density values corresponding to table X	
Rad	Average hourly global horizontal radiation	W/m ²
analysisPeriod	The selected analysis period	
year	The selected year of analysis	
nr_testPoints	The total number of grids points for which PET will be calculated	
F_veg	Vegetation fraction over the appropriate source area	
largerSVF_HW	SVF for high wind source areas (when more than 8 analysis hours are considered)	
largerSVF_LW	SVF for low wind source area (when more than 8 analysis hours are considered)	
smallerSVF_HW	SVF for high wind source areas (when less than 8 analysis hours are considered)	
largerSVF_LW	SVF for low wind source areas (when less than 8 analysis hours are considered)	

6.2.3 Validation urban air temperature calculation

The UHI calculation method appears to be accurate for application within North-Western Europe [95]. As the calculation method has been validated for cities in North-Western Europe only, accurate urban air temperature simulation in other regions cannot be guaranteed.

The correct implementation of the calculation method in Python has been validated through a sense-check: The Python calculation has been performed for varying SVF and F_{veg} after which the calculated air temperatures are compared between themselves and to values from literature. From these observations, the calculation method is evaluated based on whether the results are reasonable. Figure 6.8 shows the diurnal air temperature variation for an urban area of varying SVF (considering a default F_{veg} value of 0.3), against air temperature variation of rural weather data. From the diurnal air temperature variation, the calculation appears to have been implemented correctly in Python: In accordance with Oke’s Diurnal Cycle [74], the urban-rural air temperature differences are most pronounced in the evening and at night, whereas they are negligible around four hours after sunrise. As expected, decreasing SVF leads to higher urban air temperatures. Additionally, the magnitude of UHI_{max} is in line with expectations from literature as it approaches 6 °C for calm weather conditions, considering a fairly urbanised area (low F_{veg} and SVF) [89]). The overall air temperature calculation thus seems to have been implemented correctly. Considering assumed correct implementation of the air temperature calculation method, and validation of the calculation method for cities in North-Western Europe, the implemented method is considered appropriate for application in the PET calculation model.

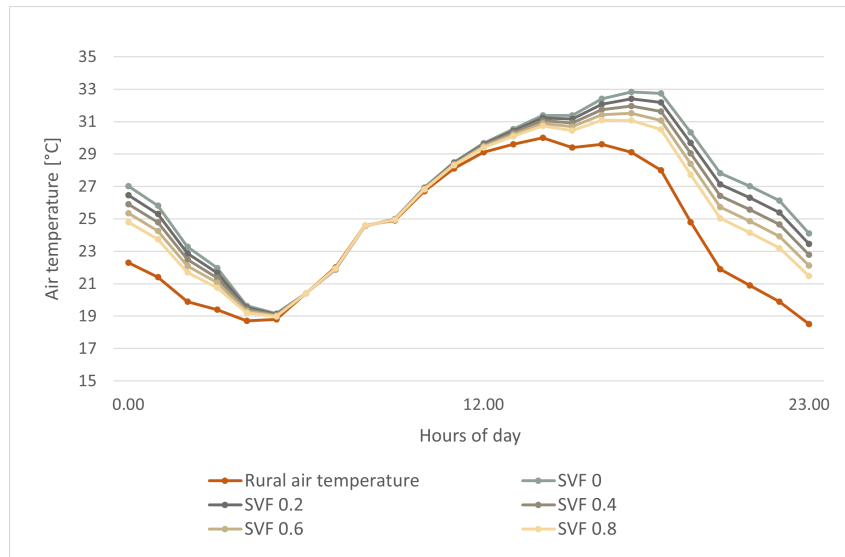


Figure 6.8: Diurnal air temperature variation for varying SVF and a default value of F_{veg} (0.3) plotted against rural air temperature

6.3 Urban MRT calculation

The principal application of the PET calculation model will be to assess how the urban environment affects PET during heatwave situations. In situations of extreme

heat, wind speeds are often low, while skies are clear. In these situations, MRT is the dominant factor affecting thermal comfort. In contrast to urban air temperature and relative humidity, MRT shows highly variable spatial patterns [56]. It is therefore of importance that MRT calculation is performed with sufficient accuracy.

6.3.1 Honeybee Legacy Microclimate Map MRT calculation

Mackey et al. [60] have developed a workflow for MRT calculation, which is programmed in the "Microclimate Map" component that comes with the Honeybee Legacy Grasshopper3D plugin. Within the Microclimate Map, longwave- and shortwave MRT are calculated separately, after which the total MRT is calculated (figure 6.9).

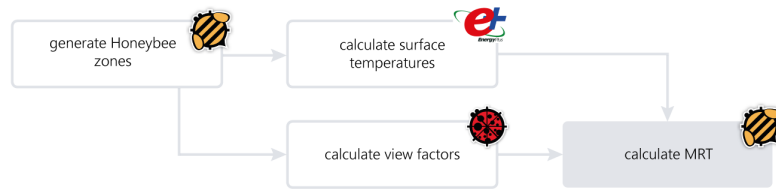


Figure 6.9: Honeybee Legacy Microclimate Map MRT calculation workflow

The **longwave MRT** is dependent on the temperature of surrounding surfaces and the longwave sky temperature (T_i). For MRT calculation, these surrounding temperatures are weighed by their corresponding view factors (F_i) (equation 6.5). View factors describe the portion of the spherical view that is taken up by surrounding surfaces, observed from a given point for which one wants to calculate MRT. Grasshopper performs the view factor calculation by ray-tracing [22].

$$MRT_{longwave} = \left(\sum_{i=1}^n F_i T_i^4 \right)^4 \quad (6.5)$$

The temperatures of surrounding surfaces are modelled through use of an external simulation engine: Energyplus (E+) [101]. The surrounding surface temperatures are calculated by the "Honeybee Export to OpenStudio" component. The longwave sky temperature calculation, on the other hand, is programmed into the "Honeybee Microclimate Map" component itself. Within the component, longwave sky temperature is calculated according equation 6.6 [52]. The horizontal infrared radiation ($IR_{horizontal}$) is obtained from rural weather data, the emissivity of a person (ϵ_{person}) is assumed to have a value of 0.95 and the Stefan-Boltzmann constant (σ) is equal to $5.667 \cdot 10^{-8}$.

$$T_{sky} = \left(\frac{IR_{horizontal}}{\epsilon_{person} \cdot \sigma} \right)^{0.25} - 273.15 \quad (6.6)$$

For calculation of **shortwave MRT**, the indoor SolarCal model by Arens et al. [7] has been altered for outdoor situations to create an effective radiant field (ERF) (equation 6.7), which is used for shortwave MRT calculation (equation 6.8).

$$ERF_{solar} = \left(0.5f_{eff}f_{svv} (I_{diff} + I_{THR})R_{floor} \right) + \frac{A_p F_{bes} I_{dir}}{A_D} \left(\frac{\alpha_{SW}}{\alpha_{LW}} \right) \quad (6.7)$$

$$MRT_{solar} = \frac{ERF_{solar}}{f_{eff}h_r} \quad (6.8)$$

In these equations, f_{eff} presents the portion of the body that radiates heat (assumed to be 0.725), f_{svv} is the sky exposure factor and f_{bes} is either equal to 1 (person subjected to direct sun) or 0 (person in shade). I_{diff} , I_{TH} and I_{dir} are the diffuse sky- global horizontal- and direct normal radiation. A_p and A_D are factors related to human geometry, whereas α_{SW} and α_{LW} present human clothing characteristics. The reflectance of ground surfaces is accounted for through R_{floor} . h_r from the latter equation refers to the radiation heat transfer coefficient [60].

6.3.2 Limitations Honeybee Legacy Microclimate Map MRT calculation

Both longwave- and shortwave MRT calculations have been somewhat simplified in the Microclimate Map calculation procedure: The surface emissivity (ϵ) is omitted in **longwave MRT** calculation, based on the assumption that the emissivity coefficients of all surrounding surfaces are equal. Since most building materials have similar emissivity values (not far from unity), this assumption is considered acceptable [23]. Additionally, the calculation of surface temperatures, and subsequently the calculation of longwave MRT, is moderately simplified by the exclusion of reciprocity in longwave radiation exchange between the considered surfaces [22].

A more significant simplification in MRT calculation, however, is related to **shortwave MRT**. As a consequence of using the shortwave calculation method by Arens et al. [7], the Honeybee Legacy Microclimate Map workflow does not consider reflected shortwave radiation by surrounding objects, except for the ground surface [22, 40]. Since research has shown that reflected shortwave radiation is expected to have a considerable effect on MRT [40, 92, 83, 55, 93], accurate modelling of shortwave radiation is highly significant. Various studies propose the use of Radiance, a ray-tracing algorithm, for radiation simulations in MRT calculation [38, 79]. As accurate modelling of radiation is required to answer evaluate the effect of facade albedo on PET (research question 2), the next section suggests a method for improvement of the original Honeybee Legacy Microclimate Map calculation method through application of Radiance.

6.3.3 Application of Radiance for improved MRT calculation

Radiance can be implemented in the MRT calculation through use of a function within the SolarCal library, imported from the Ladybug Tools Python software development kit (SDK). The specific function to address is the "Ladybug-comfort Solarcal Shortwave_from_horiz_solar" function. The SolarCal function can be imported in Grasshopper through a GHPython component (figure 6.10) and requires

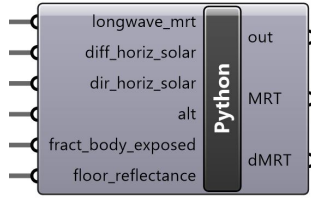


Figure 6.10: Python component for MRT calculation via the Ladybug-comfort.solarcal.shortwave_from_horiz_solar function

input as listed in table 6.4 to calculate MRT [53]. Figure 6.11 presents an overview of the overall MRT calculation.

Table 6.4: Input parameters for MRT calculation via Ladybug_comfort.solarcal.shortwave_from_horiz_solar function. Retrieved from [53]

Parameter	Required input	Unit
longwave_mrt	The longwave mean radiant temperature (MRT)	°C
diff_horiz_solar	Diffuse horizontal solar irradiance (result from a Radiance study)	W/m ²
dir_horiz_solar	Direct horizontal solar irradiance (result from a Radiance study)	W/m ²
alt	The altitude of the sun	°
fract_exposed	A number between 0 and 1 representing the fraction of the body exposed to direct sunlight	
floor_reflectance	A number between 0 and 1 that represents the reflectance of the floor	

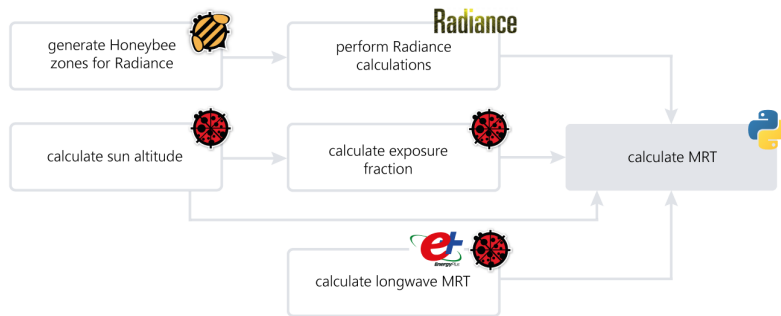


Figure 6.11: Flow chart of the MRT calculation procedure using Radiance for radiation inputs

The **longwave MRT** calculation in this method is similar to the longwave MRT calculation in the Honeybee Legacy Microclimate Map component. However, whereas the longwave MRT calculation in the Microclimate Map method is programmed into the Python script of the component, for this calculation method, longwave MRT calculation is deconstructed from the final MRT calculation. Building surface temperatures, view factors and the longwave sky temperature are calculated using the same simulation engines and equations. Subsequently, longwave MRT is calculated through the "Ladybug MRT calculator" component, which performs the calculation of equation 6.5 (figure 6.12).

The **diffuse- and direct solar horizontal irradiance** received in all grid-points are calculated using the external simulation engine Radiance [30]. In MRT calculation, the ray-tracing capabilities of Radiance are used to calculate directly received irradiance, irradiance received upon scattering in the atmosphere and irradiance received indirectly via reflection by surrounding geometry. For calculation of received irradiance, a model containing the building- and ground geometry, including information on reflectance of used materials, is created. An upward sensor grid is added for calculation of both diffuse- and direct received irradiance. The diffuse irradiance is calculated by subtracting the direct irradiance from the total irradiance (figure 6.13). Note that the diffuse irradiance contains both diffusely reflected irradiance by particles in the atmosphere and reflected irradiance by surrounding

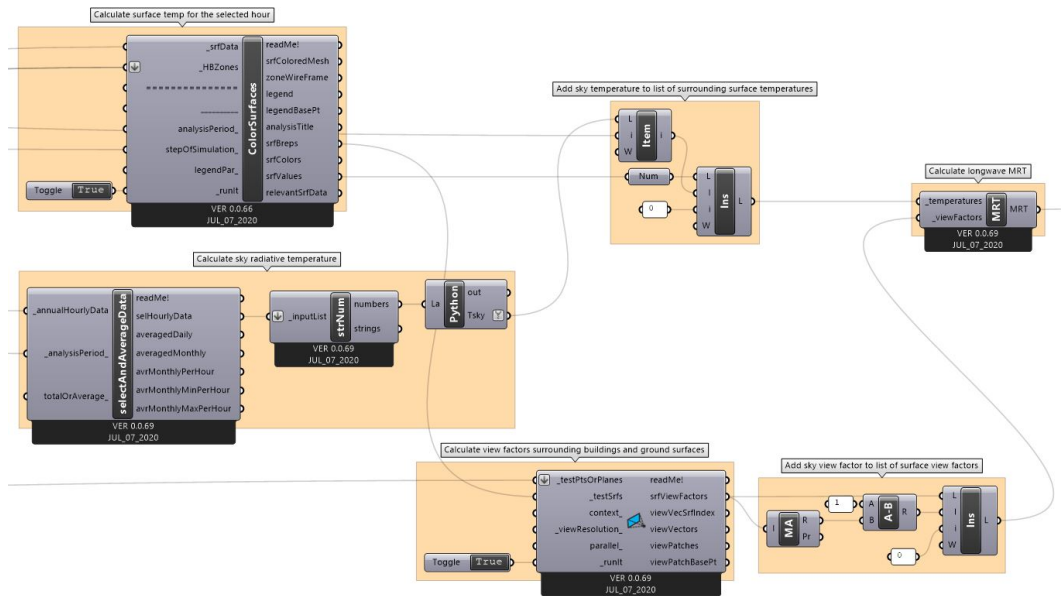


Figure 6.12: An overview of the longwave MRT calculation workflow

geometry. By increasing the number of ambient bounces (ab) of the Radiance calculation, an increasing number of bounces of the radiation rays by particles in the sky and surrounding objects are considered. Note that increasing the number of ambient bounces significantly affects calculation time. Ground-reflected irradiance is accounted for through the **floor reflectance** input, which is set to a number between 0 and 1, representing the ground albedo.

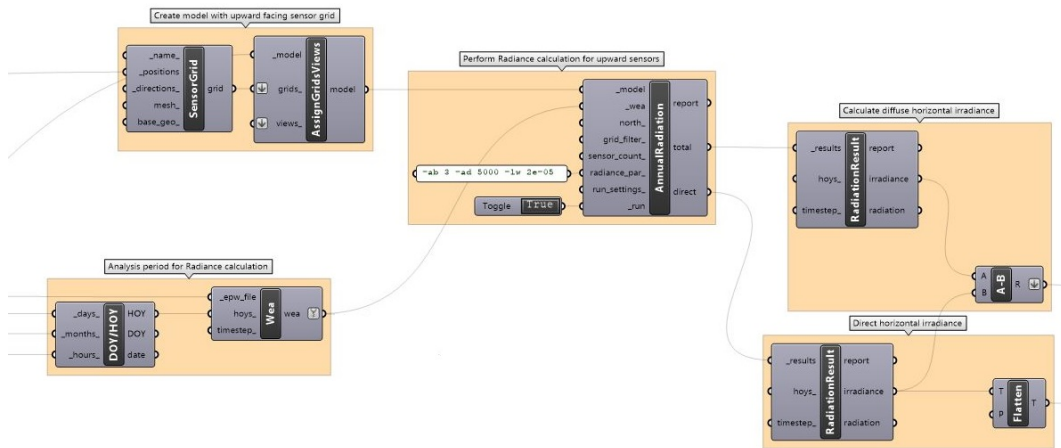


Figure 6.13: Radiance workflow

The sun **altitude** is received from the "Ladybug Sunpath" component. This component is also used for calculation of the **fraction of body exposed to sunlight**. This latter input parameter takes either a value of 0 (when the center point of the body is located in a shaded area) or 1 (when the center point of the body is exposed to direct sunlight). The sun vectors of the Ladybug Sunpath component are used to draw the shadow outline of buildings cast onto the analysis plane. Dependent on whether an analysis point is located within the shadow outline or not, either the value 0 or 1 is attributed to the point through a script written in Python (figure 6.14, appendix D).

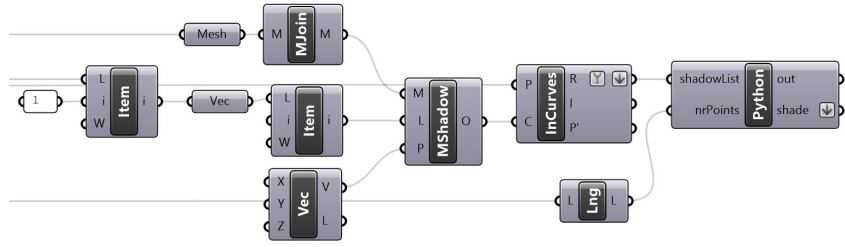


Figure 6.14: Calculation of fraction of body exposed to sunlight

A comparative study between the two described methods for calculation of MRT is described in the next section. In the next paragraph, the method that uses the original Honeybee Legacy Microclimate Map component is referred to as the original MRT method, and the method that uses Radiance for its irradiance input calculation is referred to as the Radiance-based method.

6.3.4 Comparison of both calculation methods

The Microclimate Map- and Radiance method are compared for an urban canyon building typology (figure 6.15). The urban canyon has street length of 40 [m] and street width of 12 [m]. The street is enclosed by 2-storey buildings on either side. The buildings have brick facades and the street is constructed using concrete. A window-to-wall ratio (WWR) of 0.4 is applied. The comparative study is performed for this geometry as this is the geometry that will be studied further for answering research questions 2.a - 2.c in the parametric study in section IV.

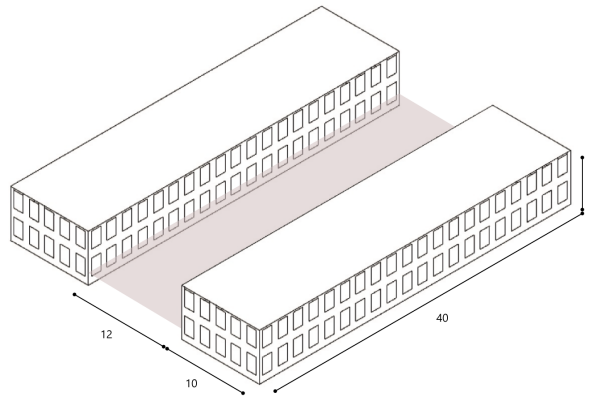


Figure 6.15: The urban canyon for comparison of MRT calculation methods

The MRT values for both methods have been compared on a warm summer day over a time interval in the afternoon (13.00 - 17.00) (figure 6.16). These time steps have been chosen as they are representative for the warmest hours of the day, for which the PET evaluation study in section IV will be carried out. Since the calculation of longwave MRT is the same for both methods, any differences in MRT are the result of differences in shortwave MRT only. From figure 6.16 and 6.17, it appears that the Radiance method results in a moderately larger MRT within the urban canyon. This is reasonable, as with application of Radiance in the MRT calculation workflow, any additional reflected shortwave irradiance is considered as well, which results in a larger MRT. Considering the congruent and sensible results of the Radiance method

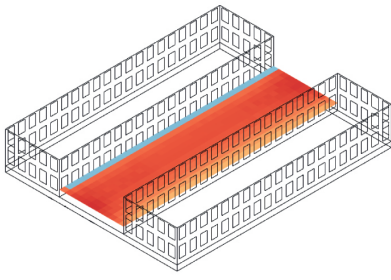
as compared to the Microclimate Map method, the Radiance method will be used for research into design heat mitigation measures. In the next section, validation of the Radiance method for application in PET Calculation is discussed.

6.3.5 Validation of MRT calculation

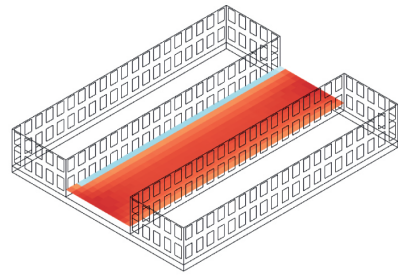
A disadvantage of implementing the novel Radiance-based MRT calculation method is the absence of validation of the calculation procedure in literature. As opposed to the Radiance-based method for MRT calculation, the original Ladybug Tools MRT calculation method has been reviewed in literature, albeit to a limited extent. The original calculation procedure is based on indoor MRT calculations, which have been altered for outdoor use. While these indoor MRT calculations have been confirmed to be accurate [7], the alteration of the MRT calculation into the original calculation procedure, and subsequent application of the original method for outdoor use appears to be less accurate: Substantial differences between MRT simulated by the original MRT method in Grasshopper and MRT field measurements are observed [71, 28, 21]. The reported differences commonly go up to to 6 °C, with Elwy et al. [21] reporting outlier differences of up to 20 °C. Other studies have attempted to validate the original calculation method with MRT simulation by ENVI-met. While some studies show good agreement between both simulation methods [39], others show significant differences [21, 70]. Depending on urban geometry, time of day and year and geographic location, some studies show over-estimation of MRT by the original MRT calculation method, whereas others show under-estimation. Due to the limited amount of comparative studies as well as incongruity between study results, it is not possible to draw firm conclusions on the accuracy of the Ladybug Tools original MRT calculation method. Since temporal and spatial variation between simulated MRT, ENVI-met simulated MRT and field measurements are comparable, the original Ladybug Tools MRT calculation method is considered to be sufficiently accurate for MRT estimation in the early design stage. However uncertainties related to precise MRT magnitude should be considered carefully when interpreting the results of PET calculation.

Since the original MRT calculation method is considered sufficiently accurate, the Radiance-based method for MRT is considered sufficiently accurate accordingly: The differences between the original MRT simulation and Radiance-based simulation are marginal compared to the differences between various calculation software and observed field measurements. Besides, the Radiance-based method, which performs a more accurate irradiance calculation, is considered an improvement in comparison with the original calculation, as in literature, inaccuracies in the original Ladybug Tools calculation method are often attributed to inaccurate calculation of received irradiance [28].

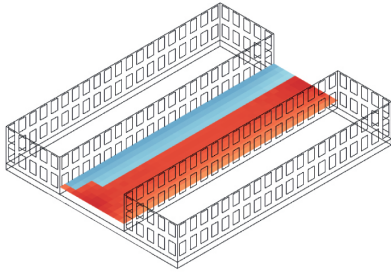
The correct implementation of irradiance in the Grasshopper workflow is validated through a sense-check: For a simple urban geometry (a singular building in an open field (figure 6.18)) the effect of increasing facade albedo on diffuse irradiance values at 1.2-m height is discussed. The check is performed at noon, and from the distribution of diffuse irradiance received over the analysis area (figure 6.19), one can clearly see the expected decrease in received irradiance in the shaded section of the analysis area (on the north side of the building). Considering low albedo values (0 - 0.4), lower irradiance values close to the building occur on the sun-facing side as well. This effect is most vividly pronounced for zero albedo facades. From these



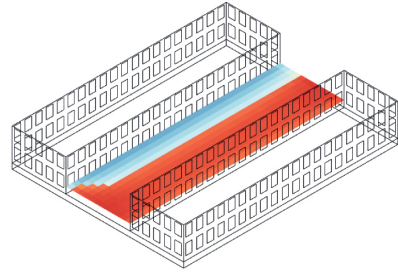
(a) MRT 13.00: Microclimate Map



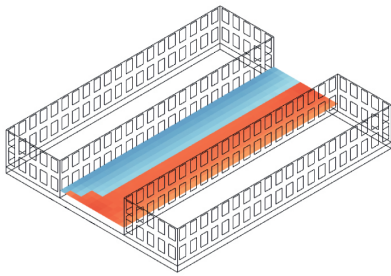
(b) MRT 13.00: Radiance



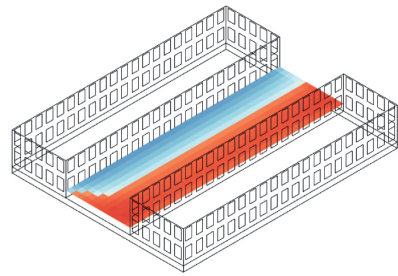
(c) MRT 14.00: Microclimate Map



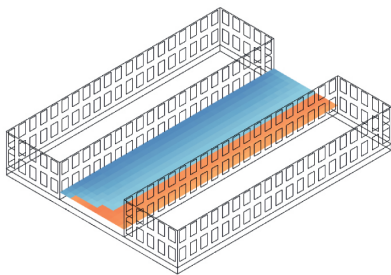
(d) MRT 14.00: Radiance



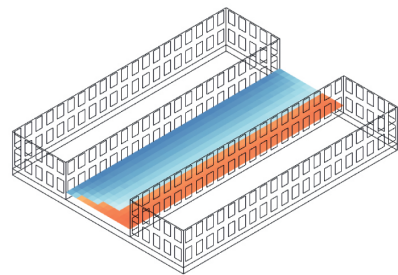
(e) MRT 15.00: Microclimate Map



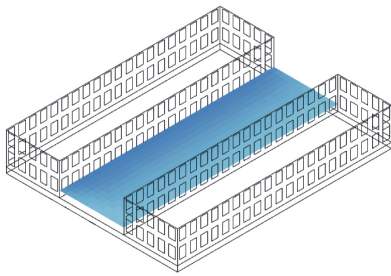
(f) MRT 15.00: Radiance



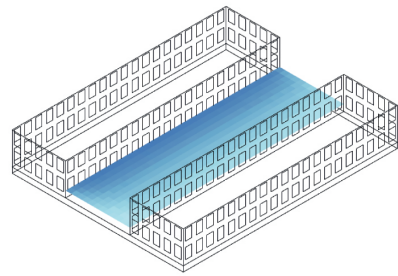
(g) MRT 16.00: Microclimate Map



(h) MRT 16.00: Radiance



(i) MRT 17.00: Microclimate Map



(j) MRT 17.00: Radiance

Figure 6.16: MRT comparison for Microclimate Map- and Radiance method for different times of day (afternoon)

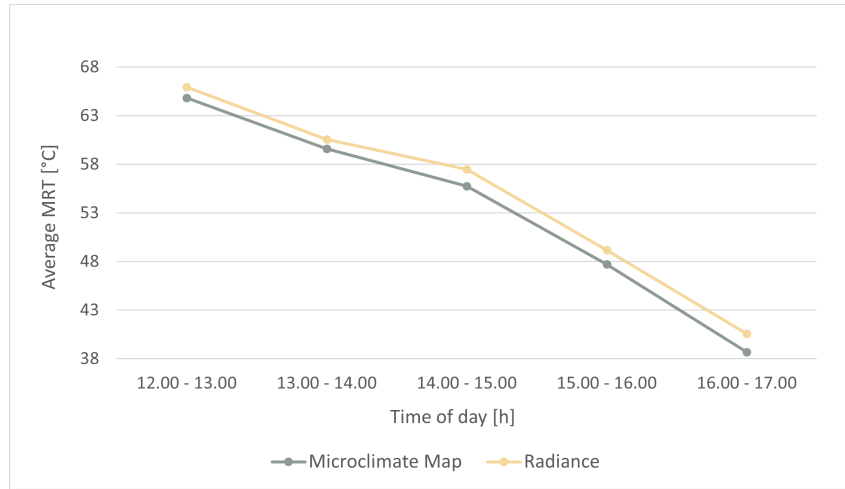


Figure 6.17: The urban canyon for comparison of MRT calculation methods

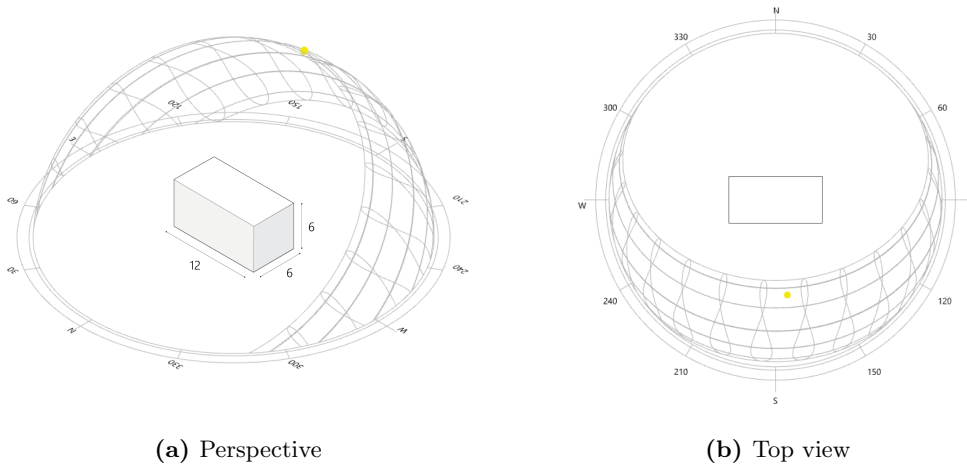


Figure 6.18: Urban geometry for Radiance sense-check

figures one can derive that, for low albedo situations, diffusely reflected irradiance by particles in the sky hemisphere is governing over diffusely reflected irradiance by building surfaces. In close proximity to either side of the building, one is sheltered by the building: Part of the diffusely reflected irradiance within the sky hemisphere is blocked, resulting in less received irradiance when standing close to the building. Further away from the building, spatial distribution of received irradiance becomes equal as the sheltering effects of the building fade away. At a facade albedo of 0.6 a turning point is seen: On the south-side of the building, the received irradiance becomes larger than the irradiance received in the open field (at the edges of the analysis area). Now, it appears that diffusely reflected irradiance by the facade has considerable impact: For increasing facade reflectance, increased amounts of diffuse irradiance are received when standing close to the building. From albedo 0.6 or higher, the effect of reduced irradiance close to the building facades due to the 'sheltering effect' of buildings is thus cancelled out by increased reflectance by building facades.

The temporal and spatial patterns of irradiance distribution obtained through Radiance calculation are thus in line with what's expected: Impact of shading patterns is clearly visible and increased facade albedo leads to an increase in diffusely reflected irradiance in close proximity to the reflecting surfaces. From these results, the irra-

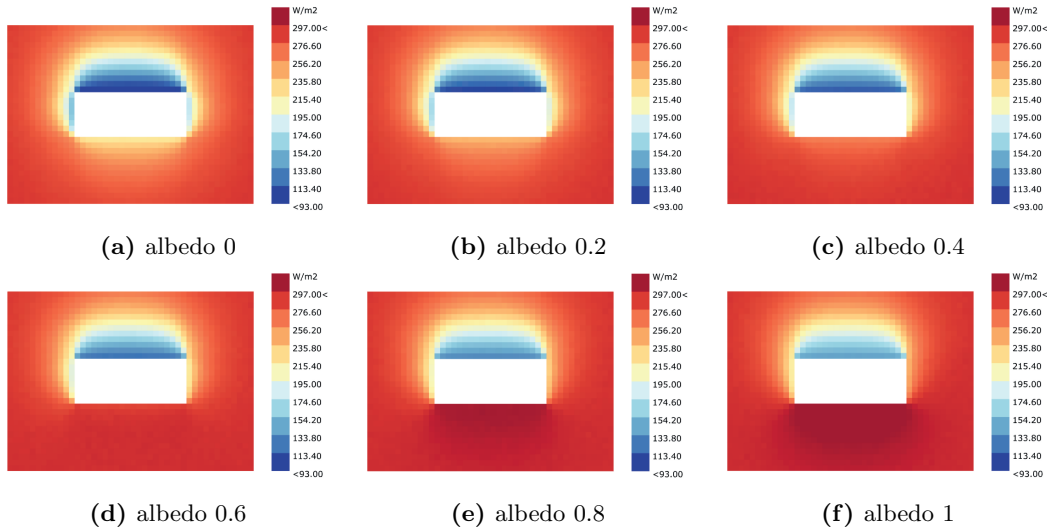


Figure 6.19: Diffuse irradiance received at 1.2 [m] height for varying facade albedo at 12.00 (top view of analysis area)

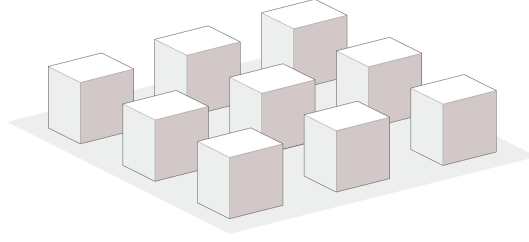
diance calculation appears to have been implemented correctly in the Grasshopper workflow.

6.4 Urban relative humidity calculation

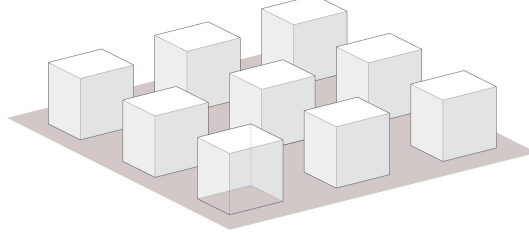
The transformation of rural relative humidity values to urban relative humidity values has been omitted: Hourly rural values will be used as input data for PET calculation. The decision to omit the transformation of rural relative humidity to an urban equivalent is based on the relative insignificance of differences between rural and urban values. Weather data from both rural and urban weather stations has demonstrated that relative humidity values vary up to 4 % only between rural and urban environments during daytime in the summer months, with the severity of reduction in relative humidity in urban environments dependent on both increased air temperatures as well as decreased vegetated land cover (reduced evapotranspiration) [54, 33]. Consequently, the neglect of reduced urban relative humidity in PET calculation is considered acceptable as the reduction rates are generally low.

6.5 Urban wind speed calculation

Accurate simulation of highly spatially- and temporally variable local wind speed patterns through CFD simulations is omitted in the PET calculation model for multiple reasons: Most importantly, the enormous time-savings achieved by omitting CFD simulations are beneficial for overall PET calculation time, which is desirable for PET evaluation in the early design stage. Additionally, in the early design stage, detailed information regarding complex local wind patterns is not required. One is rather interested in large scale effects of building density on average wind speeds. A final argument for wind speed simplification is the application of the model for situations of extreme heat, in which wind speeds are generally very low and thus of little importance in thermal comfort calculation.



(a) Frontal surface area (oriented towards the wind direction) A_f



(b) Underlying surface area A_d

Figure 6.20: Constituents of frontal area density λ calculation

A suitable model for detecting the large-scale effects of urban massing on the wind speed profile is that of MacDonald, developed in 1999 [58]. In accordance with wind-tunnel data for arrays of cubes, MacDonald's method describes how the general logarithmic wind-profile (equation 6.9, table 6.5) is altered by the urban environment below the atmospheric roughness sublayer (RSL)ⁱⁱ.

$$u(z) = \frac{u^*}{k} \ln\left(\frac{z-d}{z_0}\right) \quad (6.9)$$

The departure of measured wind tunnel data from the logarithmic wind profile is shown in figure 6.21. Within the urban canopy layer (UCL), the wind profile takes the shape of an exponential profile (equation 6.10, table 6.5), with 'a' equal to 9.6λ , where λ refers to the frontal area density (equation 6.12, figure 6.20). From equation 6.10, one can derive that geometric characteristics of the urban area (λ and H) determine the shape of the exponential profile, and thus determine the rate of wind speed reduction in urban areas.

In the upper part of the RSL, the exponential profile is transitioned to the logarithmic profile as exemplified in equation 6.13 (table 6.5). Thus, within three different height intervals, three different wind profiles are governing (figure 6.21).

$$u(z) = u_H \exp\left(a\left(\frac{z}{H} - 1\right)\right) \quad (6.10)$$

$$a = 9.6\lambda \quad (6.11)$$

$$\lambda_f = \frac{A_f}{A_d} \quad (6.12)$$

ⁱⁱThe RSL typically extends up to a height of 2-3 times the average building height.

Table 6.5: Parameters for wind calculation

Parameter		Parameter	
Parameter wind profile interpolation	A	Frontal area density	λ_f
Underlying surface area cubes	A_d	Friction velocity	u^*
Frontal area (towards wind) cubes	A_f	Wind speed at height z	$u(z)$
Parameter wind profile interpolation	B	Wind speed at cube height	u_H
displacement height	d	Considered height	z
Cube height	H	Roughness length	z_0
von Kármán constant (= 0.4)	k	Top of the RSL	z_w

$$u(z) = \frac{u^*}{B} \ln\left(\frac{A + Bz}{A + BH}\right) + u_H \quad (6.13)$$

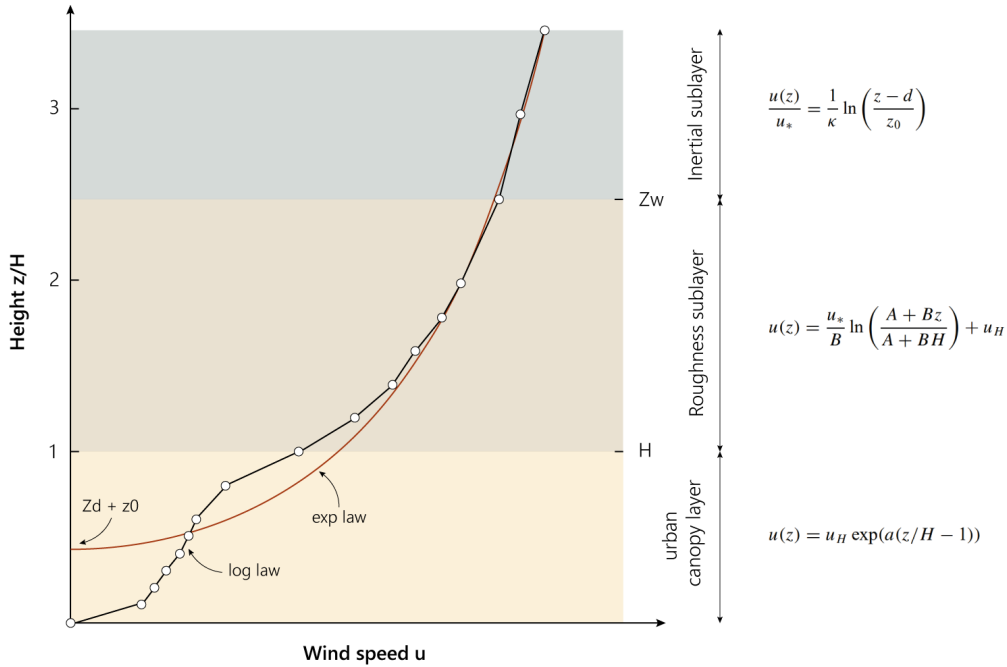


Figure 6.21: afbeelding. Adapted from [75]

The MacDonald method as described above, has been adapted by Koopmans et al. [51] for the development of PET heat maps of real urban environments with highly in-homogeneous spatial characteristics. As the adapted calculation method describes an approach for application of the MacDonald method in real urban environments, the latter calculation method is used as a starting point for wind speed calculation in the PET model. The calculation steps as presented in [51] have been somewhat modified for application in the Grasshopper environment. The calculation steps for calculating urban wind speeds at 1.2 [m] as used in the Grasshopper PET model are displayed below.

1. Begin with a normalized wind speed of 1 [m/s] at 10 [m] height, describing wind speeds as measured at rural reference stations. In step 12, this normalized wind speed will be translated to the actual wind speed.

2. Transform the normalized wind speed to a height of 60 [m] in accordance with the logarithmic law: $u_{60} = 1.3084 u_{10}$
3. For each point in space for which wind speeds are calculated: Determine the average building- and tree height (H) weighted to their footprint (A) (equation 6.14) within a 280x140 [m] source area (figure 6.22) surrounding the calculation point. If rural wind speeds (measured at 10 [m] height) are below 1.5 [m/s], a 175x175 [m] source area should be used.

$$H_{avg} = \frac{H_{building,i}A_{building,i} + H_{tree,j}A_{tree,j}}{\sum A_{building,i} + \sum A_{tree,j}} \quad (6.14)$$

4. Calculate the frontal areas perpendicular to the prevailing wind direction of both buildings and trees ($A_{frontal}$). To obtain the frontal area density (λ): Divide the total frontal area of both buildings and trees within the considered source area by the appropriate source surface area ($A_{source\ area}$) (equation 6.15 and 6.16).

$$\lambda_{buildings} = A_{frontal\ buildings} / A_{source\ area} \quad (6.15)$$

$$\lambda_{trees} = A_{frontal\ trees} / A_{source\ area} \quad (6.16)$$

5. The total frontal area density (λ_{tot}) is determined by equation 6.17. The relative impact of frontal area density for trees (λ_{trees}) on wind speed reduction is lower than the impact for buildings ($\lambda_{buildings}$), as trees are more porous than buildings.

$$\lambda_{tot} = 0.6\lambda_{buildings} + 0.3\lambda_{trees} + 0.015 \quad (6.17)$$

6. The parameters A, B, d, z_w and z_0 required for calculation with the modified wind speed profile by MacDonald [58] can be drawn from table 6.6.
7. The MacDonald wind-profile modification is applied only when the total frontal area density exceeds a threshold value (equation 6.18). If this condition is not satisfied, the urban area is assumed to have similar geometric characteristics as rural area and the general logarithmic law is used for calculation of wind speeds at 1.2 [m] height: Transform the wind speed data from a reference station (at 10 [m] height) to wind speed at 1.2 [m] height using equation 6.19.

$$0.6\lambda_{buildings} + 0.3\lambda_{trees} > \frac{25}{A_{source\ area}} \quad (6.18)$$

$$u_{1.2} = 0.6350u_{10,reference\ station} \quad (6.19)$$

8. Determine the wind speed at height of the RSL (u_{zw}).

$$u_{zw} = u_{60} \frac{\ln\left(\frac{z_w-d}{z_0}\right)}{\ln\left(\frac{60-d}{z_0}\right)} \quad (6.20)$$

9. Determine the friction velocity (u^*).

$$u^* = 0.4 \frac{u_{60}}{\ln\left(\frac{60-d}{z_0}\right)} \quad (6.21)$$

Table 6.6: Values for d , z_w , z_0 , A and B dependent on geometric properties λ_{tot} and H_{avg} [51]

λ_{tot}	d/H	z_w/H	z_0/H	A/H	B
<0.08	0.066	2	0.048	-0.35	0.56
0.08 - 0.135	0.26	2.5	0.071	-0.35	0.50
0.135 - 0.18	0.32	2.7	0.084	-0.34	0.48
0.18 - 0.265	0.42	1.5	0.08	-0.56	0.66
>0.265	0.57	1.2	0.077	-0.85	0.92

10. Determine the wind speed at average building height (u_H).

$$u_H = \frac{-u^*}{B} \ln\left(\frac{A + Bz_w}{A + BH}\right) + u_{zw} \quad (6.22)$$

11. Determine the (still normalized) wind speed at 1.2 [m] height

$$u_{1.2} = u_H \exp\left(9.6\lambda\left(\frac{1.2}{H} - 1\right)\right) \quad (6.23)$$

12. Calculate the actual hourly urban wind speed at 1.2 [m] height by multiplying the normalized wind speed at 1.2 [m] height (which is the wind speed at 1.2 [m] height when a 1 [m/s] wind speed at 10 [m] height is considered) with hourly wind speed data (at 10 [m] height) from the rural reference station (FF_{10}) and some empirically determined scaling factors (equation 6.24).

$$u_{1.2,scaled} = FF_{10}((u_{1.2} - 0.0796)0.9175 + 0.1254) \quad (6.24)$$

The proposed calculation method for wind speed provides insight into the effects of urban massing on reduced wind speed by considering both average height (H_{avg}) and building density (λ_{tot}) in close proximity (within source area) to the spatial point of interest. This method is therefore suitable for the detection of large-scale urban massing effects on urban wind speed reduction. As the PET model calculates PET on a 1-m grid of points in space, the urban wind speed on 1-m intervals should be determined. It is, however, unnecessary to perform the calculation steps as presented above on a 1-m interval, as shifting the source area by 1-m is unlikely to result in significantly different results (urban massing within two source areas over 1-m apart is approximately the same). As the only goal is to detect large scale urban massing differences that may affect urban wind speeds, the grid points for wind calculation may be shifted over 35-m intervals for improved calculation efficiency. Subsequently, wind speeds at a 1-m grid for PET calculation can be acquired by cubic interpolation. The use of 35-m intervals is in accordance with the calculation accuracy for the PET heat maps [51]

6.5.1 Implementation of wind speed calculation in PET model Grasshopper

The calculation steps as presented in the previous section have been implemented and automated in Grasshopper through generation of a component written in Python (consult appendix D for the Python script) (figure 6.23). The calculation requires

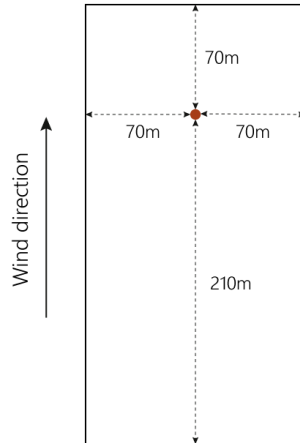


Figure 6.22: Source area for wind speed calculations

three meteorological input parameters: ruralU, hourly_windDir, all_windDir, and geometric input parameters: HW_totFootprint, HW_allFootprint, HW_allHeight, HW_frontalArea, LW_totFootprint, LW_allFootprint, LW_allHeight, LW_frontalArea (table 6.7).

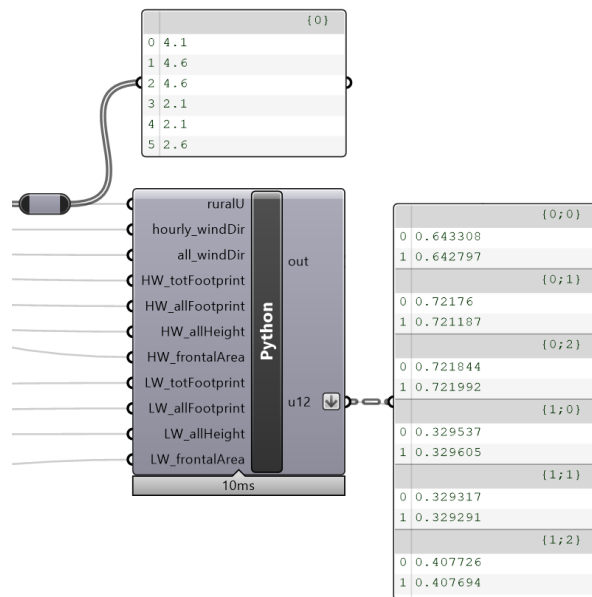


Figure 6.23: Python component for wind speed calculation

Table 6.7: Input parameters for wind speed calculation Python component

Input Parameter	Required input
ruralU	Rural hourly wind speed at 10 [m] height in [m/s]
hourly_windDir	Hourly prevailing wind direction (N, NE, E, SE, S, SW, W, NW)

continued on following page

all_windDir	A list of all angles for source area rotation corresponding to the eight potential wind directions (0, 0.25π , 0.5π , 0.75π , π , 1.25π , 1.5π , 1.75π [rad])
HW_totFootprint	Total footprint of all buildings within the source area for high wind situations in [m^2] for all potential wind directions
HW_allFootprint	Individual footprints of all buildings within the source area for high wind situations in [m^2] for all potential wind directions
HW_allHeight	Individual heights of all buildings within the source area for high wind situations in [m] for all potential wind directions
HW_frontalArea	Total frontal area of all buildings within the source area for high wind situations in [m^2] for all potential wind directions
LW_totFootprint	Total footprint of all buildings within the source area for low wind situations in [m^2] for all potential wind
LW_allFootprint	Individual footprints of all buildings within the source area for low wind situations in [m^2] for all potential wind directions
LW_allHeight	Individual heights of all buildings within the source area for high wind situations in [m] for all potential wind directions
LW_frontalArea	Total frontal area of all buildings within the source area for high wind situations in [m^2] for all potential wind directions

Both ruralU and hourly_windDir can be obtained from an .epw weather file containing weather data from a rural reference station. All_windDir is a list of integers corresponding to all potential wind directions considered for calculation. The default of considered wind directions has been set to eight, where 0 = North, 1 = North-East etc. The geometric input data for both high wind- and low wind situations is gathered from the "Ladybug Separate By Normal" component which allows for the selection of surfaces of any imported geometries. As the procedures for gathering geometric input data for low wind- and high wind speed situations are similar (only the source area over which geometry data is considered differs), solely the high wind speed procedure will be described in further detail.

The "Ladybug Separate By Normal" component is used to select the individual footprints, roofs, and facades of all imported geometry. After which all footprints, roofs, and facades that are located within the source area are selected by the "Point in Brep component". Subsequently, the area's corresponding to the selected surfaces are calculated.

6.5.2 Validation wind speed calculation

The wind speed calculation method is obtained from wind-tunnel measurements. With the wind-tunnel data, the equations to modify the log wind profile in urban areas have been verified [58]. The main question for validation of the wind speed calculation is therefore not related to the 'correctness' of the modified wind profile, but to the suitability for application in PET-analysis: Is the method sufficiently accurate for PET calculation in the early design stage? In the introduction to this chapter, it has been argued that the wind speed calculation is considered sufficiently accurate, due to the purpose of the PET model (to provide insight in PET in the early design stage for warm summer days). The use of the same wind speed calculation in the standardized PET-maps provides another argument for acceptable application in the PET model: If the wind speed calculation is considered sufficiently accurate for the PET control tool, the calculation should be considered sufficiently accurate for the developed design tool as well.

Correct implementation of the calculation in Python is validated through a sense-check: For varying frontal area density (λ) average wind speeds are calculated at 1.2 [m] height. These wind speeds are compared to the rural value as measured at the weather station (figure 6.24). As the results are sensible, increasing λ results in decreased average wind speed, the calculation method appears to be implemented correctly in Grasshopper.

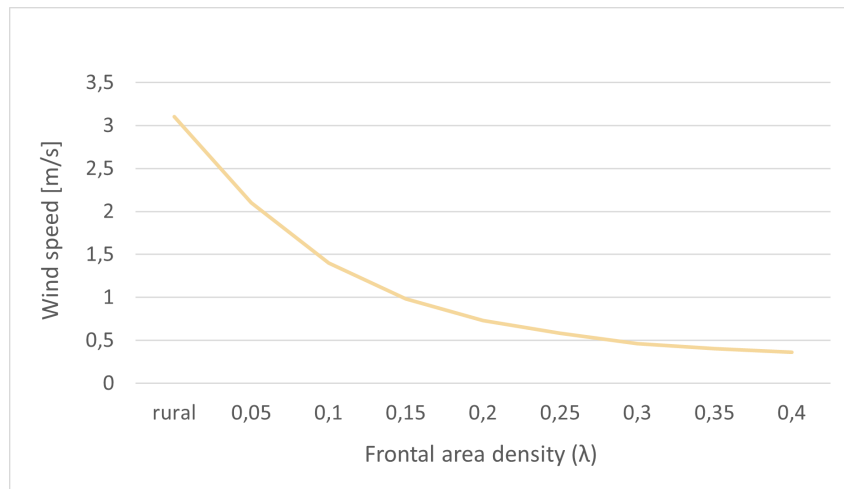


Figure 6.24: correct implementation wind speed validation

6.6 Calculation efficiency optimisation

Calculation cost is limited by careful consideration of the fastest calculation order and avoiding the use of pre-programmed components with large computation time. Additionally, the script is programmed to be 'smart': through python code, the script is capable of choosing the fastest calculation path and disconnect any non-used calculation paths. This 'fastest calculation path' determination feature is implemented for both the air temperature- and wind speed calculations. For demonstration purposes, only the implementation of the feature for air temperature calculation is discussed. Fastest calculation path selection works in a similar way for the calculation of wind speed and is demonstrated in appendix D.

Urban air temperature calculation is dependent on wind direction. In the developed PET model, 8 wind directions are considered. When the number of hours of analysis exceeds 8, it is considered more convenient to first calculate the urban air temperature increase for the 8 wind directions, and then match the results for the 8 default directions with the results of the actual occurring wind directions for each hour of analysis (in order to prevent re-calculation of air temperature for the same wind directions for a number of analysis hours). When the number of analysis hours is lower than 8, however, it is more computationally efficient to calculate air temperature for the considered hours of analysis only. A first condition for fastest calculation is thus the number of analysis hours considered. An additional condition for fastest calculation path is whether situations of low wind (rural wind speed at 10 [m] height ≤ 1.5) are considered or not. In situations of low wind, an additional calculation for the squared source area is required, which may be omitted in situations where all rural wind speeds measured at the reference station are larger than 1.5 [m/s]. Through the Python code in appendix D, the GHPython component in figure 6.25 regulates which calculation paths should be considered. Depending on the considered number of analysis hours, and whether for one (or more) of these hours a rural wind speed lower than/equal to 1.5 [m/s] has been measured, the component outputs either the command 'True' or 'False'. The command True or False regulates whether a calculation path is enabled (True) or disabled (False). For the example situation in figure 6.25 two analysis hours are considered, of which one has a measured wind speed lower than 1.5 [m/s]. The calculation path for number of hours ≥ 8 ('larger') is thus disabled through the command False and the calculation path for number of hours < 8 ('smaller') is enabled. Both the calculation paths that combine 'smaller' with high wind (HW) and low wind (LW) are enabled as one of the wind inputs has a value that is smaller than 1.5 [m/s].

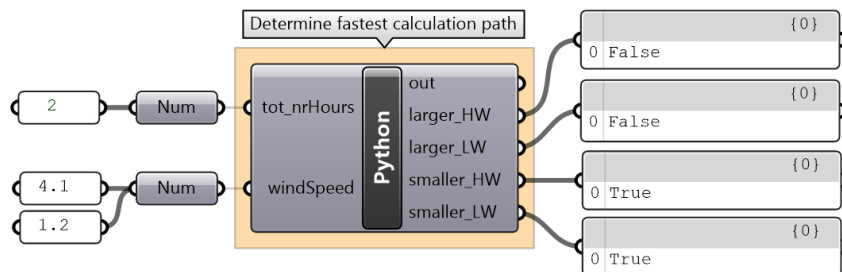


Figure 6.25: Determination of the fastest calculation path for air temperature calculation through Python

6.7 Validation

Throughout this chapter, validation of the individual calculations for rural-urban modification of the meteorological parameters has been discussed. The accuracy of the modification methods as obtained from literature is considered sufficient for application in the early design stage. Additionally, correct implementation of each method in Grasshopper has been validated through the performance of sense-checks.

In addition to the air temperature-, MRT-, relative humidity- and wind speed calculations, the Ladybug PET calculation component is considered to perform an accurate PET calculation [17]. Including the PET calculation component, all indi-

vidual calculation components of the PET model have thus been validated. It must be noted, however, that validation of the individual calculation components of the PET model does not automatically lead to validation of the PET model in its totality: While the individual deviations from reality are within an acceptable range, the sum of deviation from reality for all individual components may potentially lead to unacceptable deviation of simulated PET from PET field measurements. Here, the comparison between the Grasshopper PET model and field measurements is deliberately emphasized. As MRT and PET simulations performed by established simulation software (ENVI-met, Rayman, etc.) often distinctively differ from on-site measurements, comparing the Grasshopper PET model with these simulation software would not provide accurate information on the actual performance of the PET model. PET field measurements are a highly complex and time consuming. Due to time constraints, validation of the PET model in its totality is a subject for future research.

The absence of validation of the total model, however, does not have large implications for the usefulness of the model: While the accuracy of exact magnitude of calculated PET values will be uncertain, spatial and temporal patterns of PET distribution will be reasonably accurate due to the more detailed MRT calculation. In the early design stage, accurate spatial and temporal variation is more important than computation of precise values, since the goal of running the model in the early design stage is to provide insight into relative differences between various design options: The model should be able to show which design option performs better than others. As long as the distribution of PET is accurate, the precise PET values do not need to reach 100 percent accuracy.

Part IV

A parametric study into building-related heat mitigation strategies

Chapter 7

Research description

The PET calculation model for the early design stage as presented in section III provides urban designers with a means to quickly assess outdoor thermal comfort on the urban-block scale for multiple design variants. In addition to a rapid PET calculation tool, urban designers would greatly benefit from knowing certain rules of thumb for 'heat-proof' design. The aim of this parametric study into building-related (grey) heat mitigation strategies is to provide urban designers with basic knowledge on the efficiency of selected building-related heat mitigation strategies.

In response to the second research question, section IV ("A parametric study into building-related heat mitigation strategies") presents a study into the effect of varying H/W ratio, street orientation and facade albedo of an urban canyon on outdoor thermal comfort. In the first paragraph, the research question and sub-questions to be answered are repeated. The second paragraph presents the applied methods for answering of the research questions. Hypotheses corresponding to the research questions are drafted in the third paragraph.

7.1 Research questions

The main research question (research question 2) addressed in this section reads as follows:

How effective are the building-related heat mitigation measures identified by Kluck et al. [49] (H/W ratio, street orientation and facade albedo) in providing outdoor thermal comfort during extreme heat events in the Netherlands?

Answering of the main research question is structured according to three sub-questions:

- 2.a]** What is the individual heat mitigation effectiveness for varying the selected heat mitigation measures?
- 2.b]** How is the individual heat mitigation effectiveness of each selected heat mitigation measure affected by varying the other two heat mitigation measures? (i.e. does a dependency between the heat mitigation measures occur?)

2.c] Which combination of input values for the selected heat mitigation measures results in minimum- and maximum outdoor thermal comfort?

Note that 'effectiveness' in the research question is defined as the heat mitigation potential of a certain design measure, or in other words, the difference between maximum- and minimum average PET when varying the considered design measure between two extremes.

7.2 Methods

7.2.1 Data collection

PET data for varying H/W ratio, street orientation and façade albedo is generated using the PET model as developed in section III. With this model, PET data is calculated for a default study area and a selected analysis period and corresponding weather data. This paragraph presents the selected study area, analysis period and weather data as well as the procedure for calculation of PET.

Study area

The effect of changing H/W ratio, street orientation and façade albedo is evaluated for a representative urban form in the Netherlands: the linear urban form, or 'urban canyon' (figure 7.1) [94]. Within the urban canyon, PET is calculated at 1.2 [m] height above street level for analysis points on a 1 [m] grid.

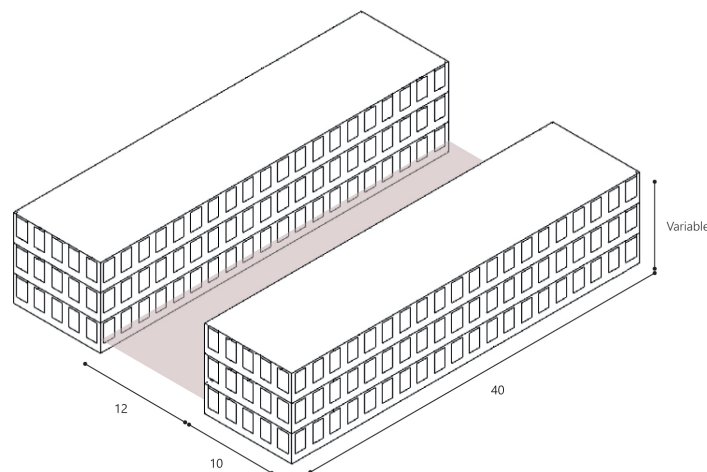


Figure 7.1: Perspective view of an example urban block with coloured analysis area. For PET calculation, the analysis area is subdivided in a 1-m grid of test points.

The variables to be evaluated for this urban canyon are varied as presented in table 7.1. The desired H/W ratio for analysis is obtained by varying the height of the flanking buildings, whilst keeping the street width fixed. Street orientation is varied

Table 7.1: Considered input for variable parameters of the parametric study

H/W ratio	1.0	0.75	0.5
Street orientation	North	North-East	East South-East
Facade albedo	Untreated facades (0.3)	White-painted facades (0.8)	

by rotating in steps of 0.25π [rad]. The cardinal directions in table 7.2 indicate the orientation of the street: North-East (NE) street orientation, for example, means the street is oriented towards the North-East rather than the facades (figure 7.2). Variation in albedo is subdivided into either the facade being painted white (albedo = 0.8) or left untreated (albedo = 0.3).

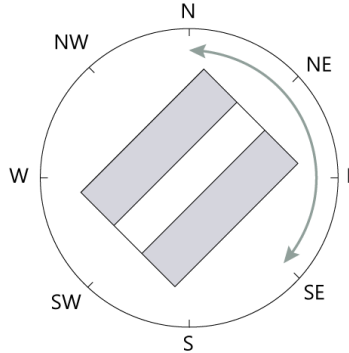


Figure 7.2: Street orientations (top view)

Besides H/W ratio, street orientation and facade albedo, the model requires additional input parameters for calculation of PET in the urban canyon (table 7.2). These parameters are kept constant throughout the analysis. The second column of table 7.2 presents the default settings for these constant parameters.

Table 7.2: Default settings for PET calculation

Design measure	Default setting
Facade albedo	<i>Variable</i>
Facade material	Brick facade
Ground material	Concrete
H/W ratio street	<i>Variable</i>
Street orientation	<i>Variable</i>
Surrounding urban environment	Representative theoretic urban area
Window-to-wall ratio (WWR)	0.4

The window-to-wall ratio (WWR) is set to 0.4, a suitable WWR for energy efficiency and sufficient daylight entrance [4]. The urban canyon is surrounded by a theoretic urban environment: For the purpose of minimizing the effects of non-uniform urban characteristics in different directions of the study area, a theoretical study area with more or less identical urban characteristics in different directions has been created. Both the building plan fraction ($\lambda_B = 0.25$), providing a measure for urban density by describing the plan area fraction of ground covered by buildings, and average height ($H_{avg} = 12$ [m]) of buildings have been adapted to average

values for Amsterdam, a representative Dutch city [19]. Randomized generation of building height, building footprint and building rotation ensures more or less equal distribution of buildings with differing heights, footprints and rotation over the surrounding study area (figure 7.3).

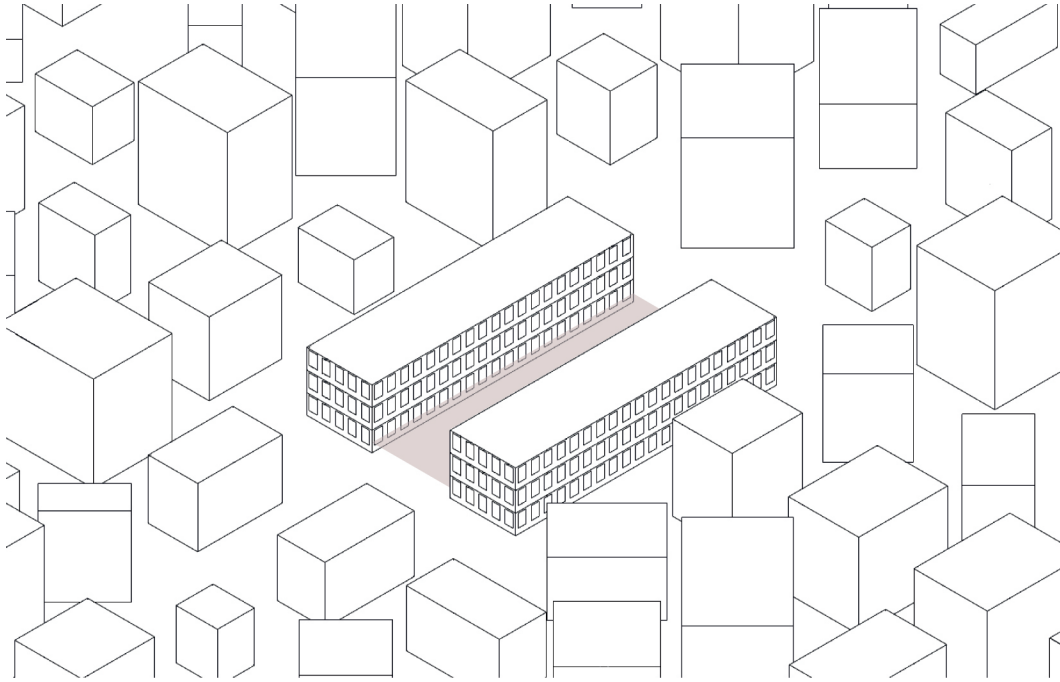


Figure 7.3: Theoretical study area set up

Analysis period and rural weather data

The objective of this study is to assess the performance of design measures for heat mitigation during extreme heat events. The analysis period for study should therefore reflect situations of above-average heat in the Netherlands: For analysis, rural weather data of a representative summer day with above average air temperatures, below average wind speeds and sunny conditions is gathered from the Amsterdam Schiphol airport weather station. Hourly values for rural air temperatures, wind speeds and sky cover conditions are displayed in table 7.3.

Only the afternoon hours (12.00 – 18.00) of the representative summer day are considered for analysis as these represent the warmest hours of the day, and heat mitigation is thus most urgent within this time-frame. An additional argument for PET assessment within this time frame, is that the PET standardized heat map uses the same time frame for PET assessment. Alignment of the control tool (PET maps) and design tool (Grasshopper PET calculation model) is desired as it facilitates comparison.

PET calculation procedure

With the constant input parameters set to their default value, PET will be calculated for varying H/W ratio, street orientation and facade albedo. Using the “Ladybug Fly Component”, the PET calculation is performed for all possible input combinations, after which the results are written to an excel file for analysis. In the paragraph

Table 7.3: Hourly values for air temperature (in [°C]), wind speed (in [m/s] at 10 [m] height) and sky cover (1 equals 1/10 covered, 10 equals total coverage)

Hour	Air temperature	Wind speed	Sky cover
0	22.3	4.6	1
1	21.4	3.6	2
2	19.9	3.1	0
3	19.4	3.1	1
4	18.7	3.1	1
5	18.8	3.1	4
6	20.4	3.6	2
7	22	3.6	2
8	24.6	3.6	1
9	24.9	3.6	1
10	26.7	4.1	1
11	28.1	4.1	1
12	29.1	4.6	4
13	29.6	4.6	2
14	30	5.1	1
15	29.4	6.2	2
16	29.6	5.1	1
17	29.1	4.6	1
18	28	3.6	1
19	24.8	2.1	1
20	21.9	2.1	2
21	20.9	2.1	1
22	19.9	1.5	2
23	18.5	1.5	1

on data analysis below, the selection of results to be written to excel for further analysis is discussed. Furthermore, the strategy for data analysis is explained.

7.2.2 Data analysis

Method for PET evaluation

The four meteorological input parameters that constitute PET, as well as PET, will be saved for each iteration in calculation. Important to note is that PET may be assessed in numerous ways. One could for example calculate the average PET, maximum PET, minimum PET or the area percentage of exceedance of a certain PET value. Local maximum or minimum values of PET are considered of little interest, as these values do not provide insight into the overall PET over the entire analysis area. Both average PET and an area percentage of PET exceedance do take into account all PET values within the analysis area, and will therefore be considered.

For calculation of **Average PET**, PET is averaged both spatially and temporally. For each hour in the analysis period, the spatially averaged PET is calculated from all PET values for individual analysis points. Subsequently, the spatially averaged PET for all individual hours are averaged to obtain the PET value averaged both

spatially and temporally. While the average value for PET in the urban canyon provides insight into the numerical values of PET in the urban canyon, an averaged value provides little insight into distribution of PET over the canyon.

Area percentage of PET exceedance provides a little more insight into the PET distribution over the canyon: For each hour of the analysis period, the percentage of the study area for which a certain threshold PET value is exceeded is calculated. This threshold value is set to 41 /degree C, the temperature at which one experiences severe heat stress. Measuring PET through a 41 /degree C exceedance percentage provides more insight into which share of the analysis area is highly uncomfortable. The disadvantage of using a 41 /degree C exceedance percentage for PET analysis is that one does not receive any information on numerical PET values.

Since the main interest of this study is to evaluate the effect of varying H/W ratio, street orientation and facade albedo on numerical PET values, the study results will be evaluated for average PET. However, the 41 °exceedance percentage will be considered as well for a small comparative study.

Analysis software

The input and output data written to excel will be analysed using DesignExplorer, an interface for visual design analysis [17].

7.3 Hypotheses

Corresponding to the research questions, hypotheses for expected study outcome have been drafted.

7.3.1 Hypotheses corresponding to sub-question 2.a

Various studies show large effects of changing **H/W ratio** on PET within the urban canyon: depending on street geometry, time of day and year and geographic location, differences of 10 °C in PET for varying H/W ratio are not uncommon [96, 43, 6]. It must be noted, however, that these studies focus warm and dry climate zones that are not characteristic for the Dutch climate. However, as the study is performed for a warm summer day in the Netherlands, the effect of changing H/W ratio on PET in the urban canyon is expected to lead to similar results as seen in literature. The expected relationship between H/W ratio and PET in the urban canyon is negative: Increasing H/W ratio is expected to lead to decreased PET values.

In addition to H/W ratio, PET is largely affected by **street orientation**: Various studies show significant effects of street orientation on PET in warm and dry climates [96, 6]. From literature, the effects of varying street orientation on PET appear to be slightly lower than the effects of changing H/W ratio. Note, however, that a comparison of the effectiveness of both design measures is dependent on the considered H/W ratio's and street orientations as well as geographic location and time of analysis.

Taleghani et al. [94] have performed a study into the effects of changing street orientation for an urban canyon in the Netherlands. A combined model of ENVI-met and Rayman has been used to assess PET in an urban canyon on a warm summer day ($T_{max} = 33\text{ }^{\circ}\text{C}$) for both N-S and E-W street orientations. Considering an analysis period of 24 hours, the N-S street orientation is significantly cooler as it receives less sun throughout the day. Since the largest effect of changing street orientation on PET is a result of shading patterns, it is expected that different street orientations perform better for different times of day. The effect of street orientation on thermal comfort in the urban canyon is thus highly dependent on the analysis period. Considering an analysis interval consisting of the afternoon hours, NE - SW street orientations are expected to result in the largest average PET values, as these orientations are most consistently subjected to direct sunlight.

Increased **facade albedo** is known to mitigate UHI as it decreases outdoor air temperatures [27]. Application of ‘light’ facade materials is therefore often considered as a heat mitigation strategy. However, from a thermal comfort perspective, application of light facades should be considered carefully: An increased amount of reflected shortwave radiation received by pedestrians will result in higher radiation-related thermal discomfort [55]. While Salvati et al. [83] classify the overall effects of increased received shortwave irradiance on outdoor thermal comfort negligible and Shashua-Bar et al. [86] find a slightly negative relation between facade albedo and PET, most studies report a positive relation between increasing facade albedo and increasing PET [92, 55, 81, 85, 27]: These studies suggest that the effect of decreased air temperatures as a result of increased facade albedo is not sufficient to offset the increased received irradiance.

In the temperate climate of the Netherlands, an approximate $0.8\text{ }^{\circ}\text{C}$ increase in PET has been determined for every 0.1 increase in albedo [92]. For a similar German climate, an approximate 0.75 – 1.25 increase in PET for every 0.1 increase in albedo is seen, dependent on exposure of the facade to direct sunlight or not [55]. Note that, again, it is difficult to draw a general conclusion on the exact effect of varying facade albedo on PET valid in all situations, as the effect of facade albedo on PET is affected by urban morphology, weather conditions, analysis period (time of day and day of year) and geographic location.

7.3.2 Hypotheses corresponding to sub-question 2.b

The impact of H/W ratio is dependent on street orientation and vice versa as both impact PET by affecting shading patterns. The dependency between the two design measures is conditional to the position of the sun, and thus time of day and year and geographic location. Considering an analysis interval consisting of the afternoon hours, H/W ratio is expected to impact PET to a lesser extent for NE-SW street orientations than NW - SE orientations as obstruction of direct sunlight by NW - SE building orientation is larger during this time interval.

The relative impact of facade albedo on PET is expected to be dependent on H/W ratio and vice versa, since increased building height leads to a larger exposure to facade area within the canyon. Additionally, the impact of facade albedo on PET is expected to be dependent on street orientation and vice versa, as the exposure of facades to direct sunlight is dependent on street orientation.

7.3.3 Hypotheses corresponding to sub-question 2.c

From the individual effectiveness of heat mitigation measures as discussed in the previous paragraphs, the combination of H/W ratio 0.5, SE street orientation and untreated facades is expected to result in lowest average PET, while the combination of H/W ratio 1.0, NE street orientation and white-painted facades is expected to result in highest average PET.

Chapter 8

Results

The results to the parametric study are displayed on the next page. Figures 8.1, 8.2 and 8.3 show PET results for varying H/W ratio, street orientation and facade albedo respectively. Both average PET (Avg_PET) and 41 °C PET exceedance percentage (perc_PET) are displayed. In figure 8.1, H/W ratio 1.0 is indicated by the blue lines, H/W ratio 0.75 by the purple lines and H/W ratio 0.5 by the red lines. In figure 8.2, SE street orientation is displayed in blue, E orientation in dark purple, NE orientation in light purple and N orientation in red. In figure 8.3, white-painted facades (albedo 0.8) are represented by blue lines and untreated facades are represented (albedo 0.3) by red lines.

Figure 8.4 provides an overview of all considered configurations. From left to right, canyon configurations with increasing average PET values are displayed. Blue circles indicate a H/W ratio of 1, purple circles a H/W ratio of 0.75 and red circles a H/W ratio of 0.5. The street orientation of the urban canyons is displayed below each configuration.

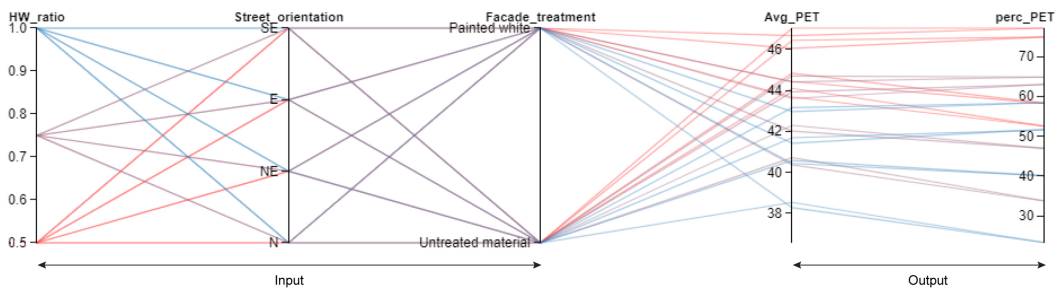


Figure 8.1: PET results for varying H/W ratio

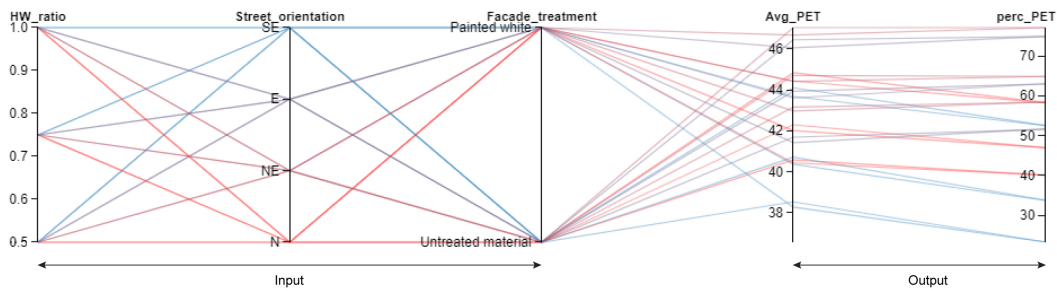


Figure 8.2: PET results for varying street orientation

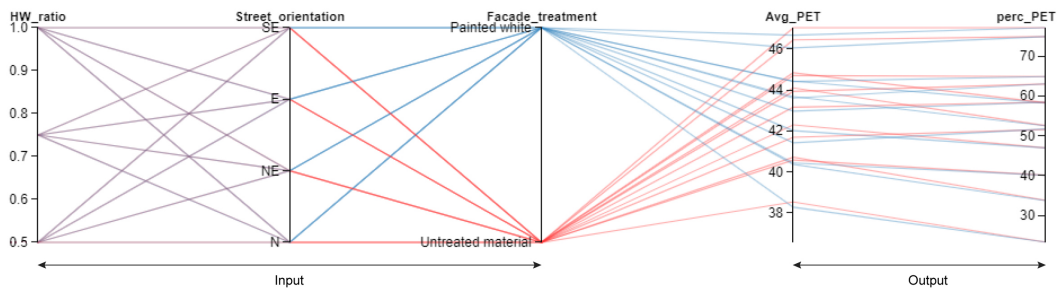


Figure 8.3: PET results for varying facade albedo

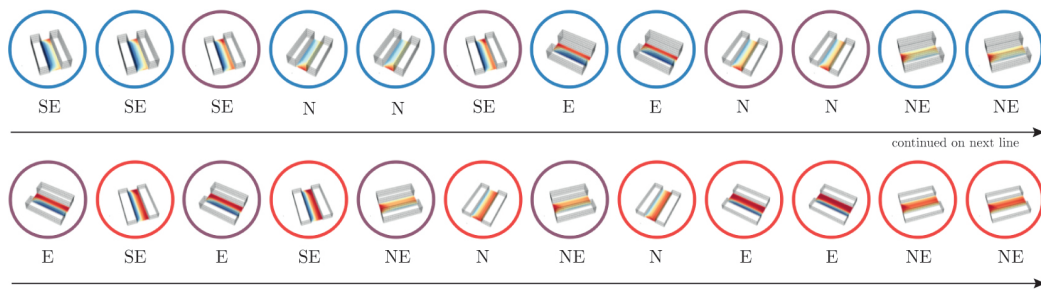


Figure 8.4: Overview of all considered urban configurations for increasing average PET values from upper left to lower right (continues on next line). Blue circles indicate a H/W ratio of 1.0, purple circles a H/W ratio of 0.75 and red circles a H/W ratio of 0.5.

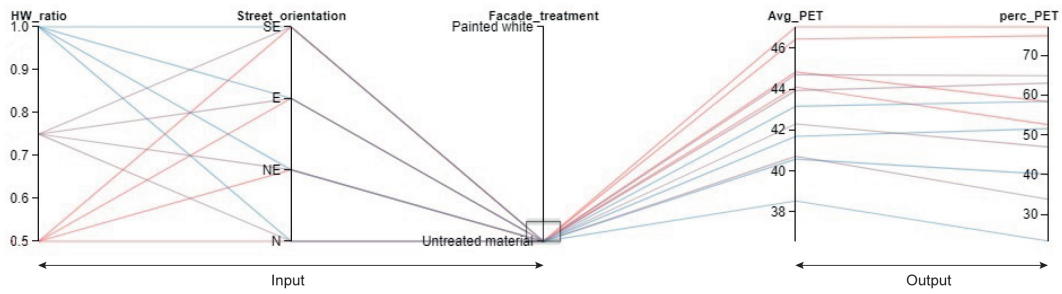
Chapter 9

Interim exploration and discussion of study results

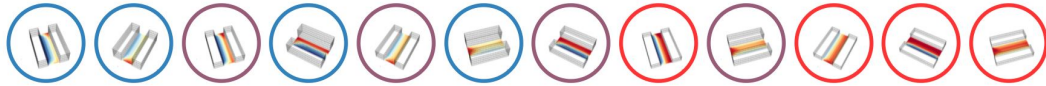
In this chapter, the study results as presented in chapter X are discussed. The heat mitigation effectiveness of H/W ratio, street orientation and facade albedo is assessed for average PET. The consequences of choosing for assessment of average PET rather than 41 °C PET exceedance percentage are explained in the first paragraph through a comparative study for both evaluation methods. Subsequently, the individual heat mitigation performance of H/W ratio, street orientation and facade albedo are discussed (research question 2.a). For each of these individual input parameters, the effect of the residual two input parameters on the heat mitigation effectiveness of the considered individual parameter is examined (research question 2.b). In the third paragraph, PET results of best- and worst performing urban configurations for heat mitigation (research question 2.c) are discussed. In this paragraph, the effects of chosen default settings for the urban surroundings, ground material and facade material on these average PET results are addressed. The conclusions to the parametric study are presented in chapter 11, section "Discussion, conclusion and future studies".

9.1 A comparison of PET evaluation methods for heat mitigation assessment

While spatially and temporally averaged PET results provide information on the average numerical value of PET in the urban canyon, 41 °C PET exceedance percentage provides information on the area percentage within the urban canyon that is highly uncomfortable. From figure 9.1, it is clearly shown that these PET evaluation methods do not necessarily result in similar assessment of best performing urban configurations for heat mitigation: From left to right, these figures rank urban configurations with increasing average PET (figure 9.1b) and increasing 41 °C PET exceedance percentage (figure 9.1c). Comparing these two figures, it is apparent that the ranking of best- to worst performing urban configurations from left to right differs depending on the PET evaluation method chosen for assessment. The difference in ranking of urban configurations for average PET and 41 °C PET exceedance percentage can be explained by taking a closer look at two particular urban configu-



(a) Considered combinations of input parameters in Design Explorer

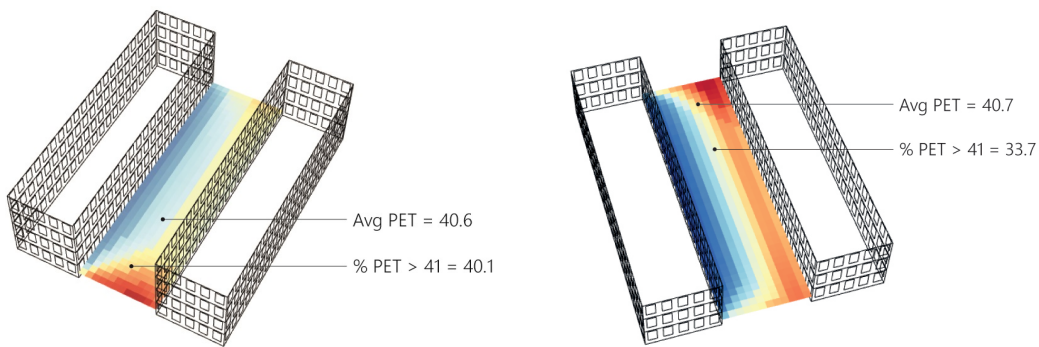


(b) Ranked by average PET



(c) Ranked by 41 °C PET exceedance

Figure 9.1: A comparison of best- to worst performing facades considering both average PET (b) and 41 °C PET exceedance percentage (c)



(a) H/W ratio 1.0 N street orientation

(b) H/W ratio 0.75 SE street orientation

Figure 9.2: A comparison of PET evaluation by average PET and 41 °C PET exceedance percentage for two urban canyons

rations: The combination of H/W ratio 1 & N street orientation and the combination of H/W ratio 0.75 a& SE street orientation (figure 9.2). The right canyon (H/W ratio 0.75 & SE) performs significantly better when considering the percentage of PET over 41, as one side of the canyon is shaded throughout most of the afternoon, whereas the left canyon (HW ratio 1 & N) has a more equally distributed PET pattern. However, since PET values in the non-shaded part of the right canyon reach relatively high values, this canyon performs (slightly) worse when considering average PET. The choice of PET evaluation method for heat mitigation assessment in urban planning should thus carefully be considered by urban designers.

9.2 Assessment of individual heat mitigation strategies and identification of interdependencies

9.2.1 H/W ratio heat mitigation performance

General assessment of individual performance H/W ratio

PET results for varying H/W ratio are presented in figure 8.1. From this figure it appears that increasing H/W ratio results in decreased average PET and vice versa. Whether the PET results will decrease further when increasing the H/W ratio above 1.0 is dependent on whether the maximum shading in the canyon has yet been achieved. The PET results are expected to reach a minimum threshold value when complete shading of the canyon is reached, however, from these results the pattern of average PET decrease for H/W ratios above 1.0 cannot be determined.

Effect of street orientation and facade albedo on H/W ratio heat mitigation effectiveness

The effect of varying street orientation and facade albedo on heat mitigation effectiveness¹ of H/W ratio is assessed by comparing the difference between maximum average PET (H/W ratio 0.5) and minimum average PET (H/W ratio 1.0) for all possible combinations of street orientation and facade albedo. Table 9.1 presents the differences in average PET between H/W ratio 0.5 (maximum PET) and H/W ratio 1.0 (minimum PET) that occur for varying street orientation and facade albedo.

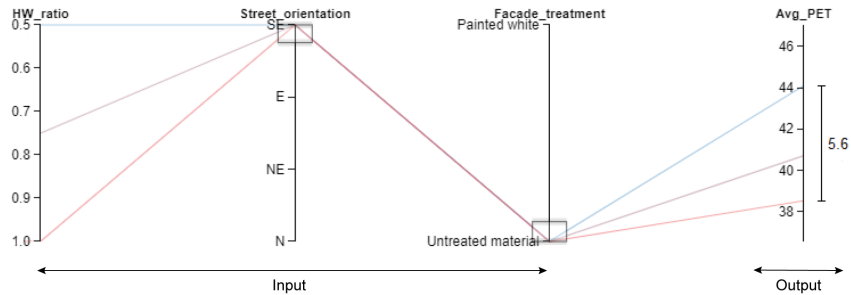
Table 9.1: Difference (in °C) between maximum average PET (H/W ratio 0.5) and minimum average PET (H/W ratio 1.0) for various combinations of street orientation and facade treatment

	Untreated	Painted white
SE	5.6	5.4
E	4.8	4.6
NE	3.9	3.7
N	4.2	4.0

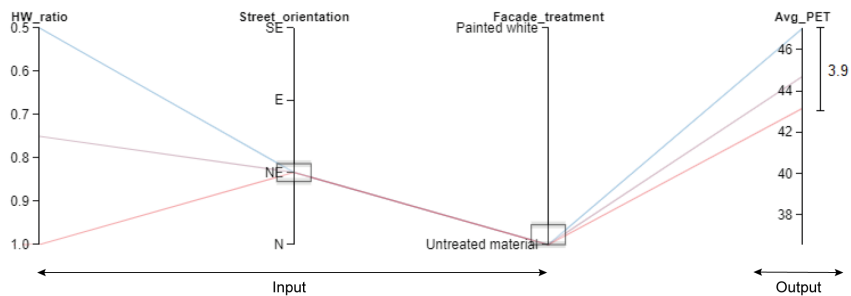
From table 9.1 it is shown that street orientation moderately affects the effectiveness of varying H/W ratio: For SE street orientations, H/W ratio-related differences in average PET are significantly larger than for NE street orientations (figure 9.3). Increasing H/W ratio for the purpose of heat mitigation thus seems more effective when applied to SE street configurations. However, With effectiveness defined as the heat mitigation potential of varying H/W ratio, or in other words the magnitude of difference between maximum- and minimum average PET corresponding to H/W ratio 0.5 and 1.0 respectively, this statement should be interpreted with some caution: Whilst increasing H/W ratio leads to the largest PET reduction for SE street orientations, the application of larger building height to streets with SE orientation is not necessarily a better design decision than application of larger building height to streets with other orientations: Since average PET in SE oriented streets appears

¹Note that effectiveness refers to the heat mitigation potential of varying H/W ratio, or in other words the difference between maximum- and minimum average PET as a result of varying between H/W ratio 0.5 and 1.0.

to be significantly lower than for other street orientations (figure 9.3), the need for heat mitigation in SE oriented streets is generally less critical than for other street orientations.



(a) Difference in average PET between H/W ratio 1.0 and 0.5 for SE street orientation and untreated facade material equals 5.6 °C



(b) Difference in average PET between H/W ratio 1.0 and 0.5 for NE street orientation and untreated facade material equals 3.9 °C

Figure 9.3: The effect of street orientation on heat mitigation effectiveness of H/W ratio. For demonstration purposes, the facade treatment has been kept constant.

Note that the maximum heat mitigation potential of 5.6 °C is somewhat lower than differences mentioned in literature (paragraph 7.3. This discrepancy may be caused by either differences in analysis period or differences in maximum building height considered.

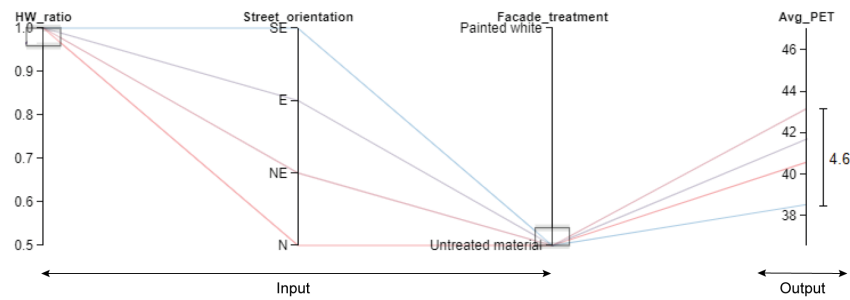
Average PET differences between H/W ratio 1.0 and H/W ratio 0.5 are marginally more pronounced for untreated facade material than for white-painted facades. However, as these differences are relatively small and the accuracy of the impact of facade albedo is open to debate (sub-paragraph 9.2.3), the effect of facade albedo on the effectiveness of varying H/W ratio is considered insignificant.

9.2.2 Street orientation heat mitigation performance

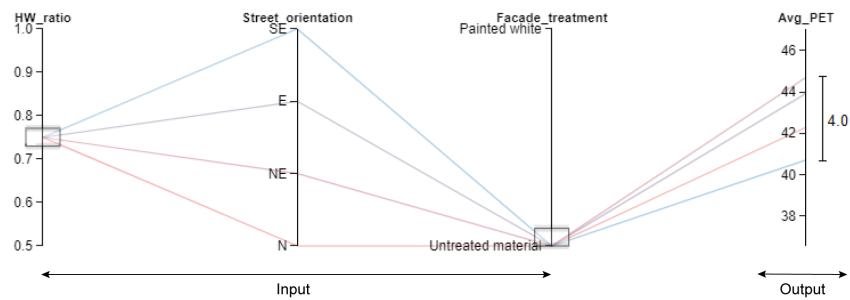
General assessment of individual performance street orientation

The effect of varying street orientation on PET values is shown in figure 8.2. Blue lines represent SE orientation, dark purple lines represent E orientation, light purple lines NE orientation and red lines N orientation. For demonstration purposes, figure 9.4a, 9.4b and 9.4c show PET results for varying street orientation considering a constant H/W ratio of 1.0, 0.75 and 0.5 respectively and constant untreated facade material. These figures show more clearly that, for each considered configuration, SE street orientations result in the lowest average PET, followed by N and E street orientations. NE street orientations lead to largest average PET values within the

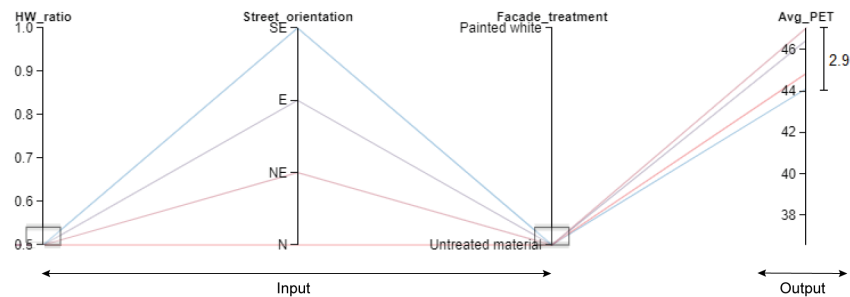
urban canyon. Note that, for demonstration clarity, only the PET results for untreated facade material are displayed here. For white-painted facades, similar results (same order of PET magnitude for varying street orientations) are measured.



(a) Difference in average PET between NE and SE street orientations for H/W ratio 1.0 (equals 4.6 °C)



(b) Difference in average PET between NE and SE street orientations for H/W ratio 0.75 (equals 4.0 °C)



(c) Difference in average PET between NE and SE street orientations for H/W ratio 0.5 (equals 2.9 °C)

Figure 9.4: The effect of H/W ratio on heat mitigation effectiveness of street orientation. For demonstration purposes, the facade treatment has been kept constant.

Effect of H/W ratio and facade albedo on street orientation heat mitigation effectiveness

The effect of varying H/W ratio and facade albedo on heat mitigation effectiveness of street orientation is assessed by comparing the difference between maximum average PET (NE street orientation) and minimum average PET (SE street orientation) for all possible combinations of street orientation and facade albedo. Table 9.2 presents the differences in average PET between NE street orientations (maximum PET) and SE street orientations (minimum PET) that occur for varying H/W ratio and facade albedo.

Table 9.2 shows that with increasing H/W ratio, the heat mitigation effectiveness of varying between best- and worst performing street orientations (SE and NE) in-

creases: For a larger H/W ratio, the difference between minimum- and maximum average PET values becomes larger. This effect is also clearly demonstrated in figure 9.4. Rotating street orientation from worst performing NE orientation to best performing SE orientation is thus most effective when larger H/W ratios are considered. These results are sensible as they correspond to the interdependency between H/W ratio and street orientation as discussed in the previous sub-paragraph: However, in this sub-paragraph the results are interpreted from a street orientation perspective instead of a H/W ratio perspective. Note that, due to the definition of effectiveness in this discussion, the statement regarding the effectiveness of varying street orientation for different H/W ratios should be interpreted with some caution: Whilst varying between worst performing (NE) and best performing (SE) street orientation leads to the largest PET reduction for a H/W ratio of 1.0, the overall effects are more critical for lower H/W ratios: For lower H/W ratios, larger average PET values are measured in the urban canyon, and varying street orientation for the purpose of heat mitigation could thus be considered more pressing.

Table 9.2: Difference between maximum average PET (NE street orientation) and minimum average PET (SE street orientation) for various combinations of H/W ratio and facade treatment

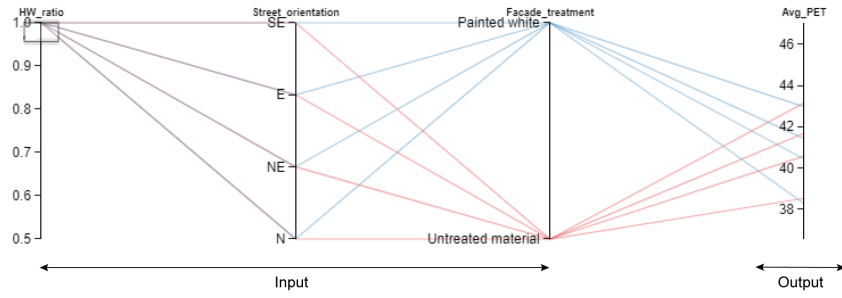
	Untreated	Painted white
H/W 1.0	4.6	4.7
H/W 0.75	4.0	4.1
H/W 0.5	2.9	3.0

For each H/W ratio, average PET differences between the best performing- and worst performing street orientation are marginally more pronounced for white painted facade material than for untreated facades. However, these differences are relatively small. Because of these small differences and an additional uncertainty regarding the accuracy of facade albedo consideration in the calculation (sub-paragraph 9.2.3), the effect of facade albedo on the effectiveness of varying street orientation is considered insignificant.

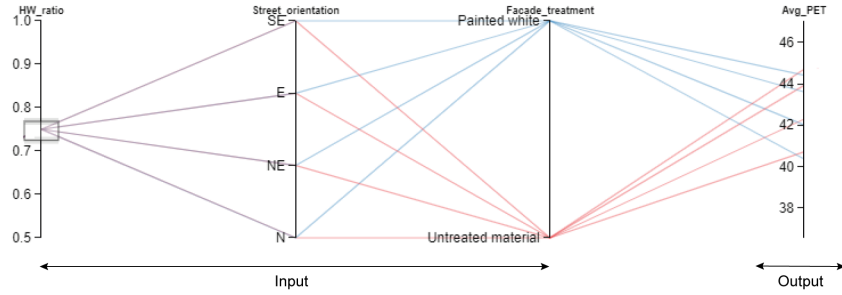
9.2.3 Facade albedo heat mitigation performance

General assessment of individual performance facade albedo

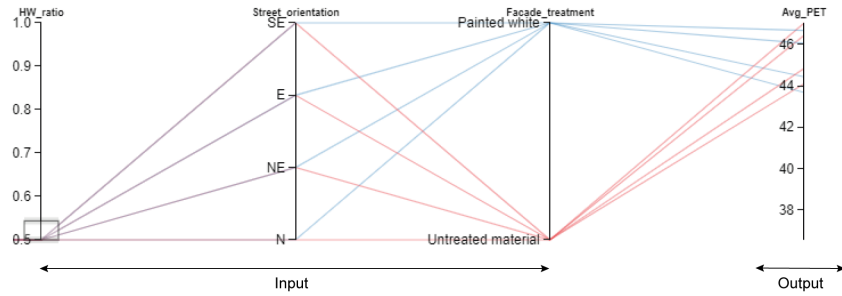
In figure 8.3, the impact of facade albedo on PET is shown. The blue lines show PET results for white-painted facades (albedo = 0.8) and the red lines show PET results for untreated facades (albedo = 0.3). For clear demonstration of the heat mitigation effect of facade albedo, figure 9.5 shows the PET results for varying facade treatment decomposed for individual H/W ratio. This figure shows that for each combination of H/W ratio and street orientation, untreated facades result in slightly higher average PET values than white-painted facades. These results contradict the study expectations as formed in paragraph 7.3.1. To explain these results, the PET calculation for varying facade albedo is assessed in greater detail. Since the results are similar for each urban configuration (untreated facades result in higher average PET than white-painted facades for each possible combination of input parameters) it is sufficient to perform this analysis for one combination of H/W ratio and street orientation input only: A combination of H/W ratio 0.75 and N street orientation has randomly been selected for further analysis.



(a) Average PET differences for varying facade albedo for H/W ratio 1.0



(b) Average PET differences for varying facade albedo for H/W ratio 0.75



(c) Average PET differences for varying facade albedo for H/W ratio 0.5

Figure 9.5: Differences in average PET between untreated facades (red lines) and white painted facades (blue lines) for all possible combinations of H/W ratio and street orientation. For clarity of demonstration, the Design Explorer images have been displayed for individually selected H/W ratio.

Because varying facade albedo at a small scale does not affect wind speed and air temperature in the calculation model, the unexpected PET results can be explained by assessment of MRT only. For the selected urban canyon geometry, spatially averaged MRT is slightly lower for high albedo facades compared to low albedo facades (figure 9.6), which is in accordance with the lower average PET values for high facade albedo. Two major factors contribute to MRT: surface temperature of urban geometry (which affects MRT in the longwave spectrum) and received shortwave irradiance (either direct or diffuse). For the considered urban configuration, high albedo (white-painted) facades lead to lower longwave MRT within the urban canyon. However, high albedo facades simultaneously lead to a greater amount of diffuse shortwave irradiance receivedⁱⁱ, and thus higher shortwave MRT, within the urban canyon (figure 9.7). The lower longwave MRT for high albedo facades can be explained by differences in facade temperature for low- and high albedo facades (figure 9.8): Increased solar reflectance by the facade (high albedo), leads to lower warming of the facade, and thus lower surface temperatures. The larger diffuse irradiance for high albedo facades is a result of increased solar reflectance by the facade. While lower longwave MRT leads to lower MRT values, increased diffuse shortwave irradiance (and thus increased shortwave MRT) increases MRT values for

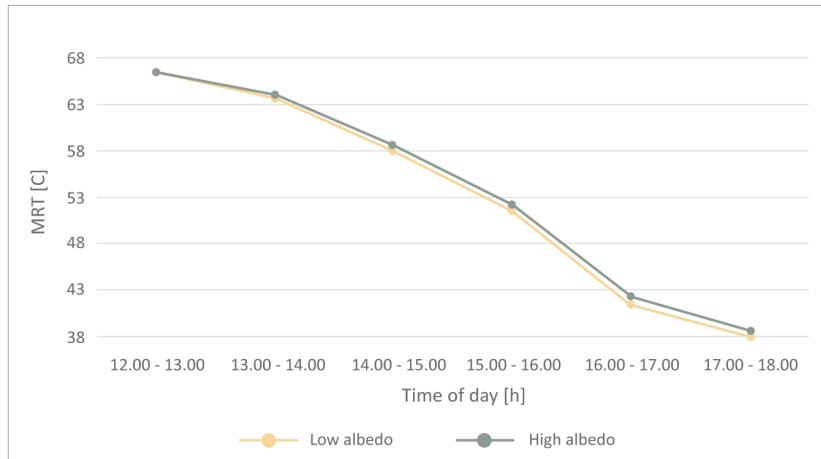


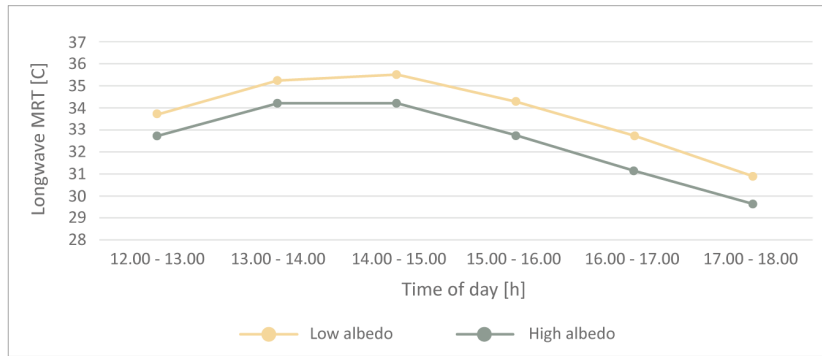
Figure 9.6: Spatially averaged MRT over all analysis hours for low albedo (0.3) and high albedo (0.8) facades

high albedo facades. As the total MRT for high albedo facades is lower than for low albedo facades, the effect of reduced surface temperature that comes with the application of high albedo facades thus outweighs the effect of increased diffuse solar irradiance.

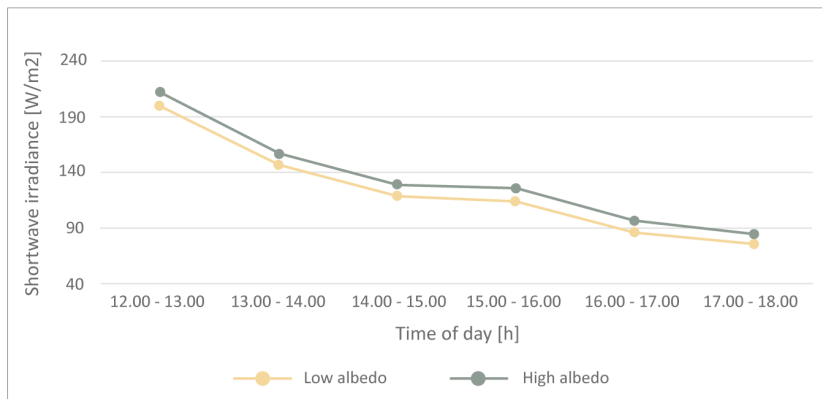
For all results generated in the parametric study, the effect of increasing albedo on surface temperatures is dominant over the effect of increasing albedo on received diffuse shortwave irradiance. However, the amount of reflected shortwave irradiance within the urban canyon is dependent on the number of bounces performed by Radiance. Varying the number of ambient bounces in the Radiance calculation may therefore affect the observed results. The parametric study has been performed for a default ambient bounces (ab) value of two. To assess the impact of increasing the number of ambient bounces, the results in figure 9.6 and 9.7, which have been calculated for two ambient bounces, are compared to results calculated for four ambient bounces (figure 9.9). In this graph, the original calculations, performed with 2 ambient bounces, are presented by the dotted lines. From this figure, the effect of increasing the number of bounces on the calculation results is evident: Since increasing the number of bounces increases the amount of diffuse irradiance received, increasing the number of bounces results in larger MRT for both the low albedo and high albedo scenario. However, the relative impact of increasing the number of bounces for high albedo facades is larger than for low albedo facades (figure 9.10). This difference is large enough to reverse the results that were obtained using two bounces in the calculation: For four bounces, the high albedo facade results in larger MRT compared to the low albedo facade. With longwave MRT left unaffected by changing the number of bounces, the effect of increasing albedo on received diffuse solar irradiance is now larger than the effect of increasing albedo on surface temperatures.

From this analysis, it is apparent that the Radiance number of bounces is a matter for discussion when using the PET analysis model. While a lower number of bounces significantly reduces calculation time, the number of bounces moderately affects the effect of facade albedo on PET. At the time of writing, it is unclear which value

ⁱⁱNote that consideration of diffuse shortwave irradiance only is sufficient, as received direct shortwave irradiance is dependent on geometric considerations which remain equal for varying facade albedo

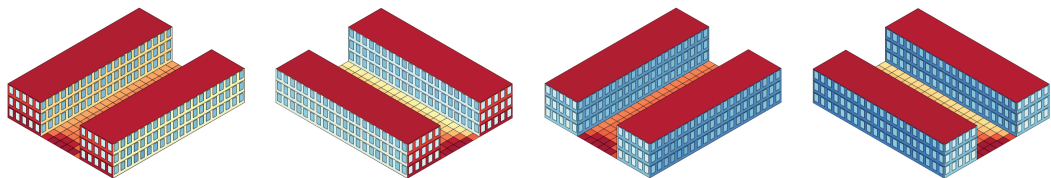


(a) Spatially averaged longwave MRT for the considered analysis hours



(b) Spatially averaged diffuse shortwave irradiance for the considered analysis hours

Figure 9.7: A comparison of spatially averaged longwave MRT in the urban canyon for low- and high albedo facades (a) and spatially averaged received diffuse shortwave irradiance (b)



(a) Low albedo SE perspective (b) Low albedo SW perspective (c) High albedo SE perspective (d) High albedo SW perspective

Figure 9.8: Temporally averaged facade surface temperatures for varying facade albedo

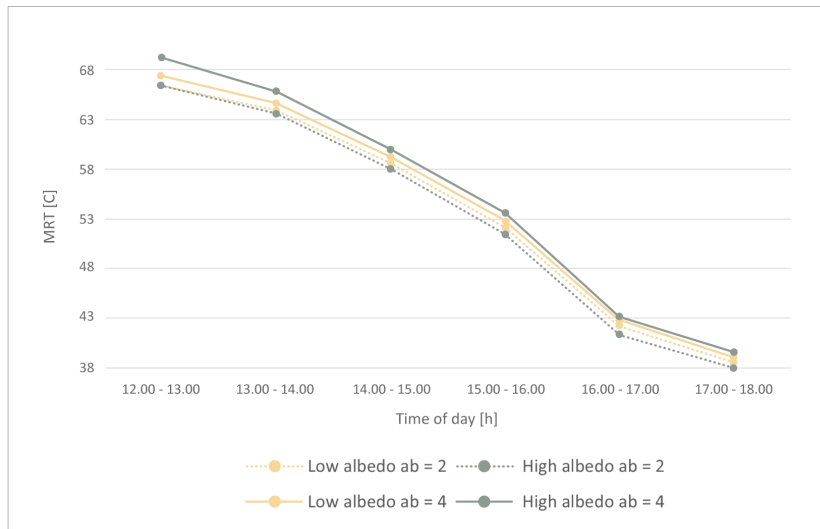


Figure 9.9: Spatially averaged MRT (longwave + shortwave) for low- and high albedo facades, considering two and four ambient bounces for calculation.

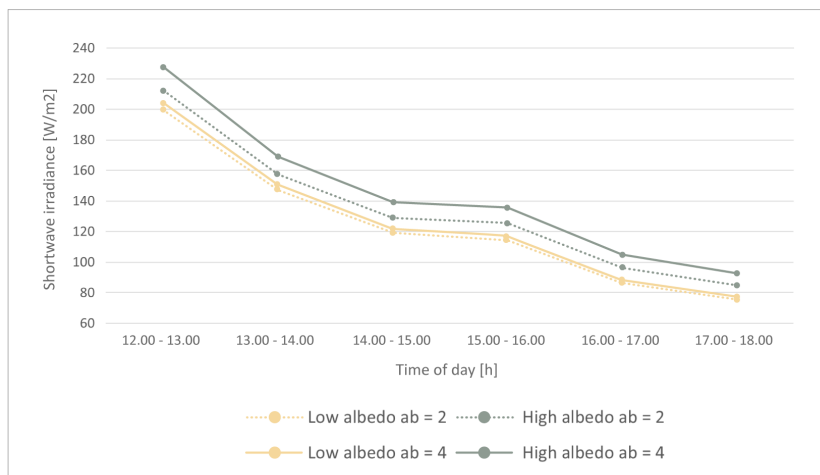


Figure 9.10: Spatially averaged diffuse shortwave irradiance received for low- and high albedo facades, considering two and four ambient bounces for calculation.

of ambient bounces results in a realistic display of reflected shortwave radiation as seen in reality. The number of bounces to be considered in the early design stage is thus open to discussion.

Effect of H/W ratio and street orientation on facade albedo heat mitigation effectiveness

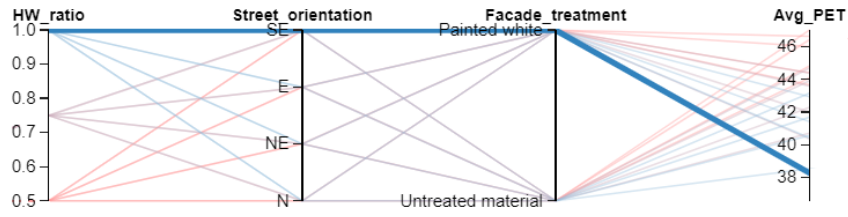
Since the effects of facade albedo as seen from the parametric study are marginal, and the correctness of their magnitude is debatable due to uncertainty about correct implementation of number of bounces in the Radiance calculation, no significant statement on the effect of H/W ratio and street orientation on facade albedo heat mitigation effectiveness can be presented.

9.3 Interpretation of numerical average PET results

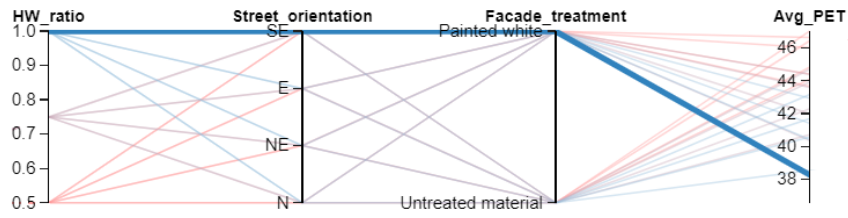
Figure 8.4 ranks all considered urban canyons according to their heat mitigation performance. From left to right, urban canyons with increasing average PET values are displayed. The blue circled canyons have a H/W ratio of 1.0, the purple circled canyons a H/W ratio of 0.75 and the red circled canyons a H/W ratio of 0.5. Below each canyon, the street orientation is displayed. As expected, a combination of H/W ratio 1.0 and SE street orientation results in the lowest average PET. Depending on the number of ambient bounces considered in the Radiance calculation, either the combination with an untreated facade ($ab = 4$) or the combination with a white painted facade ($ab = 2$) leads to lower average PET (figure 9.11). Considering $ab = 2$, the lowest spatially and temporally averaged PET value measured in the urban canyon equals $38.28\text{ }^{\circ}\text{C}$. Oppositely, a combination of NE street orientation and H/W ratio 0.5 results in highest average PET within the urban canyon. Again, the number of ambient bounces considered determines whether the combination with untreated facade material ($ab = 2$) or a white painted facade ($ab = 4$) leads to the highest average PET (figure 9.12). For calculation with two ambient bounces, the highest spatially and temporally averaged PET equals $47.04\text{ }^{\circ}\text{C}$

The exact numerical value, however, is not solely determined by the variable input parameters as studied: In addition to H/W ratio, street orientation and facade albedo, the input parameters kept constant in the parametric study (table 7.2) may affect the PET results. The effect of surrounding environment, facade material and ground material on PET results is explored through comparison of the default settings with alternative settingsⁱⁱⁱ. Since the nature of this sub-study is exploratory, the effect of surrounding environment, facade material and ground material is studied for one urban configuration with default settings as presented in table 9.3 only. For each studied input parameter, only the input for the parameter in question is varied, while all other parameters are kept constant to their default value. In the sub-paragraphs below, the results of the exploration into the effect of surrounding environment, facade material and ground material on PET results are presented. Consult appendix E for a more in-depth description of the exploratory study.

ⁱⁱⁱThe effect of WWR is left out of the scope of this exploration

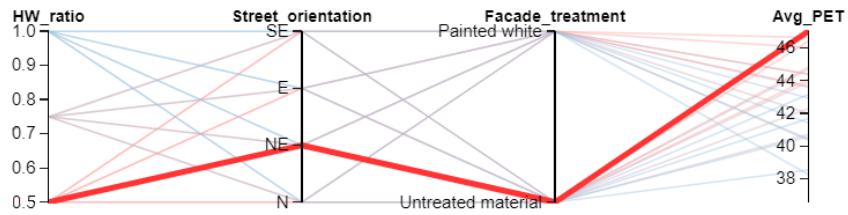


(a) H/W ratio 1.0, SE street orientation and white-painted facades

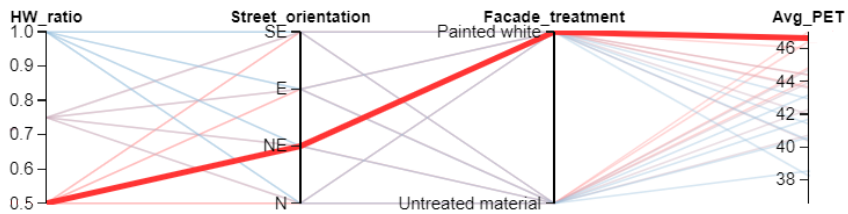


(b) H/W ratio 1.0, SE street orientation and untreated facades

Figure 9.11: Best performing (lowest average PET) urban canyons



(a) H/W ratio 0.5, NE street orientation and untreated facades



(b) H/W ratio 0.5, NE street orientation and white-painted facades

Figure 9.12: Worst performing (highest average PET) urban canyons

Table 9.3: Default settings for exploration of effects surrounding environment, ground material and facade material on PET results

Input parameter	Default setting
Facade albedo	Untreated facade material
Facade material	Brick facade
Ground material	Concrete
H/W ratio street	0.75
Street orientation	N
Surrounding urban environment	Representative theoretic urban area
Window-to-wall ratio (WWR)	0.4

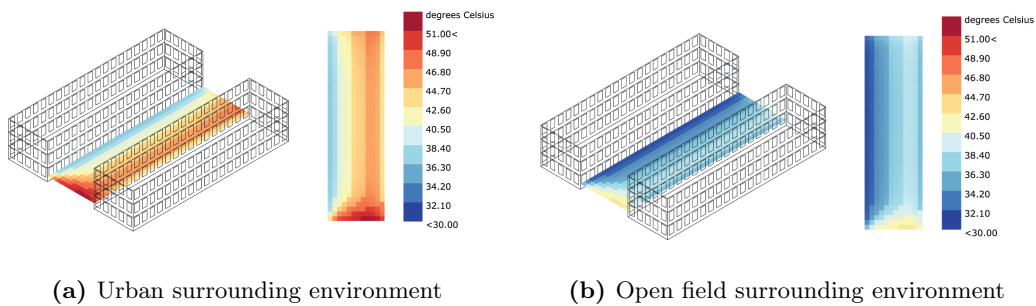


Figure 9.13: Temporally averaged PET (12.00 - 18.00) for an urban surrounding environment (a) and open field surrounding environment (b)

9.3.1 Effect of surrounding environment on PET results

The effect of the surrounding environment on PET results is explored through comparison of two different environments: the representative theoretic urban environment (paragraph 7.2.1) and an open field. Figure E.1 and E.2 show the temporally averaged PET for the urban- and open field environment respectively. Table E.1 shows the spatially and temporally averaged PET results for both environments and the diurnal evolution of spatially averaged PET for the afternoon hours is presented in figure E.3. From these results it appears that the surrounding environment largely affects PET as measured within the urban canyon: with an open field environment resulting in significantly lower PET values than urban surroundings. Urban designers should thus always consider the large scale urban environment, also when assessing PET at a smaller scale.

Table 9.4: Spatially and temporally averaged PET values

Surrounding Environment	Urban	Open field
Average PET in °C	42.20	35.27

9.3.2 Effect of facade material on PET results

For exploration of the effect of facade material on PET results, three different facade constructions are considered: the brick facade as applied in the parametric study, a timber facade and a facade with aluminium cladding. Figure E.4, E.5 and E.6 show

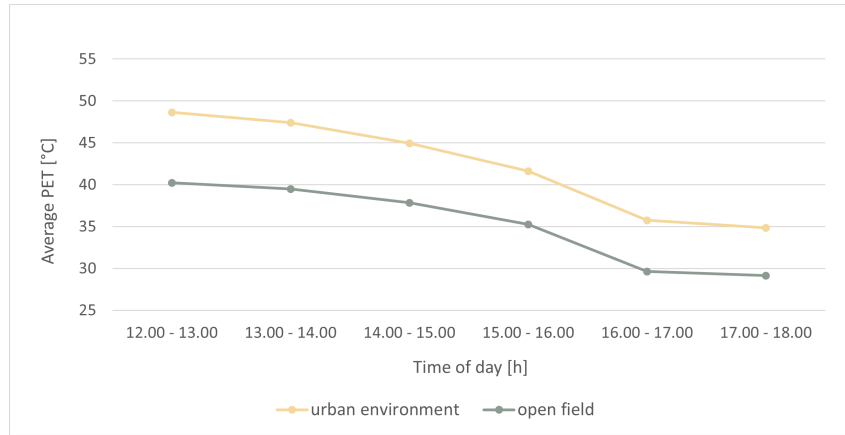


Figure 9.14: Hourly PET (12.00 - 18.00) for surroundings and open field

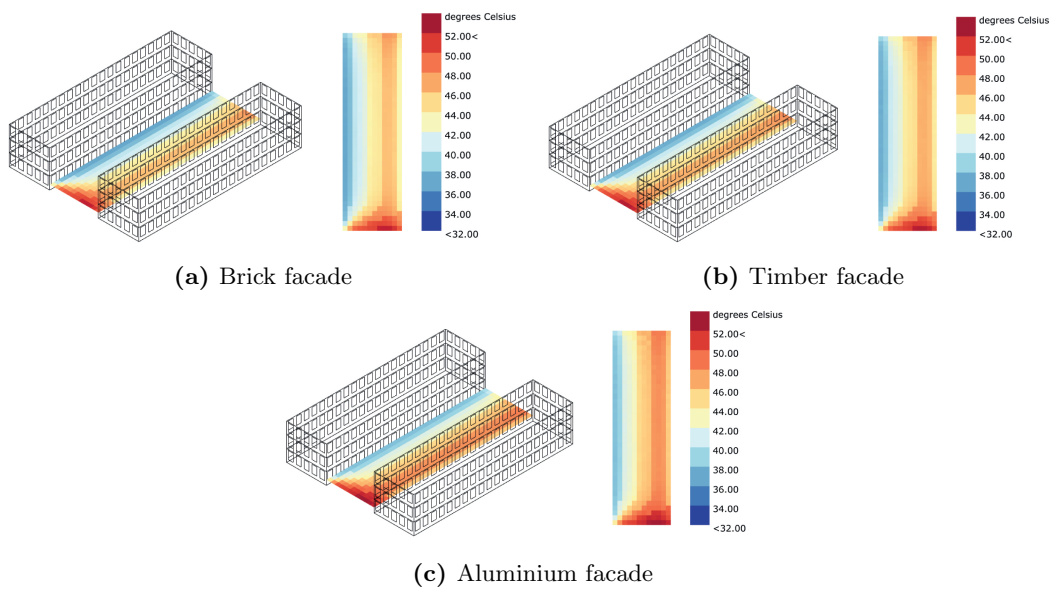


Figure 9.15: Temporally averaged PET (12.00 - 18.00) for a brick facade (a), a timber facade (b) and an aluminium facade

the temporally averaged PET for the brick-, timber- and aluminium facade. Table E.2 shows the spatially and temporally averaged PET results for the considered facades. The diurnal evolution of spatially averaged PET for the afternoon hours is presented in figure E.7. For the considered urban canyon, varying facade material moderately affects PET: the brick facade leads to the lowest PET, closely followed by the timber facade. The aluminium facade results in somewhat higher PET values. Note that the magnitude of facade material effects on PET appear to be highly dependent on urban morphology, time of day and year considered for analysis as well as geographic location of the study area.

Table 9.5: Spatially and temporally averaged PET values

	Brick	Timber	Aluminium
Average PET [in °C]	42.31	42.76	43.65

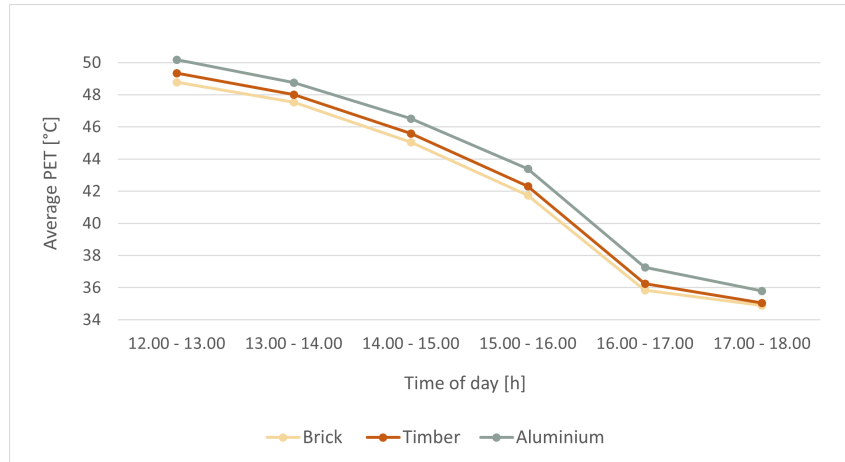


Figure 9.16: Hourly PET (12.00 - 18.00) for different facade materials

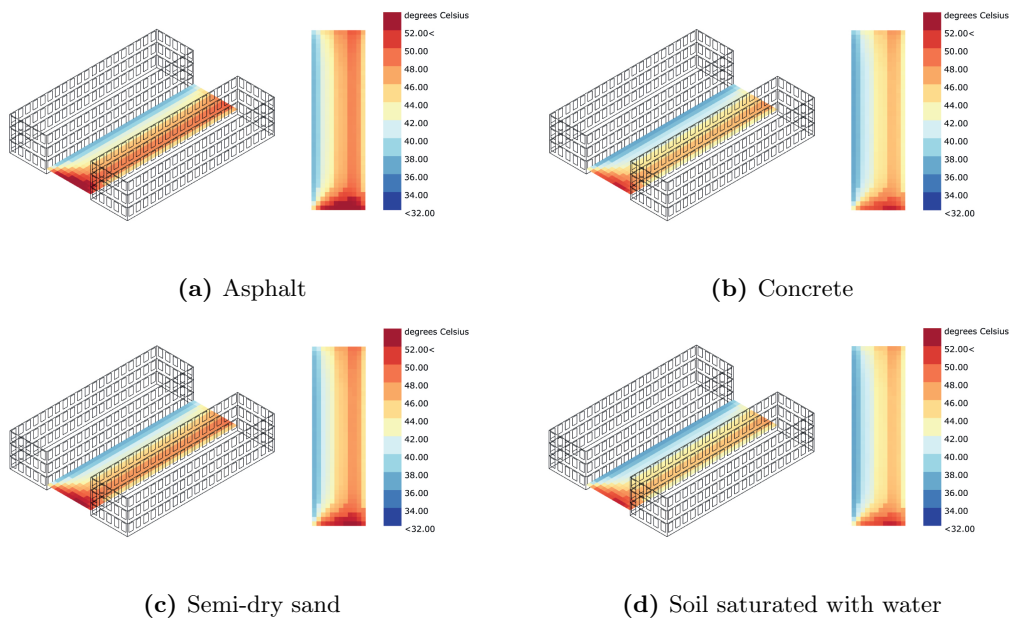


Figure 9.17: Temporally averaged PET (12.00 - 18.00) for asphalt (a), concrete (b), semi-dry sand (c) or soil saturated with water (d) ground material

9.3.3 Effect of ground material on PET results

The effect of ground material on PET results is explored for four different ground materials: Asphalt, concrete, semi-dry sand and soil saturated with water. Figures 9.17a - E.11 show the spatially and temporally averaged PET results for the considered ground materials. Table E.3 shows the spatially and temporally averaged PET results for the considered facades. The diurnal evolution of spatially averaged PET for the afternoon hours is presented in figure E.12. Particularly for the hours in which the ground area is exposed to direct sunlight, ground material appears to significantly affect PET: While the PET results for concrete and soil saturated with water are very similar, both asphalt and semi-dry sand lead to significantly larger PET values in the urban canyon. Again, it must be noted that the magnitude of ground material effects on PET appear to be highly dependent on urban morphology, time of day and year considered for analysis as well as geographic location of the study area.

Table 9.6: Average PET for all analysis hours and over all test points

	Asphalt	Concrete	Sand	Soil
Average PET [in °C]	44.08	42.31	43.42	42.15

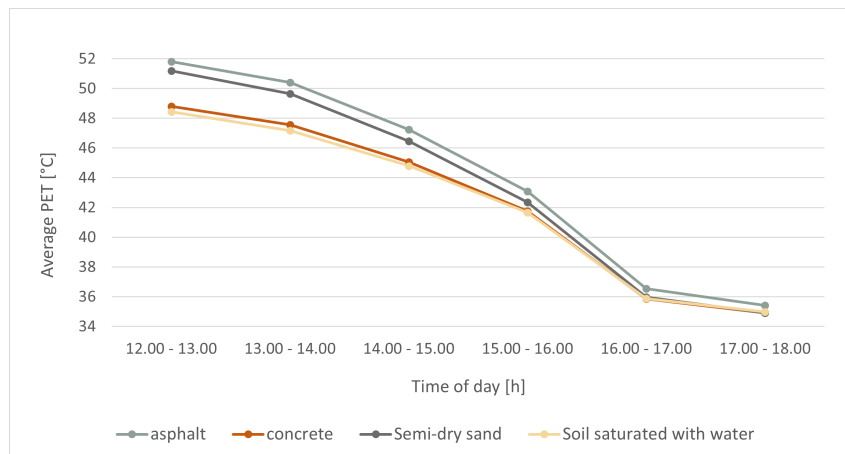


Figure 9.18: Hourly PET values (averaged over all test points) for different ground materials

Part V

Discussion, conclusion and future studies

Chapter 10

Discussion

For the reference urban geometry as assessed in the parametric study, the developed PET model takes approximately 11 minutes to calculate PET. This is a large improvement of time-efficiency in comparison to traditional PET calculation models, which may take up to multiple hours to calculate PET for similar configurations. From a time-perspective, the model thus seems highly suitable for the early design stage. In this chapter, the compromised accuracy at the cost of improved time-efficiency of the PET calculation model is discussed. Inaccuracies of the overall PET calculation are explained through inaccuracies embedded in the sub-calculation of the meteorological input parametersⁱ. Subsequently, the effect of limitations of the PET calculation model on results of the parametric study are discussed.

The effect of the urban environment on increase in **urban air temperature** relative to rural air temperature is implemented in the model through a first-order approximation diagnostic equation for urban-rural air temperature differences [95]. The equation appears to be relatively robust for Western-European cities (RMSE 0.91 K and MEAE 0.58 K) and is thus expected to have little effect on inaccuracy of overall PET. Note that, as the equation has been validated for Western-European cities only, sufficient accuracy for urban air temperature calculation through the equation cannot be guaranteed for non-Western-European cities. Additionally, it should be emphasised that the equation does not account for varying input of building materials and albedo, as these properties are assumed to be generally similar for Western-European cities. This implies that, when altering material characteristics and albedo on the large scale, any effects on urban air temperatures are not considered. However, as the PET model will mostly be used for urban design projects on the smaller scale located in existing cities (which do comply with the characteristic materials and albedo the equation has been developed for), this is in general not expected to affect the accuracy of PET calculation. A final limitation to the equation is its restricted applicability from April to September. The PET model can thus only be used for heat assessment in spring- and summer months.

MRT calculation is implemented in the PET calculation model through a recently developed calculation method in the Ladybug Tools Python SDK, which uses Radi-

ⁱNote that the individual calculations methods for meteorological input parameters have been validated in literature and application of these calculations in the PET model has been assessed through a sense-check. The individual sub-calculations themselves are thus considered sufficiently accurate.

ance for improved accuracy of shortwave MRT calculation. Note that the calculation method is a draft version, and has thus not been validated in literature at time of writing. However, as the calculation method builds on the original Ladybug Tools method for MRT calculation, which is largely similar and has been assessed in literature, a literature review of the original Ladybug Tools method has been performed to evaluate validation of MRT calculation. From literature it appears that simulation of exact MRT magnitude using Ladybug Tools is difficultⁱⁱ, and depending on time of day and considered urban geometry, may misrepresent actual MRT values up to \pm a few degrees Celsius. Although it appears from literature that Ladybug Tools is not capable of simulating the exact correct MRT magnitude, both the sense-checks performed with the PET calculation model and the results from the parametric study do show similar spatial and temporal MRT patterns as seen in literature. In the early design stage, when the model is predominantly used for comparison of various design variants, correct assessment of spatial and temporal MRT patterns is considered more important than calculation of exact correct MRT in the early design stage (provided that the discrepancy between simulated- and actual MRT does not exceed the few degrees Celsius of maximum discrepancy as mentioned in literature). The original Ladybug Tools MRT calculation method is thus considered sufficiently accurate for the early design stage. Additionally, application of Radiance in the newly developed MRT calculation method, potentially improves the accuracy of the original MRT simulation, as in literature, inaccuracies of the Ladybug Tools MRT calculation are often attributed to inaccurate shortwave MRT simulation. However, future studies should validate the Radiance-based MRT calculation method (and appropriate number of ambient bounces used in calculation) as it is currently a draft method, and from the parametric study, increased shortwave irradiance as a result of increasing facade albedo appears to be somewhat lower than measured in literature.

As rural **relative humidity** values are generally similar to urban relative humidity values, rural relative humidity from rural weather data has directly been used as input for the PET calculation. This is considered acceptable as the direct application of rural relative humidity to PET calculation is performed in the PET heat maps (which will be used as control tool) as well.

Wind speed calculation is based on the MacDonald method for calculating wind-profile modification in urban areas. Accurate simulation of highly spatially- and temporally variable local wind speed patterns through CFD simulations is omitted in this study for multiple reasons: Most importantly, the enormous time-savings achieved by omitting CFD simulations are beneficial for overall PET calculation time, which is desirable for PET evaluation in the early design stage. Additionally, in the early design stage, detailed information regarding complex local wind patterns is not required. One is rather interested in large scale effects of building density on average wind speeds. As the MacDonald method accounts for large scale building density effects on average wind speeds, the method is considered sufficiently accurate for the early design stage. Note, however, that the accuracy is limited to relatively low wind speeds, as for situations of high wind, wind speeds become relatively more important in thermal comfort determination. The model is thus encouraged to be applied for its designated purpose only: assessment of PET for extreme heat events

ⁱⁱNote that discrepancies between simulated MRT and field measurements are not uncommon for established MRT simulation tools such as ENVI-met either, and that any measured discrepancies might be the result of inaccurate MRT measurements, as it is generally considered difficult to perform accurate field measurements.

when wind speeds are generally low.

Provided that limitations to the individual input parameters (f.e. limited application the months April-September), are considered carefully, the summation of individual inaccuracies is believed to result in an overall PET calculation inaccuracy that is acceptable for the early design stage. Moreover, by careful consideration of relative importance of the input parameters and corresponding distribution of computational cost for more detailed calculation where needed, an adequate balance between time-efficiency and sufficient accuracy is believed to have been achieved. The results of the parametric study, which in general show sensible spatial and temporal variation, are a first step towards confirmation of the suitability of the model for the early design stage. This initial insight should be further confirmed through a field measurement validation study.

Since the parametric study complies with the formulated constraints of the PET model, inaccuracies in PET results as a consequence of simplifications of the PET model are considered acceptable. Facade albedo results, however, should be interpreted with some caution as the validity of the draft Radiance calculation cannot be guaranteed at time of writing. This is subject for future research.

Chapter 11

Conclusion

The objective of this thesis has been twofold:

1. To create a computationally efficient parametric model for PET calculation to be used by urban designers in the early design stage
2. To quantify how building-related grey heat mitigation strategies on the urban block scale impact outdoor PET values in the Netherlands during extreme heat events

This chapter presents the core findings and conclusions to the research questions corresponding to the objectives listed above. The first main research question is addressed in the first paragraph, whereas the second main research question is addressed in the second paragraph.

11.1 Conclusions to the first research question

The first main research questions reads as follows:

”How can a parametric computational model be set up for outdoor PET calculation with an adequate balance between time-efficiency and sufficient accuracy for the early design stage?”

In this paragraph, the set up of the parametric model is explained and decisions for improved calculation efficiency whilst maintaining sufficient accuracy of PET calculation are substantiated. Note that, even though answers to the supporting sub-questions to main research question are not answered separately in this paragraph, the answers are embedded in the overall conclusion.

The parametric computation model for outdoor PET calculation is set up in the Grasshopper3D environment of Rhinoceros (McNeelAssociates). Grasshopper3D is a visual programming interface, highly suitable for early design stage PET calculation due to its availability of plugins with pre-programmed (environmental) calculation components and inter-operability with external simulation engines (such as EnergyPlus and Radiance), but more importantly the ability for users to adapt any calculations to their personal preference.

The outdoor PET computation model calculates PET through the pre-programmed PET calculation "Ladybug Thermal Comfort Indices" component based on the original PET Fortran code by Höpfe [37]. The PET calculation component requires the input of four meteorological parameters for outdoor thermal comfort calculation: Urban air temperature, urban MRT, urban relative humidity and urban wind speed at 1.2 [m] height. The developed model transforms rural weather data into the urban meteorological input parameters for PET calculation. As the PET calculation itself takes up to a few seconds only, computational efficiency of the model is largely dependent on computation methods for transforming rural- into urban weather data.

Sufficient accuracy of the model is ensured by spatially- and temporally detailed simulation of MRT which, in situations of extreme heat (low wind speeds and clear skies), is the most important parameter affecting thermal comfort. Detailed calculation of MRT is achieved by enhancing the original Method for MRT calculation (which uses EnergyPlus for simulation only), through additional use of external simulation engine Radiance for increased accuracy of MRT simulation in the shortwave spectrum. By varying the number of ambient bounces for Radiance calculation, one can significantly adapt MRT calculation time to what's considered suitable for the project. Note that altering the number of ambient bounces may affect the PET outcome up to approximately one °C.

An adequate balance between time-efficiency and sufficient accuracy of the model is achieved by more rapid assessment of the parameters with lower relative importance in extreme heat situations: air temperature, relative humidity and wind speed. Air temperature is calculated through a diagnostic equation developed by Theeuwes et al. [95] and implemented in Grasshopper through Python script, which has been proven to be valid for western European cities. The use of a diagnostic equation avoids use of complex energy modelling and is thus considered rather time efficient. Urban relative humidity is approximately equal to rural relative humidity. Therefore, rural values are directly used as input to the PET calculation avoiding any computational expenses. The largest time saving in comparison with traditional PET calculation models (such as ENVI-met), however, is achieved by application of a simplified calculation method for urban wind speed, developed by MacDonald [58]. The MacDonald method is used for detection of large scale effects of urban massing on the wind speed profile, and subsequent calculation of wind speeds at 1.2 [m] height. Note that from this method, any local effects of wind speed are not accounted for. Additionally, time efficiency is increased by implementation of a python script that automates determination of the fastest calculation path and subsequent PET calculation via the fastest path.

For the urban configurations as assessed in the parametric study, the model takes approximately 11 minutes to calculate PET per configuration. This is a large reduction of computation time compared to traditional PET simulation models such as ENVI-met, which may take multiple hours for a similar calculation. Since all individual calculation methods applied are validated, and the initial overall PET results obtained by the model from the parametric study appear to be sensible, an adequate balance between time-efficiency and sufficient accuracy for the early design stage is considered to have been achieved by the developed PET calculation model. Note that, as the Radiance-based MRT calculation is a draft version, and the increase of average PET for increasing facade albedo as seen in the parametric study appears to be somewhat lowⁱ, further evaluation MRT simulation accuracy is suggested.

ⁱWhile the increase of average PET for increasing facade albedo appears to be somewhat low

Note that, for correct application of the developed model, a few limitations should be taken into consideration:

- Due to simplifications for wind speed calculation, the model is not sufficiently accurate in situations of high-wind, when the effect of wind speed on thermal comfort is relatively important.
- The model cannot be applied for winter thermal comfort calculations, since the wind speed calculation is unlikely to be sufficiently accurate and the air temperature calculation method is only valid from April to September.
- The air temperature calculation of the model has been validated for Western-European cities only. One should thus be cautious when applying the model outside of Western-Europe.

11.2 Conclusions to the second research question

The second main research question reads as follows:

How effective are the building-related heat mitigation measures identified by Kluck et al. [49] (H/W ratio, street orientation and facade albedo) in providing outdoor thermal comfort during extreme heat events in the Netherlands?

Conclusions corresponding to the second research question are formulated based on the results of the parametric study in chapter X. This paragraph outlines the conclusions of the parametric study structured according to the sub-questions to research question two. For each considered heat mitigation measure, the individual heat mitigation performance and the effect of varying the residual two heat mitigation measures on the individual heat mitigation performance are described (answering sub-question 2.a and 2.b). Subsequently, the combination of input values for H/W ratio, street orientation and facade albedo resulting in minimum- and maximum outdoor thermal comfort are presented (answering sub-question 2.c).

Note that, for correct interpretation of answers to the research questions, a few things should be carefully considered:

- The exact numerical results as presented are only valid for the considered urban configuration, analysis period, weather data and geographic location.
- Outdoor thermal comfort is assessed using temporally and spatially averaged PET. The chosen PET evaluation method (either average PET or 41 °C PET exceedance percentage) may affect whether a certain urban canyon performs better than others or not. For urban designers, it is thus essential to critically consider how to define PET when performing a heat-mitigation analysis.
- In this research, effectiveness of a heat mitigation measure has been defined as the heat mitigation potential of the considered design measure. This effectiveness is assessed by evaluation of the largest difference between maximum- and

in comparison to similar studies performed in the Netherlands [91] and Germany [55], some studies do suggest a lower increase of average PET for increasing albedo.

minimum PET when varying the design measure. It should be emphasised here that the largest difference between maximum- and minimum PET does not always occur in the most 'critical' situation for heat mitigation: Consider an example situation in which varying of a design measure under condition A leads to an average PET decrease from 35 [°C] to 30 [°C]. Varying the same design measure under condition B leads to an average PET decrease from 40 [°C] to 38 [°C]. While varying the design measure under condition A appears to be most effective (largest decrease in average PET), one may argue that varying the design measure for condition B more critical because of the higher initial PET.

11.3 Conclusion to sub-questions 2.a and 2.b

The sub-questions answered in this section are listed below. For each individual heat mitigation design measure (H/W ratio, street orientation and facade albedo), conclusions regarding the individual heat mitigation effectiveness, and how this effectiveness is affected by the other two design measures, are listed.

- 2.a]** What is the individual heat mitigation effectiveness for varying the selected heat mitigation measures?
- 2.b]** How is the individual heat mitigation effectiveness of each selected heat mitigation measure affected by varying the other two heat mitigation measures? (i.e. does a dependency between the heat mitigation measures occur?)

H/W ratio heat mitigation performance

In response to the parametric study results, the following conclusions regarding the heat mitigation effectiveness of varying H/W ratio are drawn:

- Corresponding to the hypotheses, increasing H/W ratio from 0.5 to 0.75 and 1.0 results in decreased average PET and vice versa.
- The heat mitigation effectiveness of H/W ratio is significant: differences between maximum- and minimum average PET for varying H/W ratio of up to 5.6 °C have been measured.
- Street orientation moderately affects the effectiveness of varying H/W ratio: Differences between minimum- and maximum average PET are most pronounced for SE street orientation (up to 5.6 °C difference) and least pronounced for NE street orientations (up to 4.2 °C difference). Increasing H/W ratio as a heat mitigation strategy is therefore considered most effective when applied to SE street orientations and least effective when applied to NE street orientations.
- Facade albedo does not significantly affect the effectiveness of varying H/W ratio for heat mitigation purposes.

Street orientation heat mitigation performance

- Corresponding to the hypotheses, SE street orientations result in lowest average PET, while NE street orientations lead to the highest average PET. E and N street orientations result in intermediate average PET values, with E orientations leading to higher average PET than N orientations.
- The heat mitigation effectiveness of street orientation is considerable: Varying between SE and NE street orientations shows differences between minimum- and maximum average PET of up to 4.7 °C.
- H/W ratio affects the effectiveness of varying street orientation: For a H/W ratio of 1.0, the heat mitigation potential of varying between SE and NE street orientations is largest (up to 4.7 °C). For a H/W ratio of 0.5, the heat mitigation potential of varying between SE and NE street orientations is smallest (up to 2.9 °C).
- Facade albedo does not significantly affect the effectiveness of varying street orientation for heat mitigation purposes.

Facade albedo heat mitigation performance

- The Radiance number of ambient bounces considered in the calculation model largely affects the impact of varying facade albedo on average PET in the urban canyon: For $ab = 2$, low albedo facades lead to higher average PET in the canyon than high albedo facades. This is reversed when more ambient bounces are considered. For $ab = 4$, low albedo facades lead to lower average PET in the urban canyon than high albedo facades, which corresponds to the hypotheses as drafted in paragraph 7.3.
- Both for $ab = 2$ and $ab = 4$, the effectiveness of varying facade albedo on average PET within the urban canyon is substantially lower than the effectiveness of varying H/W ratio and varying street orientation: Varying between untreated facades (low albedo of 0.3) and white-painted facades (high albedo of 0.8) results in a heat mitigation potential of up to 0.73 °C. The magnitude of heat mitigation potential is somewhat lower than expected from literature.

From the conclusions of heat mitigation effectiveness of H/W ratio, street orientation and facade albedo, it thus follows that, in general, H/W ratio is the most effective heat mitigation design measure, closely followed by street orientation. From the study results, varying facade albedo appears to be a considerably less effective strategy for heat mitigation. While the order of effectiveness corresponds to the drafted hypotheses, further validation of the facade albedo calculation is required to draw a firm conclusion regarding the exact magnitude of facade albedo effectiveness.

11.4 Conclusion sub-questions 2.c

- 2.c] Which combination of input values for the selected heat mitigation measures results in minimum- and maximum outdoor thermal comfort?

- A combination of SE street orientation and H/W ratio 1 results in lowest average PET. Depending on the number of ambient bounces considered in the Radiance calculation, either the combination with an untreated facade ($ab = 4$) or the combination with a white painted facade ($ab = 2$) leads to lower average PET. Considering two ambient bounces, the lowest spatially and temporally averaged PET value is measured for the combination of SE street orientation, H/W ratio 1 and white painted facades and equals 38.28 °C. Oppositely, a combination of NE street orientation and H/W ratio 0.5, results in highest average PET within the urban canyon. Again, the number of ambient bounces considered determines whether the combination with untreated facade material ($ab = 2$) or a white painted facade ($ab = 4$) leads to the highest average PET. For calculation with two ambient bounces, the highest spatially and temporally averaged PET equals 47.04 °C and is measured for the combination of NE street orientation, H/W ratio 0.5 and untreated facades.
- The numerical outcome is largely affected by choice of urban surroundings. Urban designers should thus always consider the large scale urban environment when modelling for PET on the urban block scale.
- Both ground- and facade material moderately affect the numerical outcome of PET in the urban canyon. These parameters could thus be considered design measures for heat mitigation themselves and are suggested to be added to the overview of grey heat mitigation design measures by Kluck et al. [49] (table 1.3).

Chapter 12

Recommendations

Recommendations for future research are subdivided into two categories: recommendations for future research (paragraph 12.1) and recommendations for practice (paragraph 12.2).

12.1 Recommendations for future research

- Validation of the developed PET model is considered most important for future research. Note that the model should be validated through field measurements rather than through comparison with existing simulation models, as these models appear to not be completely accurate either. For fair comparison, one should measure spatially and hourly averaged wind speed in the reference canyon for actual PET calculation, as the simulated PET does not account for local spatial and temporal variation in wind speed: simulated PET for averaged wind speeds in the urban canyon cannot reasonably be compared with the actual highly variable wind patterns in the urban canyon. An additional footnote to the comparison is that the field measurements should be performed for a situation that complies with the weather data-, time of year- and geographic constraints of the PET model.
- The application of Radiance for MRT calculation should be developed further and validated. From the results of the parametric study, the impact of increasing facade albedo on average PET in the urban canyon appears to be relatively low in comparison to earlier researchⁱ. It should be validated whether these discrepancies are the result of differences in research set up or the result of inaccuracies in the Radiance MRT model. Additionally, further research into the effect of the number of ambient bounces in Radiance calculation is suggested. Currently, it is unclear which number of ambient bounces provides accurate results. This should be validated, preferably against field measurements.
- 'Green' (vegetation-related) heat mitigation measures have been left out of the scope of this research. However, implementation of vegetation in the PET model is an important topic for future research, as green mitigation measures

ⁱNote that not all considered reference studies find larger PET results for increased facade albedo. However, two studies performed in Germany and the Netherlands that appear to be similar to the parametric study do find this relationship.

are highly desirable due to both their effectiveness in heat mitigation and positive impact of liveability in urban areas. In addition to shading (when considering trees), evaporation is an important cooling principle of green heat mitigation measures. Through geometric modelling of trees, the effects of tree shading can be accounted for. Additionally, the effect of evaporation on city-wide air temperature decrease is estimated through varying the vegetation fraction (F_{veg}) in urban air temperature calculation. The effect of trees and large grass-covered areas is thus expected to be modelled reasonably accurate already. Note that, this should be validated in future studies. The effects of green-facades, however, are expected to be slightly more complex as both surface temperatures and reflected shortwave irradiance are affected by application of green facades. An interesting topic for future research is thus to evaluate how green facades can be modelled appropriately for PET calculation.

- The largest inaccuracies in PET calculation are expected to be the result of inaccurate wind speed modelling. Improved wind speed calculation could be desirable for more accuracy in the PET calculation, however enhanced accuracy often comes at large computation cost when CFD simulations are involved. Increase of computational heaviness of the model should be avoided. Therefore, research into application of more rapid accurate wind modelling, for example through machine learning algorithms or fast fluid dynamics (FFD), could be an interesting topic for future research.
- In this thesis, selected design measures from the overview of Kluck et al. [49] have been evaluated for their heat mitigation performance. From the exploration into the effects of ground- and facade material on the obtained research results, it appears that both ground- and facade material significantly affect average PET in the urban canyon. The effects appear to be even higher than the effects of varying facade albedo. It is therefore suggested to add ground- and facade material to the list of grey heat mitigation measures by Kluck et al. While the exploration into the effects of ground- and facade material provides a first insight into the behaviour of certain materials and effects on outdoor thermal comfort, further research is needed to quantify the precise effects of various ground- and facade materials on PET for varying urban configurations.

12.2 Recommendations for practice

- It is important for urban designers to select the evaluation method of PET cautiously: Results may be different when assessing for spatially averaged PET compared to a 41 °C PET exceedance percentage for example. While the former evaluation method (average PET) provides more insight in numerical outcome of PET, the latter evaluation method (41 °C PET exceedance percentage) provides more insight into spatial distribution of (un)comfortable areas.
- From the exploration into the effect of the surrounding environment of the urban canyon on average PET, it appears that average PET is significantly affected by varying the surrounding environment. When an urban configuration on the urban block scale is modelled, one should thus always model (part of) the surrounding urban environment to the area one's interest in.

- The Radiance-based MRT calculation method is in ongoing development. At time of writing, a draft version that combines the original method of longwave MRT determination, with shortwave MRT determination through Radiance and a draft set of Python equations from the Ladybug Tools SDK is implemented in the PET calculation model. This deconstructed method of MRT calculation may soon be replaced by an all-encompassing Ladybug Tools MRT calculation component (containing both longwave- and shortwave calculation), once the next stable release of Ladybug Tools (version 1.3.0) is launched. An all-encompassing MRT calculation component is expected to somewhat improve accuracy of the calculation, but more importantly: is expected to significantly improve calculation time.
- The model may be modified for application in either an earlier or later design stage, when less- or more detailed PET calculations are required. The model can be simplified by enlarging the grid size of calculation, decreasing the number of sub-surfaces for which facade temperatures are calculated, replacement of the MacDonald wind calculation by the less accurate "Ladybug Wind Speed Calculator" component and reduction of number of ambient bounces in the Radiance calculation (note the consequences for average PET). Oppositely, more detail can be embedded in the model through decreasing the grid size, increasing the number of sub-surfaces for facade temperature calculation and increasing the number of ambient bounces (Radiance), but most importantly, replacement of the MacDonald wind calculation by CFD calculation.
- The Grasshopper environment in which the PET model has been created allows for easy coupling of PET calculation with calculations for additional KPI's. Coupling of calculations is highly recommended as it allows for well-considered total design.
- Future weather scenarios can be assessed with the model by implementation of future weather data. Readily made future weather data .epw files may be purchased online or current weather data can be transformed to future weather data using calculation procedures as described in literature [68, 51].
- Currently, urban design does not have to comply with any standards for outdoor thermal comfort. Some design guidelines to support urban designers in designing for outdoor thermal comfort have been drafted, however, these guidelines are formulated rather broadly in terms of shade percentage and distance to 'cool' places to stay. From an interview with Laura Kleerekoper [49], this is partly due to absence of easy-to-use outdoor thermal comfort design tools. However, the developed PET method is created in response to the absence of early design stage PET calculation tools, and thus eliminates this as a reason for not formulating design guidelines more strictly: Once urban designers are equipped with the appropriate PET calculation tool, a first step towards overcoming the hurdle of implementing outdoor thermal design standards (for the purpose of regulating heat-proof design) is taken. Additionally, the model could be used as tool for assessment of appropriateness of (re)formulating outdoor thermal comfort in terms of PET.

List of Figures

1	The vast impact of urbanisation on change of natural landscape is well exemplified by the urban sprawl of Mexico city, altering the characteristics of surrounding hills (Barcroft Media, 2013)	1
1.1	Extreme weather events such as heatwaves or excessive precipitation compromise comfort, health and safety of urban dwellers	5
1.2	A trend of increased number of summer days (air temperature > 25 °C) in the Netherlands from 1920 - 2020. Retrieved from [5]	6
1.3	The urban heat issue	7
1.4	Positioning of the new tool	9
1.5	Report outline	13
3.1	Heat fluxes of the human energy balance. Adapted from [34]	18
3.2	Planck curves of blackbody emitters at temperatures of the sun and the earth-atmosphere system. Adapted from [75]	19
3.3	title here	23
3.4	title here	24
4.1	An example PET map of Wageningen, created using the Dutch standardized PET calculation method	28
6.1	Structure of the PET calculation model in Grasshopper	32
6.2	Example configuration of an urban block with corresponding analysis points	33
6.3	Source area for calculation of spatially averaged SVF and F_{veg} . Adapted from [51]	34
6.4	Diurnal Cycle by Oke	36
6.5	Airtemp calculation	37

6.6	Two-step calculation approach for Tmax, Tmin and avgU calculation	37
6.7	Average SVF calculation for a single source area	38
6.8	Diurnal air temperature variation for varying SVF and a default value of F_{veg} (0.3) plotted against rural air temperature	39
6.9	Honeybee Legacy Microclimate Map MRT calculation workflow . . .	40
6.10	Python component for MRT calculation via the Ladybug_comfort.solarcal.shortwave_from_horiz.s function	42
6.11	Flow chart of the MRT calculation procedure using Radiance for radiation inputs	43
6.12	An overview of the longwave MRT calculation workflow	44
6.13	Radiance workflow	44
6.14	Calculation of fraction of body exposed to sunlight	45
6.15	The urban canyon for comparison of MRT calculation methods . . .	45
6.16	MRT comparison for Microclimate Map- and Radiance method for different times of day (afternoon)	47
6.17	The urban canyon for comparison of MRT calculation methods . . .	48
6.18	Urban geometry for Radiance sense-check	48
6.19	Diffuse irradiance received at 1.2 [m] height for varying facade albedo at 12.00 (top view of analysis area)	49
6.20	Constituents of frontal area density λ calculation	50
6.21	afbeelding. Adapted from [75]	51
6.22	Source area for wind speed calculations	54
6.23	Python component for wind speed calculation	54
6.24	correct implementation wind speed validation	56
6.25	Determination of the fastest calculation path for air temperature calculation through Python	57
7.1	Perspective view of an example urban block with coloured analysis area. For PET calculation, the analysis area is subdivided in a 1-m grid of test points.	61
7.2	Street orientations (top view)	62
7.3	Theoretical study area set up	63

8.1	PET results for varying H/W ratio	69
8.2	PET results for varying street orientation	69
8.3	PET results for varying facade albedo	69
8.4	Overview of all considered urban configurations for increasing average PET values from upper left to lower right (continues on next line). Blue circles indicate a H/W ratio of 1.0, purple circles a H/W ratio of 0.75 and red circles a H/W ratio of 0.5.	69
9.1	A comparison of best- to worst performing facades considering both average PET (b) and 41 °C PET exceedance percentage (c)	71
9.2	A comparison of PET evaluation by average PET and 41 °C PET exceedance percentage for two urban canyons	71
9.3	The effect of street orientation on heat mitigation effectiveness of H/W ratio. For demonstration purposes, the facade treatment has been kept constant.	73
9.4	The effect of H/W ratio on heat mitigation effectiveness of street orientation. For demonstration purposes, the facade treatment has been kept constant.	74
9.5	Differences in average PET between untreated facades (red lines) and white painted facades (blue lines) for all possible combinations of H/W ratio and street orientation. For clarity of demonstration, the Design Explorer images have been displayed for individually selected H/W ratio.	76
9.6	Spatially averaged MRT over all analysis hours for low albedo (0.3) and high albedo (0.8) facades	77
9.7	A comparison of spatially averaged longwave MRT in the urban canyon for low- and high albedo facades (a) and spatially averaged received diffuse shortwave irradiance (b)	78
9.8	Temporally averaged facade surface temperatures for varying facade albedo	78
9.9	Spatially averaged MRT (longwave + shortwave) for low- and high albedo facades, considering two and four ambient bounces for calculation.	79
9.10	Spatially averaged diffuse shortwave irradiance received for low- and high albedo facades, considering two and four ambient bounces for calculation.	79
9.11	Best performing (lowest average PET) urban canyons	81
9.12	Worst performing (highest average PET) urban canyons	81

9.13	Temporally averaged PET (12.00 - 18.00) for an urban surrounding environment (a) and open field surrounding environment (b)	82
9.14	Hourly PET (12.00 - 18.00) for surroundings and open field	83
9.15	Temporally averaged PET (12.00 - 18.00) for a brick facade (a), a timber facade (b) and an aluminium facade	83
9.16	Hourly PET (12.00 - 18.00) for different facade materials	84
9.17	Temporally averaged PET (12.00 - 18.00) for asphalt (a), concrete (b), semi-dry sand (c) or soil saturated with water (d) ground material	84
9.18	Hourly PET values (averaged over all test points) for different ground materials	85
A.1	An overview of heat-mitigation strategies and their proved effectiveness in the Netherlands. – means the effect is negligible and ?? means that no effect has been proven yet. (a) Green mitigation measures. (b) Blue mitigation measures. (c) Grey mitigation measures. Retrieved from [49].	108
A.1	An overview of heat-mitigation strategies and their proved effectiveness in the Netherlands. – means the effect is negligible and ?? means that no effect has been proven yet. (a) Green mitigation measures. (b) Blue mitigation measures. (c) Grey mitigation measures. Retrieved from [49].	109
A.1	An overview of heat-mitigation strategies and their proved effectiveness in the Netherlands. – means the effect is negligible and ?? means that no effect has been proven yet. (a) Green mitigation measures. (b) Blue mitigation measures. (c) Grey mitigation measures. Retrieved from [49].	110
B.1	SEF (left) calculation and SVF (right) calculation. From [107]	111
C.1	Diurnalcycle1	112
C.2	Diurnalcycle2	113
E.1	Temporally averaged PET (12.00 - 18.00) for an urban surrounding environment in perspective (left) and top view (right)	128
E.2	Temporally averaged PET (12.00 - 18.00) for an open field as surrounding environment in perspective (left) and top view (right)	129
E.3	Hourly PET (12.00 - 18.00) for surroundings and open field	130
E.4	Temporally averaged PET (12.00 - 18.00) for a brick facade in perspective (left) and top view (right)	130

E.5	Temporally averaged PET (12.00 - 18.00) for a timber facade in perspective (left) and top view (right)	131
E.6	Temporally averaged PET (12.00 - 18.00) for an aluminium facade in perspective (left) and top view (right)	131
E.7	Hourly PET (12.00 - 18.00) for different facade materials	131
E.8	Temporally averaged PET (12.00 - 18.00) for asphalt in perspective (left) and top view (right)	132
E.9	Temporally averaged PET (12.00 - 18.00) for concrete in perspective (left) and top view (right)	132
E.10	Temporally averaged PET (12.00 - 18.00) for semi-dry sand in perspective (left) and top view (right)	132
E.11	Temporally averaged PET (12.00 - 18.00) for soil saturated with water in perspective (left) and top view (right)	133
E.12	Hourly PET values (averaged over all test points) for different ground materials	133
E.13	Air temperatures over the analysis hours. Rural weather data and air temperatures within the urban block considering an open field situation are equal, and are therefore overlapping in the graph. . . .	134
E.14	test	134
E.15	Average ground surface temperatures for an open field situation for the considered analysis period (12.00-18.00). A comparison between a paved (concrete) ground environment (left) or soil ground environment (right)	135
E.16	Average ground surface temperatures for an open field situation for the considered analysis period (12.00-18.00). A comparison between a paved (concrete) ground environment (left) or soil ground environment (right)	136
E.17	Temporally averaged longwave MRT (12.00-18.00) for a brick facade	138
E.18	Temporally averaged longwave MRT (12.00-18.00) for a timber facade	139
E.19	Temporally averaged longwave MRT (12.00-18.00) for an aluminium facade	140
E.20	Diurnal evolution (for afternoon hours) of longwave MRT for different facade materials	140
E.21	Average surface temperatures for different facades from South-East perspective	141
E.22	Average surface temperatures for different facades from South-West perspective	141

E.23 LW MRT asphalt	141
E.24 LW MRT concrete	142
E.25 LW MRT semi-dry sand	142
E.26 LW MRT soil saturated with water	142
E.27 Diurnal evolution (for afternoon hours) of longwave MRT for different ground materials	143

List of Tables

1.1	Heat mitigation design guidelines [49]	8
1.2	Grey heat mitigation as identified by Kluck et al. [49]. [??] means effects are yet unknown. [-] means effects are negligible.	10
1.3	Grey heat mitigation design measures on the urban block scale selected for further analysis	11
3.1	Meteorological variables and the corresponding heat transfer mechanism they affect	21
3.2	Surface projection factors f_p for varying solar altitude γ	22
3.3	Assumed values for the four meteorological variables for the reference indoor situation	25
3.4	Thermal perception and experienced heat stress and corresponding PET. Adapted from [11]	26
6.1	Input parameters for diagnostic UHI-equation Theeuwes et al. [95]	34
6.2	Air density corresponding to air temperature	35
6.3	Input parameters for diagnostic UHI-equation Theeuwes et al. [95]	38
6.4	Input parameters for MRT calculation via <code>Ladybug_comfort.solarcal.shortwave_from_horiz_solar</code> function. Retrieved from [53]	43
6.5	Parameters for wind calculation	51
6.6	Values for d , z_w , z_0 , A and B dependent on geometric properties λ_{tot} and H_{avg} [51]	53
6.7	Input parameters for wind speed calculation Python component	54
7.1	Considered input for variable parameters of the parametric study	62
7.2	Default settings for PET calculation	62

7.3	Hourly values for air temperature (in [°C]), wind speed (in [m/s] at 10 [m] height) and sky cover (1 equals 1/10 covered, 10 equals total coverage)	64
9.1	Difference (in °C) between maximum average PET (H/W ratio 0.5) and minimum average PET (H/W ratio 1.0) for various combinations of street orientation and facade treatment	72
9.2	Difference between maximum average PET (NE street orientation) and minimum average PET (SE street orientation) for various combinations of H/W ratio and facade treatment	75
9.3	Default settings for exploration of effects surrounding environment, ground material and facade material on PET results	82
9.4	Spatially and temporally averaged PET values	82
9.5	Spatially and temporally averaged PET values	83
9.6	Average PET for all analysis hours and over all test points	85
E.1	Spatially and temporally averaged PET values	129
E.2	Spatially and temporally averaged PET values	129
E.3	Average PET for all analysis hours and over all test points	130
E.4	SVF and F_{veg} for the urban- and open field surrounding environment	131
E.5	Air temperatures [in °C] from rural weather data (left), when an urban environment is considered (middle) and when an open field environment is considered (right)	133
E.6	Average longwave MRT for all test points over all individual hours considering open field- and urban surroundings	135
E.7	Hourly temperatures of surrounding ground surface for an open field (both situations in which soil and concrete is used considered) and an urban environment (concrete).	136
E.8	Average urban wind speed within the analysis area [in m/s] for an open field- and urban surrounding environment	136
E.9	Average longwave MRT for all analysis hours and over all test points	137
E.10	Average longwave MRT for all analysis hours and over all test points	142

Appendix A

Heat mitigation strategies review

Soort	Maatregel	Verkoelings-principe	Maatregel vooral voor		Typisch schaal-niveau waarop maatregel effectief is		Verkoelende effecten gevonden in literatuur			Extra informatie
			Dag	Nacht	Stad	Lokaal	Luchttemperatuur [°C]		Gevoels-temperatuur [°C PET]	
							Stad	Lokaal	Lokaal	
Groen	Bomen/leibomen	verdamping, beschaduwing	X		X	X	0,2 - 2,7	0,7 - 2,7	3,4 - 19,0	Effect afhankelijk van boomtype en -grootte en het lokale klimaat. Referenties zie voetnoot ¹³
	Gras/Struiken	verdamping, reflectie	X	X	X	X	0,1 - 1,1	0,9 - 1,2	0,4 - 4,9	Effect van een gezond goed verdampend grasveld. Gras heeft ook effect op oppervlakte-temperatuur (tot 20°C kouder dan beton). Referenties zie voetnoot ¹⁴
	Grasbeton-tegels	verdamping	X	X		X	--	--	--	
	Groene gevels	verdamping	X	X		X	0 - 1,9	0,2 - 1,5	??	Hoe smaller de straat, hoe groter het effect op de luchttemperatuur. Groter effect voor gevels met meer zonnestraling. Referenties zie voetnoot ¹⁵
	Groene daken (extensief)	verdamping		X	X		0 - 1,8	0 - 0,8	--	Een met sedum bedekt groen dak geeft weinig verkoeling 's nachts (vergeleken met een wit dak). Effect op stadsniveau is als 100% van alle daken in de stad groen zijn. Referenties zie voetnoot ¹⁶
	Groene daken (intensief)	verdamping	X	X	X		0 - 1,7	1,0 - 1,6	--	Effect op stadsniveau is als 100% van alle daken in de stad groen zijn. Referenties zie voetnoot ¹⁷
	Park/groene wiggen/vingers in de stad	verdamping, beschaduwing	X	X	X		??	1,1 - 2,0	1,9 - 4,2	Effect afhankelijk van vegetatietype (boom versus gras), boomgrootte, -grootte van het park en het lokale klimaat. Effect op PET gemeten in schaduw is groter dan hier genoemd. Referenties zie voetnoot ¹⁸

(a) Green heat mitigation measures

Figure A.1: An overview of heat-mitigation strategies and their proved effectiveness in the Netherlands. -- means the effect is negligible and ?? means that no effect has been proven yet. (a) Green mitigation measures. (b) Blue mitigation measures. (c) Grey mitigation measures. Retrieved from [49].

Soort	Maatregel	Verkoelings-principe	Maatregel vooral voor		Typisch schaal-niveau waarop maatregel effectief is		Verkoelende effecten gevonden in literatuur			Extra informatie
			Dag	Nacht	Stad	Lokaal	Luchttemperatuur [°C]		Gewoel-temperatuur [°C PET]	
							Stad	Lokaal	Lokaal	
Blauw	Vijvers	verdamping	X			X	0,5 - 1,3	0,5 - 0,7	0,6 - 3,6	Effect afhankelijk van het temperatuurverschil tussen water en lucht en de grootte van het waterlichaam. Referenties zie voetnoot ¹⁹
	Meer	verdamping	X		X		1,0 - 2,0	0,5 - 1,6	??	Effect afhankelijk van het temperatuurverschil tussen water en lucht en de grootte van het waterlichaam. Referenties zie voetnoot ²⁰
	Singels/ grachten/ sloten	verdamping	X			X	??	0,1 - 0,8	0,2 - 2,0	Effect afhankelijk van het temperatuurverschil tussen water en lucht en de grootte van het waterlichaam. Referenties zie voetnoot ²¹
	Rivier	verdamping, ventilatie	X		X		??	0,5 - 4,0	1,0 - 4,0	Effect afhankelijk van het temperatuurverschil tussen water en lucht en de grootte van het waterlichaam. Referenties zie voetnoot ²²
	Fontein	verdamping	X			X	--	1,0 - 4,7	1,0 - 5,0	Referenties zie voetnoot ²³
	Vernevelings- installaties	verdamping	X			X	--	0,7 - 3,0	??	Data zijn van Japanse studies. Referenties zie voetnoot ²⁴
	Besprekings- straten	verdamping	X			X	--	0,8 - 3,0	??	Referenties zie voetnoot ²⁵
	Polderdaken	verdamping	X		X		??	--	--	Effect vergelijkbaar met dat van een intensief groendak. Referenties zie voetnoot ²⁶

(b) Blue heat mitigation measures

Figure A.1: An overview of heat-mitigation strategies and their proved effectiveness in the Netherlands. -- means the effect is negligible and ?? means that no effect has been proven yet. (a) Green mitigation measures. (b) Blue mitigation measures. (c) Grey mitigation measures. Retrieved from [49].

Soort	Maatregel	Verkoelings-principe	Maatregel vooral voor		Typisch schaal-niveau waarop maatregel effectief is		Verkoelende effecten gevonden in literatuur			Extra informatie	
			Dag	Nacht	Stad	Lokaal	Luchttemperatuur [°C]		Gevoels-temperatuur [°C PET]		
							Stad	Lokaal	Lokaal		
Grijs	Parasols/ doeken/per-gola's/arcades/loggia's/lufels/schuttingen	beschaduwng	X			X		–	0 - 1,0	2,0 - 17,0	Genoemde effecten betreffen alleen schaduw door gebouwen. Referenties zie voetnoot ¹⁷
	Zonneschoorsteen	ventilatie	X			X		–	??	??	
	Windcorridors	ventilatie	X		X	X		??	??	??	Windcorridors verhogen de windsnelheid tot 1,5 m/s. Effect op luchttemperatuur en PET is niet gekwantificeerd. Referenties zie voetnoot ¹⁸
	Grote oppervlaktes	ventilatie	X	X	X			??	??	??	De openheid wordt weergegeven door de SVF (sky view factor). Een lage SVF leidt in de zomer tot een hogere temperatuur vanwege het blootgestelde oppervlak en het gebrek aan schaduw. Een 10% hogere SVF zorgt ook voor een toename van de windsnelheid met 8%. Totaleffect van SVF op temperatuur of PET hangt ook af van albedo, aanwezigheid van vegetatie en hoogte-breedte verhouding straten. Referenties zie voetnoot ¹⁹
	Hoogte-breedte verhouding straten	ventilatie, beschaduwng	X			X		–	??	??	Studies richten zich vaak op droge en hete klimaatzones, niet passend bij de Nederlandse context. Referenties zie voetnoot ²⁰
	Oriëntatie straten	ventilatie, beschaduwng	X			X		–	max 0,4	max 10,2	Referenties zie voetnoot ²¹
	Lichte gevels	reflectie	X			X		–	0,1 - 0,7	??	Referenties zie voetnoot ²²
	Lichte bestrating	reflectie	X			X		–	max 1,9	??	Het wordt aanbevolen om reflecterende trottoirs alleen te gebruiken als de hoogte-breedte verhouding van de straat niet groter is dan 1,0, anders wordt de straling gereflecteerd naar de gevels. Referenties zie voetnoot ²³
Witte daken	reflectie	X		X			max 0,9	–	–	0,1-0,3 °C per 10% albedo verhoging. Referenties zie voetnoot ²⁴	

(c) Grey heat mitigation measures

Figure A.1: An overview of heat-mitigation strategies and their proved effectiveness in the Netherlands. – means the effect is negligible and ?? means that no effect has been proven yet. (a) Green mitigation measures. (b) Blue mitigation measures. (c) Grey mitigation measures. Retrieved from [49].

Appendix B

SVF and SEF comparison

A final footnote to the SVF calculation is that this calculation should not be confused with that for the sky exposure factor (SEF), something that regularly occurs in practice. SEF is defined as "the proportion of the sky visible from a point to the overall sky dome" [107]. According to this definition, sky exposure is determined as the fraction between the solid angle of directly visible sky observed from a given point and the solid angle of the entire hemisphere around that point. In agreement with this definition of SEF, all parts of the sky are of equivalent importance. SVF, on the other hand does not treat all parts of the sky equally: In the calculation of SVF, visible parts of the sky are projected onto the analysis plane and subsequently weighted by their area [59]. For SVF calculation on a horizontal plane, this means that visible sky patches are adjusted by the cosine of the angle between the zenith and the visible sky patch. According to this calculation, sky patches at the top of the hemisphere are of larger importance than those at the horizon [107].

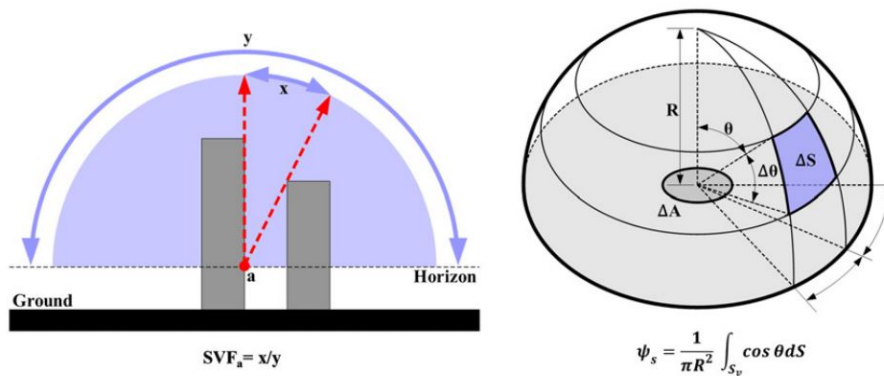


Figure B.1: SEF (left) calculation and SVF (right) calculation. From [107]

Appendix C

Diurnal Cycle

period	Sunrise / sunset (in UTC)
1 April t/m 19 April	5/18
13 April t/m 20 April	5/19
20 April t/m 19 May	4/19
20 May t/m 25 May	4/20
26 May t/m 10 July	3/20
11 July t/m 30 July	4/20
31 July t/m 21 Augustus	4/19
22 Augustus t/m 30 Augustus	5/19
31 Augustus t/m 24 September	5/18
25 September t/m 27 September	5/17
28 September t/m 30 September	6/17

Figure C.1: Diurnalcycle1

Sunrise / sunset	6/17	5/17	5/18	5/19	4/19	4/20	3/20
UTC 0	0.748	0.728	0.807	0.910	0.900	1.000	1.000
1	0.667	0.640	0.704	0.780	0.757	0.888	0.866
2	0.602	0.573	0.617	0.675	0.710	0.728	0.690
3	0.525	0.490	0.533	0.590	0.543	0.609	0.560
4	0.449	0.355	0.435	0.490	0.413	0.490	0.380
5	0.281	0.150	0.227	0.320	0.150	0.256	0.107
6	0.127	0.078	0.095	0.120	0.057	0.079	0.015
7	0.063	0.025	0.032	0.040	0.000	0.007	-0.020
8	0.019	-0.013	-0.009	-0.005	-0.020	-0.020	-0.007
9	-0.015	-0.020	-0.020	-0.020	-0.005	-0.006	0.007
10	-0.020	-0.001	-0.003	-0.004	0.013	0.010	0.029
11	0.000	0.025	0.020	0.016	0.037	0.033	0.050
12	0.030	0.056	0.048	0.042	0.063	0.056	0.074
13	0.065	0.090	0.080	0.071	0.090	0.082	0.108
14	0.117	0.165	0.136	0.111	0.150	0.128	0.161
15	0.205	0.270	0.215	0.176	0.222	0.184	0.228
16	0.335	0.413	0.325	0.270	0.318	0.270	0.312
17	0.532	0.600	0.485	0.386	0.450	0.366	0.424
18	0.747	0.803	0.662	0.546	0.600	0.506	0.556
19	0.906	0.920	0.849	0.716	0.762	0.651	0.695
20	0.975	0.978	0.932	0.877	0.890	0.803	0.838
21	1.000	1.000	0.979	0.941	0.950	0.901	0.911
22	0.931	0.925	1.000	0.981	0.982	0.958	0.964
23	0.849	0.830	0.918	1.000	1.000	0.983	0.984

Figure C.2: Diurnalcycle2

Appendix D

Python code PET simulation model

D.1 Transform datetime information

```
import rhinoscriptsyntax as rs
from datetime import date, timedelta, datetime

print "the current analysis period is:" + str(currentDate)

#convert tuples containing the start- and enddate into
datetime data
startDate = date(year, currentDate[0][0], currentDate[0][1])
print "the start date of the analysis is:" +str(startDate)
endDate = date(year, currentDate[1][0], currentDate[1][1])
print "the end date of the analysis is:"+ str(endDate)

#find all dates in between the start- and enddate
delta = endDate - startDate

allDays = []
for i in range(delta.days + 1):
    day = startDate + timedelta(days = i)
    allDays.append(day)

print "All dates within the analysis period are:" + str(
    allDays)

allDates = []
for i in range(len(allDays)):
    allDates_add = allDays[i].strftime("%m, %d")
    allDates_tu = tuple(map(int, allDates_add.split(', ')))
    allDates.append(allDates_tu)

print allDates
```

```

#Find the successive dates of all the single dates within
the analysis period
nextDate = []

for i in range(len(allDays)):
    nextday = allDays[i] + timedelta(days=1)
    nextDate.append(nextday)

print "All successive dates of the dates within the analysis
period are:" + str(nextDate)

dateStr = []
for i in range(len(nextDate)):
    dateStr_add = nextDate[i].strftime("%m, %d")
    dateStr_tu = tuple(map(int, dateStr_add.split(', ')))
    dateStr.append(dateStr_tu)

print dateStr
successiveDates = dateStr

print successiveDates[0][0]
print successiveDates[-1][1]

RangeSuccessiveDates = [(successiveDates[0][0],
    successiveDates[0][1], 1), (successiveDates[-1][0],
    successiveDates[-1][1], 24)]
print RangeSuccessiveDates

nrDays = len(allDays)

#Get all hours in the analysis period

allHours = range(startHour, endHour + 1)
nrHours = len(allHours)

hourList = []
for day in range(nrDays):
    for hour in range(nrHours):
        hourList.append(allHours[hour] + (24*day))

```

D.2 Air temperature calculation: Find fastest calculation path

```

if tot_nrHours < 8:
    smaller_HW = 1
    larger_HW = 0
    larger_LW = 0
    print smaller_HW
    if min(windSpeed) > 1.5:

```

```

        smaller_LW = 0
    else:
        smaller_LW = 1
else:
    larger_HW = 1
    smaller_HW = 0
    smaller_LW = 0
    if min(windSpeed) > 1.5:
        larger_LW = 0
    else:
        larger_LW = 1

```

D.3 Air temperature calculation: Calculate max, min and average weather values over deconstructed days

```

import rhinoscriptsyntax as rs

#Split the hourly data for all days in lists of hourly data
of the single selected days
def splitList(aList, wantedParts):
    length = len(aList)
    return [ aList[i*length // wantedParts: (i+1)*length //
        wantedParts]
            for i in range(wantedParts) ]

TempPerDayC = splitList(HourlyTempC, nrDays)
TempPerDayS = splitList(HourlyTempS, nrDays)
UlistC = splitList(Uc, nrDays)
UlistS = splitList(Us, nrDays)

#Calculate the daily minimum and maximum temperatures
##Extract the temperatures from UTC 8 until UTC 24 for the
current days
TempListC = []
for i in range(len(TempPerDayC)):
    addTemp = TempPerDayC[i][6:]
    TempListC.append(addTemp)

##Extract the temperatures from UTC 0 until UTC 7 for the
successive days
TempListS = []
for i in range(len(TempPerDayS)):
    addTemp = TempPerDayS[i][:6]
    TempListS.append(addTemp)

##Calculate Tmax and Tmin for the selected days
Tmax = []
Tmin = []
for i in range(len(TempListC)):

```

```

HourlyTemp = TempListC[i] + TempListS[i]
addTmax = max(HourlyTemp)
addTmin = min(HourlyTemp)
Tmax.append(addTmax)
Tmin.append(addTmin)

print "Tmax_for_the_selected_days_are:" + str(Tmax)
print "Tmin_for_the_selected_days_are:" + str(Tmin)

#Calculate the daily average wind speeds
##Extract the wind speeds from UTC 8 until UTC 24 for the
current days
currentU = []
for i in range(len(UlistC)):
    addU = UlistC[i][6:]
    currentU.append(addU)

##Extract the wind speeds from UTC 0 until UTC 7 for the
successive days
successiveU = []
for i in range(len(UlistS)):
    addU = UlistS[i][:6]
    successiveU.append(addU)

##Calculate avgU for the selected days
avgU = []

for i in range(len(currentU)):
    HourlyU = currentU[i] + successiveU[i]
    Utot = sum(HourlyU)
    Ulen = len(HourlyU)
    avgUadd = Utot / Ulen
    avgU.append(avgUadd)

```

D.4 Air temperature calculation: Calculate urban air temperature

```

from datetime import date, timedelta
import clr
clr.AddReference("Grasshopper")
from Grasshopper import DataTree
from Grasshopper.Kernel.Data import GH_Path
import Rhino
import rhinoscriptsyntax as rs

list = [-22.5, 22.5, 67.5, 112.5, 157.5, 202.5, 247.5,
        292.5, 337.5]

Fveg = 0

```

```

#Fveg kan nog veranderen wanneer er groen is binnen source
  area!

#First the calculation of UHImax for each day in the
  analysis period is performed. For this calculation,
  average daily values for wind speed, air temperature and
  radiation are used.

##Calculate the nr of days in the analysis period
nrDays = range(len(avgTemp))
length_nrDays = len(avgTemp)

##Split the input in lists of hourly values into hourly
  values per day in the analysis period
def splitList(aList, wantedParts):
    length = len(aList)
    return [ aList[i*length // wantedParts: (i+1)*length //
              wantedParts]
              for i in range(wantedParts) ]

daily_ruralTemp = splitList(ruralTemp, length_nrDays)
daily_ruralU = splitList(ruralU, length_nrDays)
daily_windDir = splitList(windDir, length_nrDays)
daily_smallerSVF_HW = splitList(smallerSVF_HW, length_nrDays
)

##calculate the number of hours in the analysis period
nrHours = range(len(daily_ruralTemp[0]))
tot_nrHours = len(ruralTemp)
length_nrHours = len(daily_ruralTemp[0])

##calculate the mean downward short-wave radiation over the
  current day in kinematic units [Kms-1]

###Calculate the rounded daily average air temperatures (in
  degrees Celcius)
avgT = []
for i in nrDays:
    avgT_add = round(avgTemp[i])
    avgT.append(avgT_add)

###determine average air density over the selected days (
  dependent on average air temperature) in [kg/m3]
airtempList = range(-10,36,1)

airDensity = []
for i in nrDays:
    for j in range(len(airtempList)):
        if avgT[i] == airtempList[j]:
            airDensity.append(airdensList[j])

```

```

###determine specific heat of air in [J/kg*K]
specHeat = 1006 #value from literature: https://www.
engineeringtoolbox.com/air-specific-heat-capacity-d_705.
html

###convert directNormalRadiation to mean downward shortwave
radiation [S] in kinematic units
S = []
for i in nrDays:
    meanRad = Rad[i] / (airDensity[i]*specHeat)
    S.append(meanRad)

##Calculate the hourly sky view factor (SVF) (which is
dependent on the wind direction each hour)
SVF = []

if tot_nrHours < 8:
    for day in nrDays:
        for hour in nrHours:
            if daily_ruralU [day][hour] > 1.5:
                SVF_add = daily_smallerSVF_HW [day][hour]
                SVF.append(SVF_add)
            else:
                SVF_add = smallerSVF_LW
                SVF.append(SVF_add)
else:
    for day in nrDays:
        for hour in nrHours:
            if daily_ruralU [day][hour] > 1.5:
                if 337.5 < daily_windDir [day][hour] <= 360:
                    daily_windDir [day][hour] = 360 -
                    daily_windDir [day][hour]
                for i in range(len(list) - 1):
                    if list [i] < daily_windDir [day][hour] <=
                    list [i+1]:
                        SVF_add = largerSVF_HW [i]
                        SVF.append(SVF_add)
                else:
                    SVF_add = largerSVF_LW
                    SVF.append(SVF_add)

daily_SVF = splitList(SVF, length_nrDays)

##Calculate the average daily SVF by taking the average of
all hourly SVF values
avgSVF = []
for day in nrDays:
    avgSVF_add = sum(daily_SVF [day]) / len(daily_SVF [day])
    avgSVF.append(avgSVF_add)

##Calculate the daily UHImax

```

```

UHImax = []
for day in nrDays:
    UHImax_add = (2-SVF[day]-Fveg)*((S[day]*(Tmax[day]-Tmin[
        day])**3)/avgU[day])**3*(1/4)
    UHImax.append(UHImax_add)

##Calculate the hourly urban air temperature by adding the
    UHImax multiplied by a diurnal cycle factor to the rural
    air temperature

##Below the diurnal cycle factors are displayed
UHIfac = [[0.667, 0.64, 0.704, 0.78, 0.757, 0.888, 0.866],
[0.602, 0.573, 0.617, 0.675, 0.71, 0.728, 0.69],
[0.525, 0.49, 0.533, 0.59, 0.543, 0.609, 0.56],
[0.449, 0.355, 0.435, 0.49, 0.413, 0.49, 0.38],
[0.281, 0.15, 0.227, 0.32, 0.15, 0.256, 0.107],
[0.127, 0.078, 0.095, 0.12, 0.057, 0.079, 0.015],
[0.063, 0.025, 0.032, 0.04, 0, 0.007, -0.02],
[0.019, -0.013, -0.009, -0.005, -0.02, -0.02, -0.007],
[-0.015, -0.02, -0.02, -0.02, -0.005, -0.006, 0.007],
[-0.02, -0.001, -0.003, -0.004, 0.013, 0.01, 0.029],
[0, 0.025, 0.02, 0.016, 0.037, 0.033, 0.05],
[0.03, 0.056, 0.048, 0.042, 0.063, 0.056, 0.074],
[0.065, 0.09, 0.08, 0.071, 0.09, 0.082, 0.108],
[0.117, 0.165, 0.136, 0.111, 0.15, 0.128, 0.161],
[0.205, 0.27, 0.215, 0.176, 0.222, 0.184, 0.228],
[0.335, 0.413, 0.325, 0.27, 0.318, 0.27, 0.312],
[0.532, 0.6, 0.485, 0.386, 0.45, 0.366, 0.424],
[0.747, 0.803, 0.662, 0.546, 0.6, 0.506, 0.556],
[0.906, 0.92, 0.849, 0.716, 0.762, 0.651, 0.695],
[0.975, 0.978, 0.932, 0.877, 0.89, 0.803, 0.838],
[1, 1, 0.979, 0.941, 0.95, 0.901, 0.911],
[0.931, 0.925, 1, 0.981, 0.982, 0.958, 0.964],
[0.849, 0.83, 0.918, 1, 1, 0.983, 0.984],
[0.748, 0.728, 0.807, 0.91, 0.9, 1, 1]]

##Determine in which date interval the days within the
    analysis period fall and determine which column of the
    diurnal cycle table corresponds with the selected date
    intervals

## An overview of the date intervals and corresponding
    columns
Period = [[date(year, 4, 1), date(year, 4, 12), 2],
[date(year, 4, 13), date(year, 4, 20), 3],
[date(year, 4, 21), date(year, 5, 19), 4],
[date(year, 5, 20), date(year, 5, 25), 5],
[date(year, 5, 26), date(year, 7, 10), 6],
[date(year, 7, 11), date(year, 7, 30), 5],
[date(year, 7, 31), date(year, 8, 21), 4],
[date(year, 8, 22), date(year, 8, 30), 3],
[date(year, 8, 31), date(year, 9, 24), 2],

```

```

[date(year, 9, 25), date(year, 9, 27), 1],
[date(year, 9, 28), date(year, 9, 30), 0]]

##Transform the analysis period information into datetime
data to get all dates within the analysis period
startDate = date(year, analysisPeriod[0][0], analysisPeriod
[0][1])
endDate = date(year, analysisPeriod[1][0], analysisPeriod
[1][1])

delta = endDate - startDate

allDays = []

for i in range(delta.days + 1):
    day = startDate + timedelta(days = i)
    allDays.append(day)

##Determine the hours of the day in the analysis period to
select the correct rows from the diurnal cycle table
hoursOfDay = range(analysisPeriod[0][2] - 1, analysisPeriod
[1][2])

##Calculate the urban air temperature. The correct diurnal
cycle values are obtained by selecting the correct column
and row from the diurnal cycle table, dependent on day
and hour of the analysis period
urbanTa = []
for day in nrDays:
    for i in range(len(Period)):
        if Period[i][0] <= allDays[day] <= Period[i][1]:
            column = Period[i][2]
            for hour in nrHours:
                dc = UHIfac[hoursOfDay[hour]][column]
                urbanTa_add = daily_ruralTemp[day][hour] +
                    dc*UHImax[day]
                urbanTa.append(urbanTa_add)

##Eventueel nog de lijst hier omzetten in correcte tree met
dagen en uren. Later moet ook nog per punt the air temp
worden gegeven. Dit kan eventueel ook hier worden gedaan

daily_urbanTa = splitList(urbanTa, length_nrDays)
#print daily_urbanTa

#for day in range(length_nrDays):
#   for hour in range(length_nrHours):
#       for testpoint in range(nr_testPoints):
##           print daily_urbanTa[day][hour]
#           urban_airTemp.Add(daily_urbanTa[day][hour],
GH_Path(day, hour))

```

```

#print urban_airTemp

for day in range(length_nrDays):
    for hour in range(length_nrHours):
        urban_airTemp.Add(daily_urbanTa [day][hour], GH.Path(
            day, hour))

#hourly_u12 = splitList(u12, nr_Hours)
#
#for hour in range(nr_Hours):
#    for testpoint in range(nr_testPoints):
#        print hourly_u12[hour][testpoint]
#        urban_windSpeed.Add(hourly_u12[hour][testpoint],
#            GH.Path(hour))

```

D.5 Wind speed calculation: Find fastest calculation path

```

geometryHW = 1

if min(windSpeed) > 1.5:
    geometryLW = 0
else:
    geometryLW = 1

```

D.6 Wind speed calculation: Add up to frontal facade orientation per wind direction

```

import clr
clr.AddReference("Grasshopper")
from Grasshopper import DataTree
from Grasshopper.Kernel.Data import GH_Path
import Rhino
import rhinoscriptsyntax as rs

nrTestpoints = int(adjN.BranchCount / 3)

for dir in range(8):
    for point in range(nrTestpoints):
        if dir == 0:
            dirZero = adjNW.Branch(dir, point)[0] + adjN.
                Branch(dir, point)[0] + adjNE.Branch(dir,
                    point)[0]
            HW_frontalArea.Add(dirZero, GH_Path(dir, point))
        if dir == 1:

```

```

dirOne = adjN.Branch(dir , point)[0] + adjNE.
    Branch(dir , point)[0] + adjE.Branch(dir , point
    )[0]
HW_frontalArea.Add(dirOne , GH.Path(dir , point))
if dir == 2:
dirTwo = adjNE.Branch(dir , point)[0] + adjE.
    Branch(dir , point)[0] + adjSE.Branch(dir ,
    point)[0]
HW_frontalArea.Add(dirTwo , GH.Path(dir , point))
if dir == 3:
dirThree = adjE.Branch(dir , point)[0] + adjSE.
    Branch(dir , point)[0] + adjS.Branch(dir , point
    )[0]
HW_frontalArea.Add(dirThree , GH.Path(dir , point))
if dir == 4:
dirFour = adjSE.Branch(dir , point)[0] + adjS.
    Branch(dir , point)[0] + adjSW.Branch(dir ,
    point)[0]
HW_frontalArea.Add(dirFour , GH.Path(dir , point))
if dir == 5:
dirFive = adjS.Branch(dir , point)[0] + adjSW.
    Branch(dir , point)[0] + adjW.Branch(dir , point
    )[0]
HW_frontalArea.Add(dirFive , GH.Path(dir , point))
if dir == 6:
dirSix = adjSW.Branch(dir , point)[0] + adjW.
    Branch(dir , point)[0] + adjNW.Branch(dir ,
    point)[0]
HW_frontalArea.Add(dirSix , GH.Path(dir , point))
if dir == 7:
dirSeven = adjW.Branch(dir , point)[0] + adjNW.
    Branch(dir , point)[0] + adjN.Branch(dir , point
    )[0]
HW_frontalArea.Add(dirSeven , GH.Path(dir , point))

```

D.7 Wind speed calculation: Calculate urban wind speed

```

import rhinoscriptsyntax as rs
import math

#Take a 1 m/s normalized wind speed at a height of 10 m as
the starting point representative for open terrain in
order to create a wind reduction field
u10 = 1

#Translate this wind speed to 60-m height
u60 = 1.3084*u10

#Determine the average obstacle height H weighted to the
obstacle footprints

```

```

# sum(Hbuilding*FootprintBuilding)/allFootprints

timePoints = len(ruralU)
spacePoints = int(HW_totFootprint.BranchCount / len(
    all_windDir))
list_windDir = range(len(all_windDir))

tableMacDonald = [[0, 0.08, 0.066, 2, 0.048, -0.35, 0.56],
[0.08, 0.135, 0.26, 2.5, 0.071, -0.35, 0.5],
[0.135, 0.18, 0.32, 2.7, 0.084, -0.34, 0.48],
[0.18, 0.265, 0.42, 1.5, 0.08, -0.56, 0.66],
[0.265, 1, 0.57, 1.2, 0.077, -0.85, 0.92]]

u12 = []
for hour in range(timePoints):
    for dir in list_windDir:
        if hourly_windDir[hour] == list_windDir[dir]:
            if ruralU[hour] > 1.5:
                for testPoint in range(spacePoints):
                    totFootprint = HW_totFootprint.Branch(
                        dir, testPoint)[0]
                    sumFootprint_Height = 0
                    for building in range(len(
                        HW_allFootprint.Branch(dir, testPoint)
                    )):
                        sumFootprint_Height +=
                            HW_allFootprint.Branch(dir,
                                testPoint)[building] *
                            HW_allHeight.Branch(dir, testPoint
                                )[building]
                    avgH = sumFootprint_Height /
                        totFootprint
                    frontalArea = HW_frontalArea.Branch(dir,
                        testPoint)[0]
                    sourceArea = 280*140
                    frontal_areaDensity = frontalArea /
                        sourceArea
                    print frontalArea
                    print sourceArea
                    trees_areaDensity = 0
                    tot_areaDensity = 0.6*
                        frontal_areaDensity + 0.3*
                        trees_areaDensity + 0.015
                    if (0.6*frontal_areaDensity + 0.3*
                        trees_areaDensity) > (25 /
                        frontalArea):
                        for row in range(len(tableMacDonald)
                            ):
                            if tableMacDonald[row][0] <=
                                tot_areaDensity <
                                    tableMacDonald[row][1]:

```

```

        d = avgH * tableMacDonald [
            row][2]
        zw = avgH * tableMacDonald [
            row][3]
        zo = avgH * tableMacDonald [
            row][4]
        A = avgH * tableMacDonald [
            row][5]
        B = tableMacDonald [row][6]
        uzw = u60*(math.log((zw-d)/
            zo) / math.log((60-d)/zo)
            )
        uAsterisk = 0.4* (u60 / math
            .log((60-d)/zo))
        uH = ((-uAsterisk / B) *
            math.log((A + (B*zw))/(A
            + (B*avgH)))) + uzw
        u12add = uH * math.exp(9.6*
            tot_areaDensity*((1.2/
            avgH) - 1))
        scaledU12 = ruralU [hour]*((
            u12add - 0.0796)*0.9175 +
            0.1254)
        u12.append(scaledU12)
    else:
        u12add = 0.6350*u10
        u12.append(u12add)
else:
    for testPoint in range(spacePoints):
        totFootprint = LW_totFootprint.Branch(
            dir, testPoint)[0]
        sumFootprint_Height = 0
        for building in range(len(
            LW_allFootprint.Branch(dir, testPoint)
        )):
            sumFootprint_Height +=
                LW_allFootprint.Branch(dir,
                testPoint)[building] *
                LW_allHeight.Branch(dir, testPoint
                )[building]
        avgH = sumFootprint_Height /
            totFootprint
        frontalArea = LW_frontalArea.Branch(dir,
            testPoint)[0]
        sourceArea = 175*175
        frontal_areaDensity = frontalArea /
            sourceArea
        trees_areaDensity = 0
        tot_areaDensity = 0.6*
            frontal_areaDensity + 0.3*
            trees_areaDensity + 0.015

```

```

print frontalArea
print sourceArea
print tot_areaDensity
if (0.6*frontal_areaDensity + 0.3*
    trees_areaDensity) > (25 /
    frontalArea):
    for row in range(len(tableMacDonald)
    ):
        if tableMacDonald[row][0] <=
            tot_areaDensity <
            tableMacDonald[row][1]:
            d = avgH * tableMacDonald[
                row][2]
            zw = avgH * tableMacDonald[
                row][3]
            zo = avgH * tableMacDonald[
                row][4]
            A = avgH * tableMacDonald[
                row][5]
            B = tableMacDonald[row][6]
            uzw = u60*(math.log((zw-d)/
                zo) / math.log((60-d)/zo)
            )
            uAsterisk = 0.4* (u60 / math
                .log((60-d)/zo))
            uH = ((-uAsterisk / B) *
                math.log((A + (B*zw))/(A
                + (B*avgH)))) + uzw
            u12add = uH * math.exp(9.6*
                tot_areaDensity*((1.2/
                avgH) - 1))
            scaledU12 = ruralU[hour]*((
                u12add - 0.0796)*0.9175 +
                0.1254)
            u12.append(scaledU12)
        else:
            u12add = 0.6350*u10
            u12.append(u12add)
    else:
        pass

```

D.8 Wind speed calculation: Transform to correct data structure

```

import clr
clr.AddReference("Grasshopper")
from Grasshopper import DataTree
from Grasshopper.Kernel.Data import GH_Path
import Rhino

```

```

import rhinoscriptsyntax as rs

def splitList(aList, wantedParts):
    length = len(aList)
    return [ aList[i*length // wantedParts: (i+1)*length //
            wantedParts]
            for i in range(wantedParts) ]

print totHours
print nrDays
print nr_testPoints
nrHours = int(totHours / nrDays)
print nrHours

daily_u12 = splitList(u12, nrDays)

hourly_u12 = []
for i in range(len(daily_u12)):
    hourly_u12_add = splitList(daily_u12[i], nrHours)
    hourly_u12.append(hourly_u12_add)

print hourly_u12

for day in range(nrDays):
    for hour in range(nrHours):
        for testpoint in range(nr_testPoints):
            urban_windSpeed.Add(hourly_u12[day][hour][
                testpoint], GH_Path(day, hour))

```

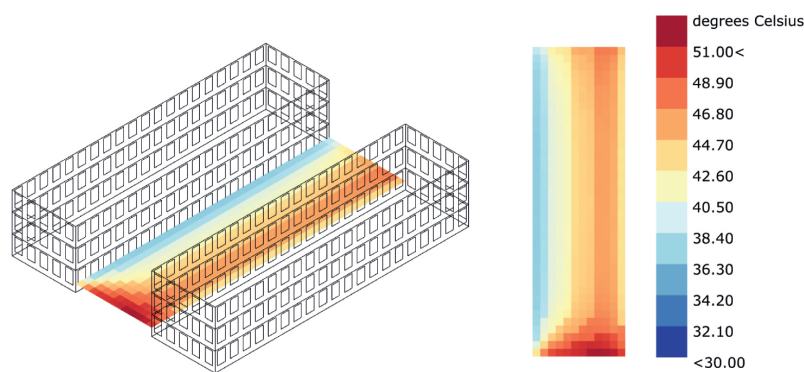
Appendix E

Exploration into the effects of varying the surrounding environment and facade- and ground material

E.1 Results exploration

E.1.1 Surrounding environment of the urban canyon

Two different environments, one urban environment and an open field, have been considered. Figure E.1 and figure E.2 show the temporally averaged PET for all afternoon hours for each individual calculation point in the analysis grid for an urban- and open field environment respectively.



From figures E.1 and E.2, the spatially and temporally averaged PET values for the considered environments are calculated (table E.1).

The diurnal evolution of spatially averaged PET for the afternoon hours is presented in figure E.3.

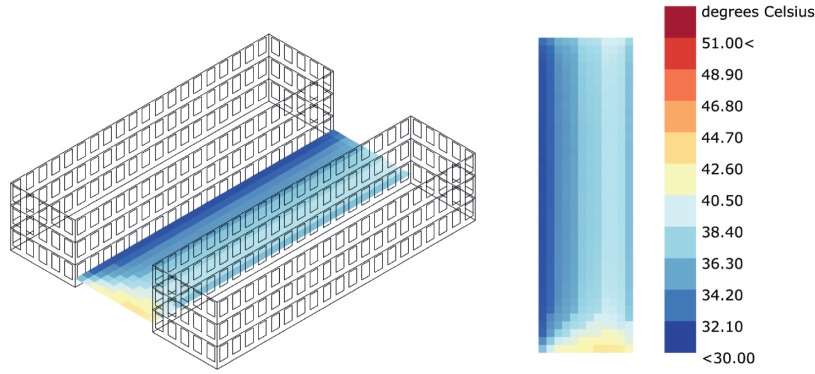


Figure E.2: Temporally averaged PET (12.00 - 18.00) for an open field as surrounding environment in perspective (left) and top view (right)

Table E.1: Spatially and temporally averaged PET values

Surrounding Environment	Urban	Open field
Average PET in °C	42.20	35.27

E.1.2 Facade material

Three different facades, a brick-, timber-, and aluminum facade have been considered. Figure E.4, figure E.5 and E.6 show the temporally averaged PET for all afternoon hours for each individual calculation point in the analysis grid, considering the brick-, timber- and aluminium facade respectively.

From figures E.4, E.5 and E.6, the spatially and temporally averaged PET values for the considered facade materials are calculated (E.2).

Table E.2: Spatially and temporally averaged PET values

	Brick	Timber	Aluminium
Average PET [in °C]	42.31	42.76	43.65

The diurnal evolution of spatially averaged PET for the afternoon hours is presented in figure E.7.

E.1.3 Ground material

Four different ground materials, asphalt, concrete, semi-dry sand and soil saturated with water, have been considered. Figure E.8, E.9, E.10 and E.11 show the temporally averaged PET for all afternoon hours for each individual calculation point in the analysis grid, considering the asphalt-, concrete-, sand- and soil ground respectively.

From figures E.8, E.9, E.10 and E.11, the spatially and temporally averaged PET values for the considered ground materials are calculated (table E.3).

The diurnal evolution of spatially averaged PET for the afternoon hours is presented in figure E.12.

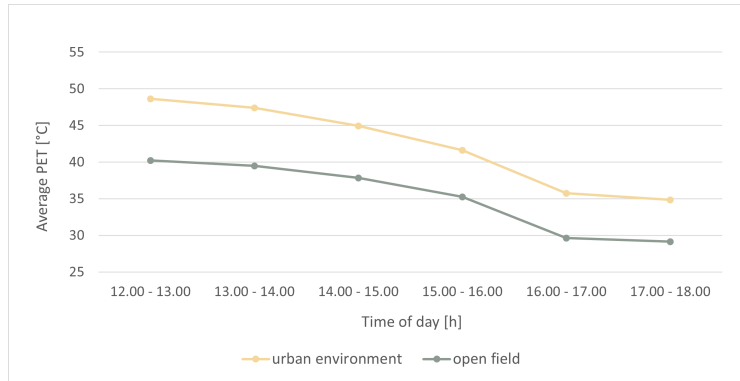


Figure E.3: Hourly PET (12.00 - 18.00) for surroundings and open field

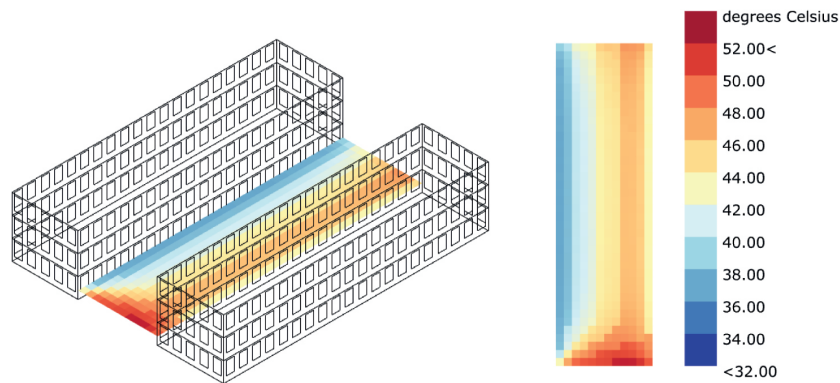


Figure E.4: Temporally averaged PET (12.00 - 18.00) for a brick facade in perspective (left) and top view (right)

E.2 Discussion of exploration

E.2.1 Surrounding environment of the urban block

Figures E.1 and E.2 show distinct differences between PET values as distributed over the analysis area. The results in these figures are translated to a difference in average PET (averaged both spatially and temporally) between the two considered surrounding environment cases of 6.93 °Celsius (table E.1).

From the results, it appears that an open field environment leads to considerable reduced PET within the analysis area of the urban block. The differences in PET between the two considered cases can be traced back by the effect of the surrounding environment on three of the four meteorological thermal comfort parameters: air temperature, MRT and wind speed. To find out the relative importance of alteration of each of these thermal comfort parameters by the surrounding environment, the affect of the surroundings on each individual thermal comfort parameter is discussed below.

Table E.3: Average PET for all analysis hours and over all test points

	Asphalt	Concrete	Sand	Soil
Average PET [in °C]	44.08	42.31	43.42	42.15

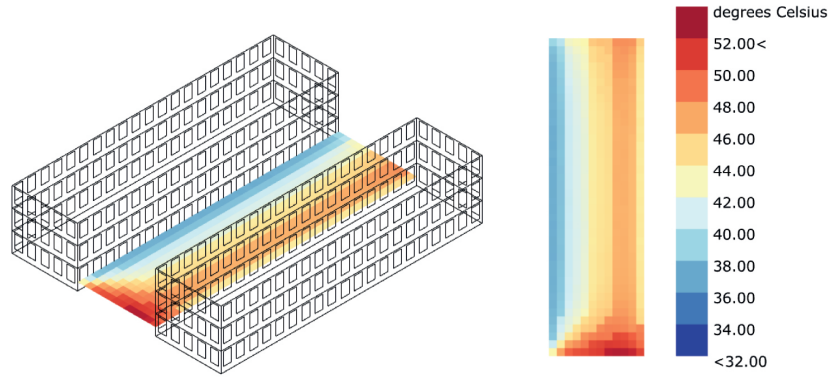


Figure E.5: Temporally averaged PET (12.00 - 18.00) for a timber facade in perspective (left) and top view (right)

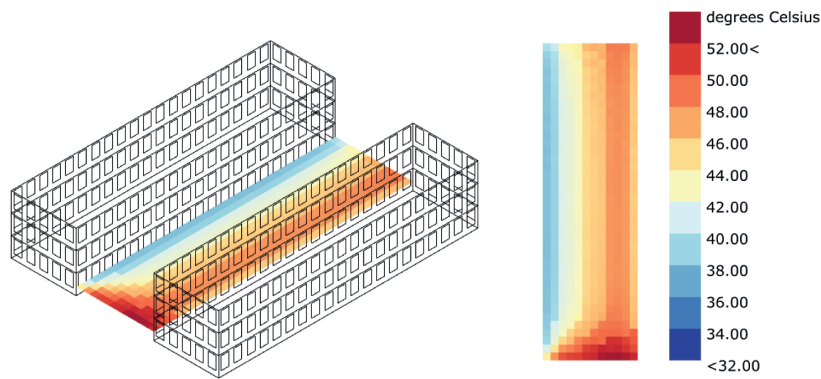


Figure E.6: Temporally averaged PET (12.00 - 18.00) for an aluminium facade in perspective (left) and top view (right)

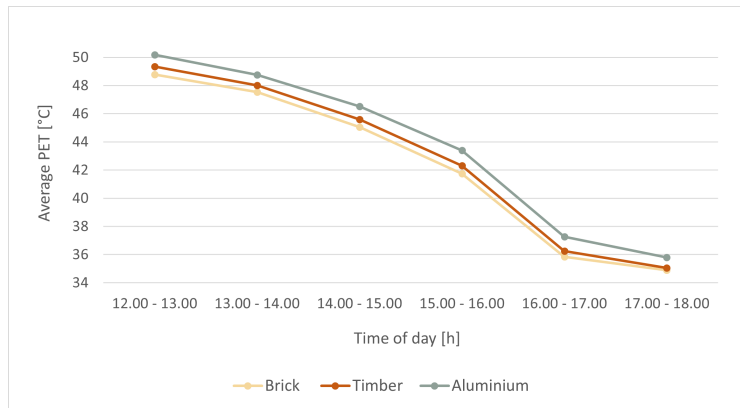


Figure E.7: Hourly PET (12.00 - 18.00) for different facade materials

Air temperature is altered by the surrounding environment due to differences in building density, leading to differences in sky view factor (SVF), and vegetation fraction (F_{veg}) (table E.4).

Table E.4: SVF and F_{veg} for the urban- and open field surrounding environment

	Urban surrounding environment	Open field surrounding environment
SVF	0.51	0.99
Fveg	0	0.99

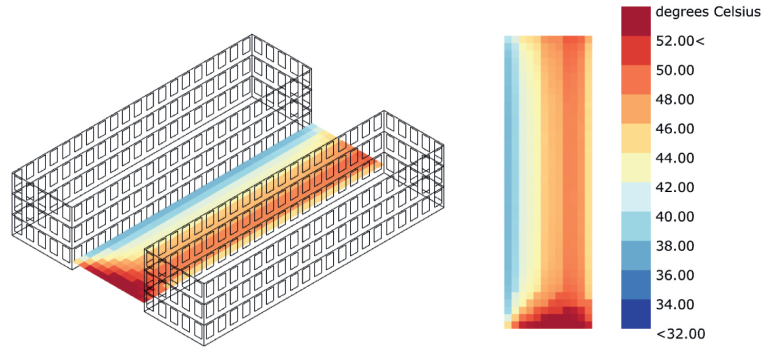


Figure E.8: Temporally averaged PET (12.00 - 18.00) for asphalt in perspective (left) and top view (right)

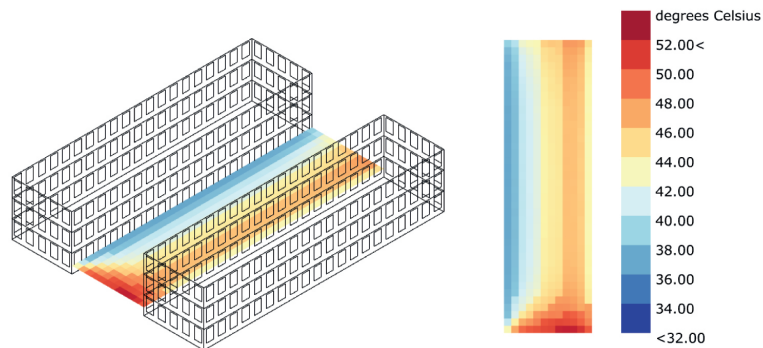


Figure E.9: Temporally averaged PET (12.00 - 18.00) for concrete in perspective (left) and top view (right)

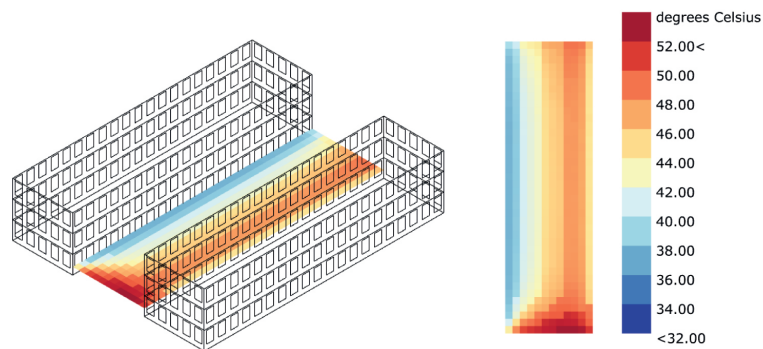


Figure E.10: Temporally averaged PET (12.00 - 18.00) for semi-dry sand in perspective (left) and top view (right)

A comparison between rural air temperatures, and air temperatures in the urban block for the urban- and open field surrounding environments, shows that, as expected, no air temperature differences occur when an open field surrounding environment is considered. For an urban environment, however, the air temperature difference between rural- and urban settings is up to 2.46 °C. These results seem

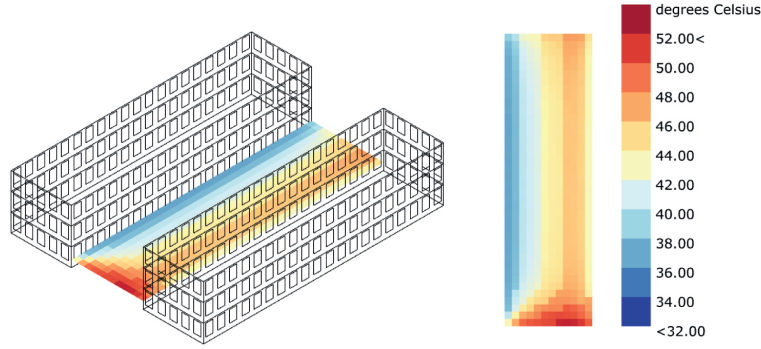


Figure E.11: Temporally averaged PET (12.00 - 18.00) for soil saturated with water in perspective (left) and top view (right)

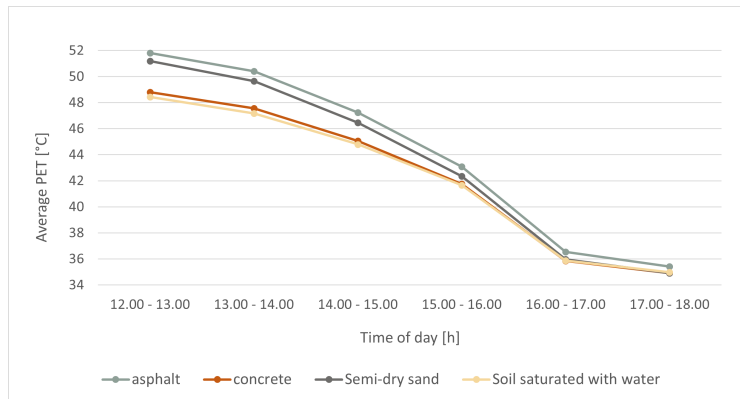


Figure E.12: Hourly PET values (averaged over all test points) for different ground materials

Table E.5: Air temperatures [in °C] from rural weather data (left), when an urban environment is considered (middle) and when an open field environment is considered (right)

rural	urban environment	open field environment
28.1	28.44	28.1
29.1	29.59	29.1
29.6	30.42	29.6
30	31.21	30
29.4	31.14	29.4
29.6	32.06	29.6

plausible as their course corresponds to the diurnal cycle for UHI effect by Oke [74], with minimal air temperature difference around noon, and increasing air temperature differences towards the evening (figure E.13). Additionally, the magnitude of the air temperature differences corresponds to what's expected from literature [89].

Mean radiant temperature is altered in the longwave spectrum only, as the short-wave share of MRT neglects the surrounding environment and is solely determined by shading patterns and reflectance of the urban block itself. Longwave MRT is only slightly affected by the presence of surrounding buildings in comparison to an open field situation (figure E.14, table E.6). Below, the origin of differences in longwave MRT for the two considered surrounding environment scenarios is explained further.

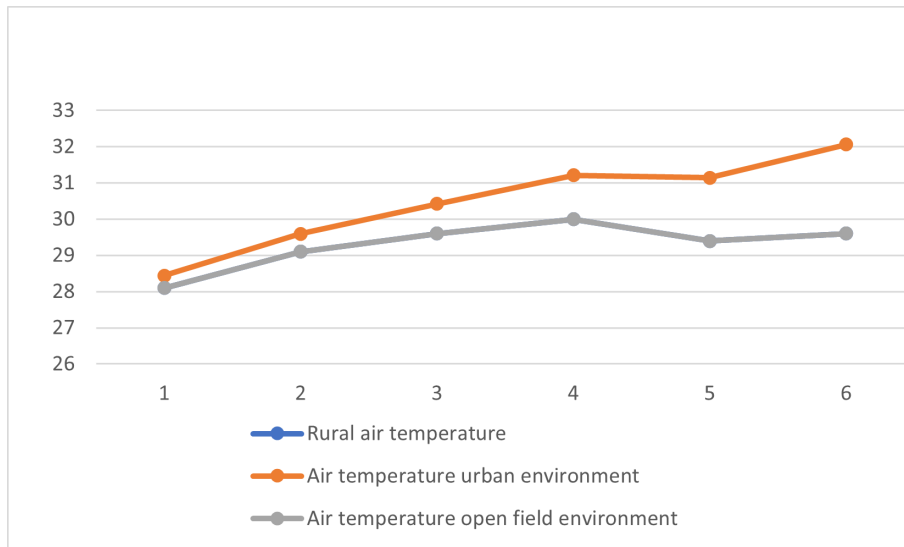


Figure E.13: Air temperatures over the analysis hours. Rural weather data and air temperatures within the urban block considering an open field situation are equal, and are therefore overlapping in the graph.

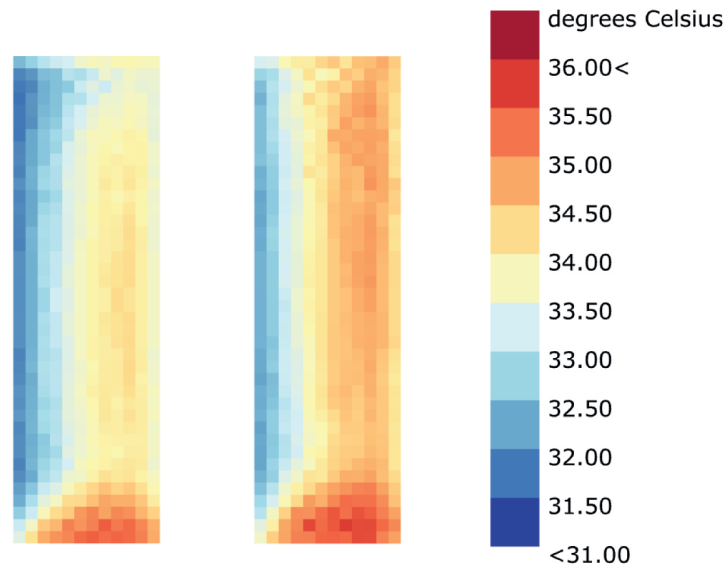


Figure E.14: test

Longwave MRT is altered by the surrounding environment as a result of temperature differences of the surrounding surfaces. These temperature differences between the situation in which an urban- and an open field surrounding environment are considered, are dependent on both differences in geometry and surrounding ground material applied in the two cases.

The impact of ground material on MRT and PET is discussed in more detail in section X. For this specific situation, the surrounding ground material seems to have a negligible impact on surrounding ground surface temperature (figure E.15 and columns 1-2 of table E.7), and is therefore assumed to have negligible impact on longwave MRT.

Accordingly, differences in surrounding surface temperatures are mainly the consequence of geometric considerations (figure E.16): On the one hand, the presence

Table E.6: Average longwave MRT for all test points over all individual hours considering open field- and urban surroundings

	Open field	Urban surroundings
12.00 - 13.00	32.89	33.79
13.00 - 14.00	34.28	35.19
14.00 - 15.00	34.74	35.45
15.00 - 16.00	33.87	34.30
16.00 - 17.00	32.61	32.82
17.00 - 18.00	30.92	31.02
Avg all hours	33.22	33.76

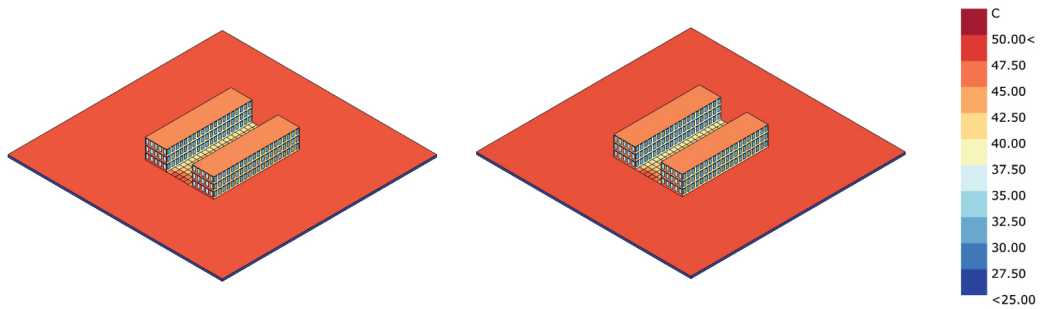


Figure E.15: Average ground surface temperatures for an open field situation for the considered analysis period (12.00-18.00). A comparison between a paved (concrete) ground environment (left) or soil ground environment (right)

of buildings in the surrounding environment leads to a substantially lower ground temperature as a result of shading (table E.7 column 3) . On the other hand, an individual in the analysis area is exposed to additional surfaces, with a surface temperature considerably larger than the longwave sky temperature. With these insights, the comparable longwave MRT results (figure E.14) can be explained: When considering an urban surrounding, the surrounding ground surface temperature is significantly lower than for the open field situation. As the emitted longwave radiation from surrounding surfaces is dependent on the surface temperature (equation x), one receives less irradiance from the surrounding ground for the urban environment situation, than for the open field situation. Conversely, the presence of surrounding buildings in the urban environment leads to a larger exposure to artificial surfaces, which have larger surface temperatures than the surrounding longwave sky temperature. Consequently, in addition to longwave irradiance received from the ground, in the urban environment, one receives additional longwave irradiance from the surrounding buildings. Compared to the open field situation, the urban environment results in decreased irradiance received from the surrounding ground surface, and increased irradiance received from surrounding buildings. From the comparable longwave MRT results for both situations, the contributions from the ground surface and buildings appear to balance each other out.

Wind speed is altered by the surrounding environment as a consequence of geometric properties of the surrounding environment: Increased obstruction by the surrounding environment leads to reduced wind speeds in the urban block. Average hourly values for wind speeds at 1.2 [m] height for both the urban- and open field environment are presented in table E.8. The presence of a representative Dutch urban environment leads to a significant reduction in wind speed.

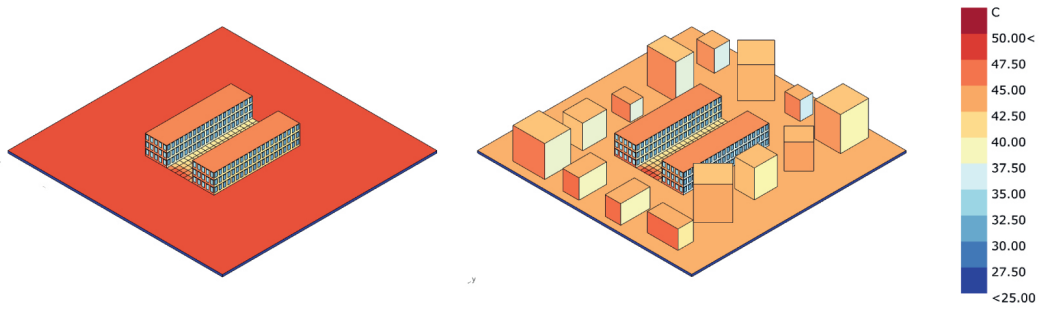


Figure E.16: Average ground surface temperatures for an open field situation for the considered analysis period (12.00-18.00). A comparison between a paved (concrete) ground environment (left) or soil ground environment (right)

Table E.7: Hourly temperatures of surrounding ground surface for an open field (both situations in which soil and concrete is used considered) and an urban environment (concrete).

	Soil (open field)	Concrete (open field)	Concrete (urban)
12-13	47.24	47.16	43.05
13-14	48.83	48.73	44.72
14-15	49.11	48.85	44.74
15-16	47.99	47.42	43.18
16-17	45.95	45.03	40.84
17-18	43.15	41.85	38.20
Avg	46.57	46.31	42.05

The results of wind speed comparison have been carried out for a default north-south street orientation only. Consequently, one may argue that the effect of street orientation has not sufficiently been considered. However, the neglect of different street orientations is justified as the wind speed calculation has been severely simplified by the MacDonald calculation method [58]: For dense urban environments, this method reduces wind speeds in accordance with building form and density averaged over a large source area. Consequently, only large scale building effects on wind speeds are noticeable, and any local affects of building form on wind speed are omitted.

Table E.8: Average urban wind speed within the analysis area [in m/s] for an open field- and urban surrounding environment

	Open field	Urban surroundings
12.00 - 13.00	2.60	0.45
13.00 - 14.00	2.92	0.51
14.00 - 15.00	2.92	0.51
15.00 - 16.00	3.24	0.56
16.00 - 17.00	3.94	0.69
17.00 - 18.00	3.24	0.57
Avg all hours	3.14	0.55

E.2.2 Facade material

From figures E.4 - E.7 and table E.2, facade materials appear to have a moderate impact on PET for this specific urban block. For the selected analysis period, application of a brick facade leads to the lowest PET, with an average value of 42.31 [°C], and application of an aluminium facade leads to the largest PET, with an average value of 43.65 [°C]. Application of a timber facade leads to an average PET which is slightly higher than the average PET of the brick facade: 42.76 [°C]. Since application of different facade material does not alter any geometric properties, all considered facades show similar patterns of PET distribution over the analysis area.

Given that the application of different facades does not affect geometry of the urban block, wind speed and air temperature are left unaffected by changing the facade material. With this statement, however, it is important to make a few comments: Considering wind speed, facade material may locally affect wind flow patterns [47]. However, as any local effects are disregarded in this study, these effects are omitted. As for air temperature, material characteristics (including albedo, thermal emissivity and heat capacity) affect UHI growth, and therefore affect air temperature [103]. Nevertheless, when applied on the local scale only, the effects on city-wide air temperature are negligible.

As any urban effects on relative humidity are considered negligible and both wind speed and air temperature are left unaffected by changes in facade materials, the only meteorological thermal comfort parameter affected by the application of different facade materials is MRT. Thus, to explain differences in PET as a result of the application of brick- timber- and aluminium facades, the impact of these facade materials on MRT should be assessed.

Different facade materials affect **mean radiant temperature** predominantly in the longwave spectrum. Any effects of different facade materials on shortwave MRT are negligible as the solar reflectance (albedo) of all facade materials is similar.

Figures E.17 -E.19 show the distribution of longwave MRT over the analysis area for the considered facades. These images clearly show the impact of facade material on longwave MRT (and consequently on PET). The aluminium facade in particular stands out, as application of this facade results in a distinctively larger longwave MRT. The longwave MRT results (table E.9, figure E.20) expectantly correspond to the PET results (table E.2, figure E.7). Differences between longwave MRT results for the various facades are larger than the differences between PET results for the various facades. Differences become less significant in the final PET calculations, as PET is not only dependent on MRT, but now also air temperature, relative humidity and wind speed are considered. Since the values for these meteorological parameters are the same for all facades, the relative differences in the final PET calculation become smaller.

Table E.9: Average longwave MRT for all analysis hours and over all test points

	Brick	Timber	Aluminium
Average longwave MRT [in °C]	33.76	34.22	36.10

As longwave MRT is dependent on surrounding surface temperatures, the difference in PET for the different facade materials is a direct result of facade surface temperature development over the selected analysis period.



Chapters/lwMRT_avg_brick.jpg

Figure E.17: Temporally averaged longwave MRT (12.00-18.00) for a brick facade

Important to note is that the chosen analysis period affects the impact of facade material on PET. Differences in heat retaining capacities, for example, may cause PET results to be different for situations in which the evening is considered. Consult appendix X for the course of surface temperatures for the facades from sunrise to midnight.

E.2.3 Ground material

From figures x - x and table x, ground materials appear to have a moderate impact on PET in the urban canyon. For the selected analysis period, application of asphalt pavement leads to the largest PET, with an average value of X [°C], and application of concrete pavement leads to the lowest PET, with an average value of X [°C]. Concrete is closely followed by semi-dry sand, which results in an average PET value of X [°C] within the urban canyon. Application of soil saturated with water as ground material results in an intermediate average PET value of X [°C]. Since application of different ground materials does not alter any geometric properties, all considered ground materials show similar patterns of PET distribution over the analysis area.

Given that the application of different ground materials does not affect geometry of the urban block, wind speed and air temperature are left unaffected by changing the ground material. Note, however that ground materials may locally affect wind flow patterns [47]. However, as these effects are expected to be marginal and any local wind effects are disregarded in this study, these effects are omitted. As for



Figure E.18: Temporally averaged longwave MRT (12.00-18.00) for a timber facade

air temperature, material characteristics affect UHI growth, and therefore affect air temperature [103]. For local application of different facade materials the effects on city-wide air temperature are negligible and may thus be neglected.

As any urban effects on relative humidity are considered negligible and marginal effects on both wind speed and air temperature by varying ground material are disregarded, the only meteorological thermal comfort parameter affected by the application of different ground materials is MRT. Thus, to explain differences in PET as a results of the application of various ground materials, it suffices to assess the impact of these ground materials on MRT.

Different ground materials affect **mean radiant temperature** predominantly in the longwave spectrum. Any effects of different ground materials on shortwave MRT are not considered, as the solar reflectance (albedo) of all ground materials are relatively low, and therefore relatively less important than the effect of increased longwave MRT.

Figures E.23 - E.26 show the spatial distribution of temporally averaged longwave MRT over the analysis area for the considered ground materials. These images clearly show the impact of ground material on longwave MRT (and consequently on PET). Figure E.27 shows the diurnal evolution of spatially averaged longwave MRT for the considered analysis period. From the graph it appears that towards the end of the afternoon, longwave MRT (and thus PET) differences for the various ground materials are less pronounced. This can be attributed to differences in surface temperature of the ground throughout the afternoon: At noon, the north-oriented canyon is fully exposed to direct sunlight. For these hours, differences in surface



Figure E.19: Temporally averaged longwave MRT (12.00-18.00) for an aluminium facade

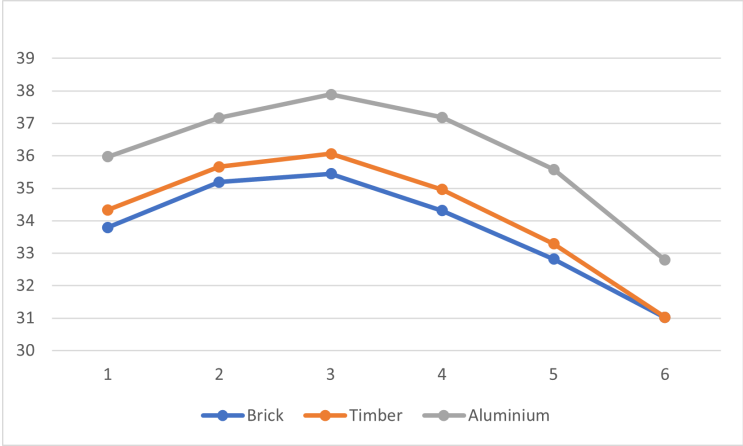


Figure E.20: Diurnal evolution (for afternoon hours) of longwave MRT for different facade materials

temperature, and consequently differences in longwave MRT are more pronounced. As the afternoon progresses, these differences become less significant when the urban canyon becomes shaded and differences between ground surface temperature for various materials are less distinct. The effect of ground material on longwave MRT and PET is thus highly dependent on exposure to sunlight. These diurnal differences highlight the importance of careful interpretation of the study results: Urban canyon configuration and analysis period appear to have large effects on the performance of various materials. For different urban configurations and different time of analysis, one may thus expect different results.

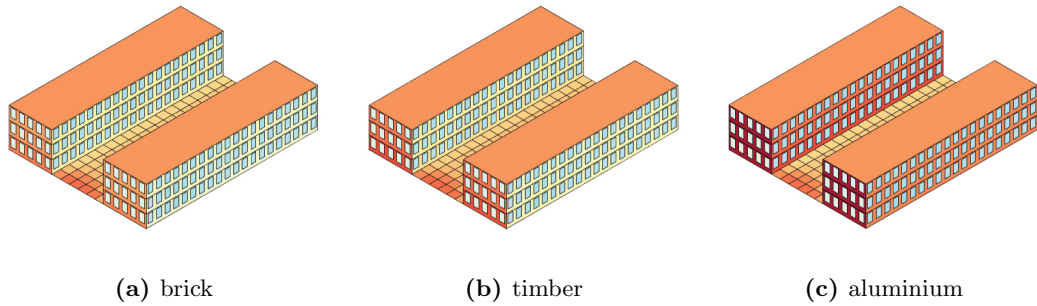


Figure E.21: Average surface temperatures for different facades from South-East perspective

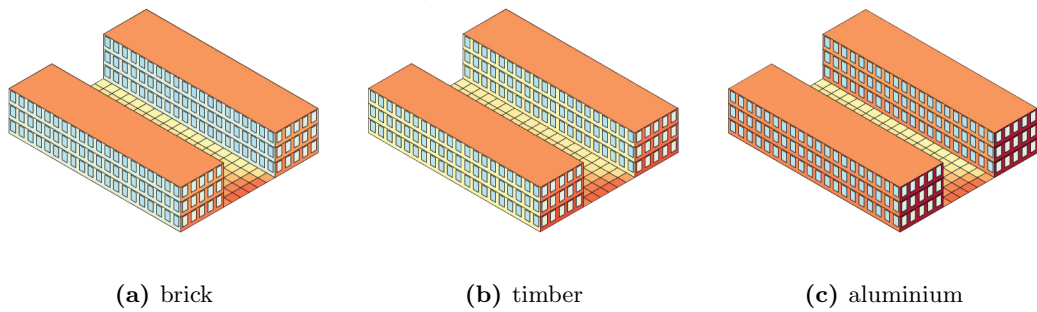


Figure E.22: Average surface temperatures for different facades from South-West perspective

Nog schrijven: Bij de facades was dit verloop minder duidelijk te zien, aangezien één kant van de facade altijd in de zon staat voor noord-zuid orientatie. Voor andere straat orientatie is dit mogelijk anders.

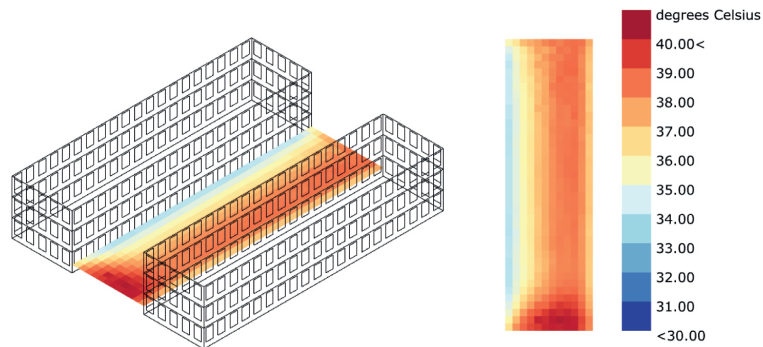


Figure E.23: LW MRT asphalt

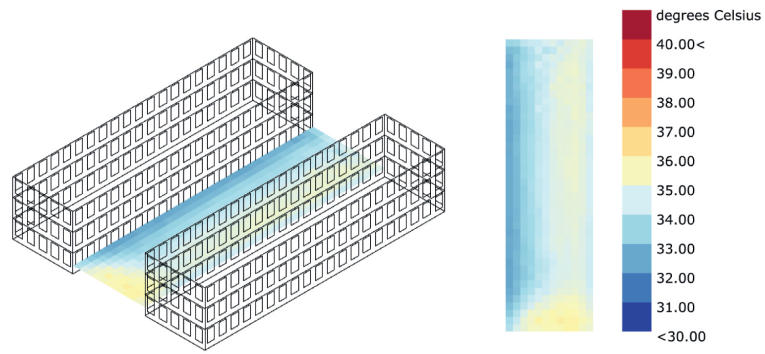


Figure E.24: LW MRT concrete

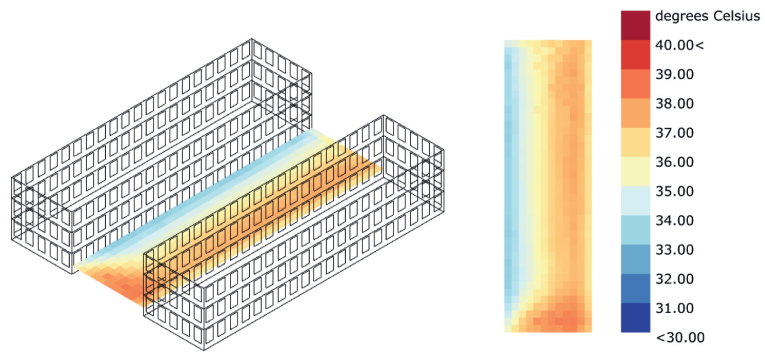


Figure E.25: LW MRT semi-dry sand

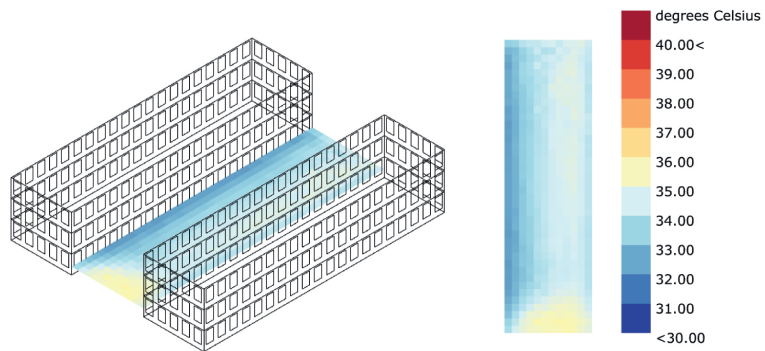


Figure E.26: LW MRT soil saturated with water

Table E.10: Average longwave MRT for all analysis hours and over all test points

	Asphalt	Concrete	Sand	Soil
Average longwave MRT [in C]	36.67	33.76	35.53	33.51

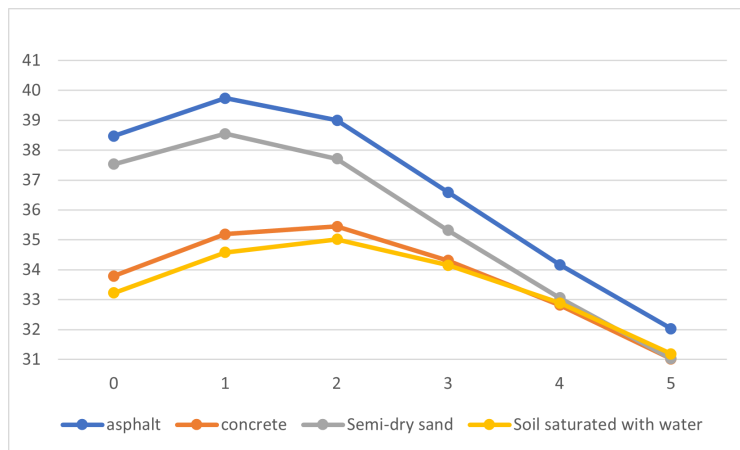


Figure E.27: Diurnal evolution (for afternoon hours) of longwave MRT for different ground materials

Bibliography

- [1] Klimaat effect Atlas.
- [2] Gil Akos and Ronnie Parsons. *Foundations: The Grasshopper primer third edition*.
- [3] O. Aleksandrowicz, M. Vuckovic, K. Kiesel, and A. Mahdavi. Current trends in urban heat island mitigation research: observations based on a comprehensive research repository. *Urban Climates*, 21:1–26, 2017.
- [4] H. Alibaba. Determination of Optimum Window to External Wall Ratio for Offices in a Hot and Humid Climate. *Sustainability*, 8(187), 2016.
- [5] AMS Institute. 100 years of Dutch summers: The clock is ticking on climate change, 2020.
- [6] E. Andreou. Thermal comfort in outdoor spaces and urban canyon microclimate. *Renewable Energy*, 55:182–188, 2013.
- [7] Edward Arens, Tyler Hoyt, Xin Zhou, Li Huang, Hui Zhang, and Stefano Schiavon. Modeling the comfort effects of short-wave solar radiation indoors. *Building and Environment*, 88:3–9, 2015.
- [8] ASHRAE. Chapter 8 Thermal Comfort. In *Handbook - Fundamentals (SI)*. 2005.
- [9] ASHRAE standard 55. Environmental conditions for human occupancy, 2004.
- [10] T Brandsma and D Wolters. Measurement and Statistical Modeling of the Urban Heat Island of the City of Utrecht (the Netherlands). *Journal of Applied Meteorology and Climatology*, 51(6):1046–1060, 2012.
- [11] Caroline Brosy, Ksenija Zaninovic, and Andreas Matzarakis. Quantification of climate tourism potential of Croatia based on measured data and regional modeling. *International Journal of Biometeorology*, 58(6):1369–1381, 2014.
- [12] William H. Brune. How Kinematic Fluxes Move Air Vertically.
- [13] M. Bruse. ENVI-met Technical Documentation, 2014.
- [14] Bruno Bueno, Aiko Nakano, and Leslie Norford. Urban weather generator: a method to predict neighborhood-specific urban temperatures for use in building energy simulations. In *9th International Conference on Urban Climate*, 2015.
- [15] Iain Campbell. Body temperature and its regulation. *Anaesthesia and Intensive Care Medicine*, 19(9):507–512, 2018.

- [16] F. Chen, H. Kasaka, R. Bornstein, J. Ching, C.S.B. Grimmond, S. Grossman-Clarke, T. Loridan, K.W. Manning, A. Martili, S. Miao, D. Sailor, F.P. Salamanca, H. Taha, M. Tewari, X. Wang, A.A. Wyszogrodzki, and C. Zhang. The integrated WRF/urban modelling system: development, evaluation, and applications to urban environmental problems. *International Journal of Climatology*, 31(2):273–288, 2011.
- [17] Chinese University of Hong Kong department of Architecture. Urban Climatic Map and Standards for Wind Environment - Feasibility Study Technical Input Report No. 1 : Methodologies and Findings of User 's Wind Comfort Level Survey Nov 2008. (1):151, 2008.
- [18] Silvia Coccolo, Jérôme Kämpf, Jean Louis Scartezzini, and David Pearlmutter. Outdoor human comfort and thermal stress: A comprehensive review on models and standards. *Urban Climate*, 18:33–57, 2016.
- [19] M. Demuzere, B. Bechtel, A. Middel, and G. Mills. Mapping Europe into local climate zones. *PLoS ONE*, 14(4), 2019.
- [20] Noël Djongyang, René Tchinda, and Donatien Njomo. Thermal comfort: A review paper. *Renewable and Sustainable Energy Reviews*, 14(9):2626–2640, 2010.
- [21] Ibrahim Elwy, Yasser Ibrahim, Mohammad Fahmy, and Mohamed Mahdy. Outdoor microclimatic validation for hybrid simulation workflow in hot arid climates against ENVI-met and field measurements. *Energy Procedia*, 153(November):29–34, 2018.
- [22] emanuele Naboni, Marco Meloni, Chris Makey, and Jerome Kaempf. The Simulation of Mean Radiant Temperature in Outdoor Conditions: A review of Software Tools Capabilities. *Proceedings of Building Simulation 2019: 16th Conference of IBPSA*, 16:3234–3241, 2020.
- [23] EnergyPlus. Engineering Reference: Mean Radiant Temperature Calculation, 2012.
- [24] Engineering Toolbox. Air - Density, Specific Weight and Thermal Expansion Coefficient at Varying Temperature and Constant Pressures, 2003.
- [25] Engineering Toolbox. Air - Specific Heat at Constant Pressure and Varying Temperature, 2004.
- [26] Yoram Epstein and Daniel S. Moran. Thermal comfort and the heat stress indices. *Industrial Health*, 44(3):388–398, 2006.
- [27] Evyatar Erell, David Pearlmutter, Daniel Boneh, and Pua Bar Kutiel. Effect of high-albedo materials on pedestrian heat stress in urban street canyons. *Urban Climate*, 10(P2):367–386, 2014.
- [28] Gianpiero Evola, Vincenzo Costanzo, Cristina Magrì, Giuseppe Margani, Luigi Marletta, and Emanuele Naboni. A novel comprehensive workflow for modelling outdoor thermal comfort and energy demand in urban canyons: Results and critical issues. *Energy and Buildings*, 216:109946, 2020.
- [29] E. Fischer and C. Schär. Consistent geographical patterns of changes in high-impact European heatwaves. *Nature Geoscience*, 3:398–403, 2010.

- [30] Randolph Fritz and A. McNeil. About Radiance, 2019.
- [31] Jonathan Graham, Umberto Berardi, Geoffrey Turnbull, and Robert McKaye. Microclimate analysis as a design driver of architecture. *Climate*, 8(6), 2020.
- [32] Selma B. Guerreiro, Richard J. Dawson, Chris Kilsby, Elizabeth Lewis, and Alistair Ford. Future heat-waves, droughts and floods in 571 European cities. *Environmental Research Letters*, 13(3):1–10, 2018.
- [33] K.D. Hage. Urban-Rural Humidity Differences. *Journal of Applied Meteorology and Climatology*, 14(7):1277–1283, 1975.
- [34] George Havenith. Heat balance when wearing protective clothing. *Annals of Occupational Hygiene*, 43(5):289–296, 1999.
- [35] George Havenith. Extreme weather events and public health responses. *Extreme Weather Events and Public Health Responses*, (January 2005):69–80, 2005.
- [36] Tsuyoshi Honjo. Thermal Comfort in Outdoor Environment. pages 43–47, 2009.
- [37] P Höppe. The physiological equivalent temperature - a universal index for the biometeorological assessment of the thermal environment. *International journal of biometeorology*, 43(2):71–75, 1999.
- [38] Jianxiang Huang, Jose Guillermo Cedeño-Laurent, and John D. Spengler. CityComfort+: A simulation-based method for predicting mean radiant temperature in dense urban areas. *Building and Environment*, 80:84–95, 2014.
- [39] Yasser Ibrahim, Tristan Kershaw, and Paul Shepherd. A methodology For Modelling Microclimates : A Ladybug-tools and ENVI-met verification study. (Figure 1), 2020.
- [40] Yasser Ibrahim, Tristan Kershaw, and Paul Shepherd. Improvement of the Ladybug-tools microclimate workflow : A verification study Department of Architecture & Civil Engineering , University of Bath , Bath , UK Abstract. 2020.
- [41] Verein Deutscher Ingenieure. Vdi-Richtlinien Vdi 3787. pages 1–2, 2008.
- [42] IPCC. Climate Change 2014 Synthesis Report: Summary for Policymakers. Technical report, 2014.
- [43] Erik Johansson. Influence of urban geometry on outdoor thermal comfort in a hot dry climate: A study in Fez, Morocco. *Building and Environment*, 41(10):1326 – 1338, 2006.
- [44] Noémi Kántor and János Unger. The most problematic variable in the course of human-biometeorological comfort assessment - The mean radiant temperature. *Central European Journal of Geosciences*, 3(1):90–100, 2011.
- [45] Kennisportaal Ruimtelijke Adaptatie. Bijsluiter gestandaardiseerde stresstest Ruimtelijke Adaptatie, 2020.
- [46] Kennisportaal Ruimtelijke Adaptatie. Bijsluiter gestandaardiseerde stresstest Ruimtelijke Adaptatie: Hitte, 2020.

- [47] L. Kleerekoper, A.A.J.F. v.d. Dobbelsteen, E. v.d. Ham, T. Hordijk, and C. Marting. Creating drafts in urban settings through coloured facades: Exploring a new climate adaptation measure based on thermal stratification. *Urban Climate*, 14(2):290–300, 2015.
- [48] A Klein Tank, Jules Beersma, J Bessembinder, B van den Hurk, and G Lenderink. KNMI '14 Klimaatscenario's voor Nederland: Herziene uitgave 2015. page 36, 2015.
- [49] Jeroen Kluck, Lisette Klok, Anna Solcerova, Laura Kleerekoper, Liesbeth Wilschut, Cor Jacobs, and Ronals Loeve. *De Hittebestendige stad*. 2020.
- [50] S. Koopmans, B. G. Heusinkveld, and G. J. Steeneveld. A standardized Physical Equivalent Temperature urban heat map at 1-m spatial resolution to facilitate climate stress tests in the Netherlands. *Building and Environment*, 181(May):106984, 2020.
- [51] S. Koopmans, B. G. Heusinkveld, and G. J. Steeneveld. Supplementary material; A standardized Physical Equivalent Temperature urban heat map at 1-m spatial resolution to facilitate climate stress tests in the Netherlands. *Building and Environment*, 181:1–11, 2020.
- [52] Big ladder software. EnergyPlus Sky Temperature Calculation.
- [53] Ladybug Tools. Ladybug Comfort SolarCal module, 2021.
- [54] H. E. Landsberg and T. N. Maisel. Micrometeorological observations in an area of urban growth. *Boundary-Layer Meteorology*, 2(3):365–370, 1972.
- [55] Hyunjung Lee and Helmut Mayer. Thermal comfort of pedestrians in an urban street canyon is affected by increasing albedo of building walls. *International Journal of Biometeorology*, 62(7):1199–1209, 2018.
- [56] Fredrik Lindberg, Björn Holmer, Sofia Thorsson, and David Rayner. Characteristics of the mean radiant temperature in high latitude cities - implications for sensitive climate planning applications. *International Journal of Biometeorology*, 58:613–627, 2014.
- [57] Igor Luginbuehl, Bruno Bissonette, and Peter J. David. Thermoregulation: Physiology and Perioperative Disturbances. pages 157 – 178. 2011.
- [58] R. W. Macdonald. Modelling the mean velocity profile in the urban canopy layer. *Boundary-Layer Meteorology*, 97(1):25–45, 2000.
- [59] C. Mackey. Sky View Factor, 2016.
- [60] Christopher Mackey, Theodore Galanos, Leslie Norford, Mostapha Sadeghipour Roudsari, and Neapoli Sdn Bhd. Wind , Sun , Surface Temperature , and Heat Island : Critical Variables for High-Resolution Outdoor Thermal Comfort Payette Architects , United States of America Massachusetts Institute of Technology , United States of America University of Pennsylvania ,. *Proceedings of the 15th IBPSA Conference*, pages 985–993, 2017.
- [61] Alberto Martilli, E. Scott Kravenhoff, and Negin Nazarian. Is the Urban Heat Island intensity relevant for heat mitigation studies? *Urban Climate*, 31(January 2019):1–4, 2020.

- [62] Andreas Matzarakis, Helmut Mayer, and Moses G Iziomon. Applications of a universal thermal index: physiological equivalent temperature. *International Journal of Biometeorology*, 43:76–84, 1999.
- [63] Andreas Matzarakis, Stefan Muthers, and Frank Rutz. Application and comparison of UTCI and pet in temperate climate conditions. *Finisterra*, 49(98):21–31, 2014.
- [64] Andreas Matzarakis, Frank Rutz, and Helmut Mayer. Modelling radiation fluxes in simple and complex environments — application of the RayMan model. *International Journal of Biometeorology*, 51:323–334, 2007.
- [65] José Meseguer, Isabel Pérez-Grande, and Angel Sanz-Andrés. Thermal radiation heat transfer. In *Spacecraft Thermal Control*. 2012.
- [66] Gerald Mills. Luke Howard and The Climate of London. *Weather*, 63(6):153–157, 2008.
- [67] Enrico Moens, Amy Hand, and Dries Hegger. Building resilience: being young and getting old in a hotter Europe. 2020.
- [68] R. E. Molenaar, B. G. Heusinkveld, and G. J. Steeneveld. Projection of rural and urban human thermal comfort in The Netherlands for 2050. *International Journal of Climatology*, 36(4):1708–1723, 2016.
- [69] Emanuele Naboni. Towards a programmable multi-domain digital design. In *Regenerative Design in Digital Practice: A Handbook for the Built Environment*, pages 55–61. Bolzano, IT: Eurac, 2019.
- [70] Emanuele Naboni, Marco Meloni, Silvia Coccolo, Jérôme Kaempf, and Jean Louis Scartezzini. An overview of simulation tools for predicting the mean radiant temperature in an outdoor space. *Energy Procedia*, 122incongr:1111–1116, 2017.
- [71] Emanuele Naboni, Luca Ofria, and Eric Danzo. A Parametric Workflow to Conceive Facades as Indoor and Outdoor Climate Givers. In *Symposium on Simulation for Architecture & Urban Design*, pages 11–18, 2019.
- [72] A. Nakano, B. Bueno, L.K. Norford, and C. Reinhart. Urban Weather Generator - a Novel Workflow ofr integrating urban heat island effect within urban design process. *Building Simulation*, 2015.
- [73] Nationaal Deltaprogramma. Deltabeslissing Ruimtelijke Adaptatie, 2014.
- [74] T. R. Oke. The energetic basis of the urban heat island. *Quarterly Journal of the Royal Meteorological Society*, 108(455):1–24, 1982.
- [75] Timothy R. Oke, Gerald Mills, Andreas Christen, and James A. Voogt. *Urban climates*. 2017.
- [76] Ken C. Parsons. *Human Thermal Environments: The effects of hot, moderate and cold environments on human health, comfort and performance*, volume 22. Taylor & Francis Inc, 2003.
- [77] PBL. Richting geven - Ruimte maken: Balans van de Leefomgeving. 2016.
- [78] Max Planck and Morton Masius. *The theory of heat radiation*. P. Blakiston’s Son & Co, 1914.

- [79] Tarek Rakha, Pouya Zhand, and Christoph Reinhart. A Framework for Outdoor Mean Radiant Temperature Simulation: Towards Spatially Resolved Thermal Comfort Mapping in Urban Spaces. *Environmental Sciences*, 19(7):1724–1731, 2017.
- [80] RIVM. Ontwikkeling Standaard Stresstest Hitte. page 121, 2019.
- [81] Federica Rosso, Iacopo Golasi, Veronica Lucia Castaldo, Cristina Piselli, Anna Laura Pisello, Ferdinando Salata, Marco Ferrero, Franco Cotana, and Andrea de Lieto Vollaro. On the impact of innovative materials on outdoor thermal comfort of pedestrians in historical urban canyons. *Renewable Energy*, 118:825–839, 2018.
- [82] Mostapha Sadeghipour Roudsari and Michelle Pak. Ladybug: A parametric Environmental Plugin for Grasshopper to Help Designers Create an Environmentally-Conscious Design. *Proceedings of the 13th International conference of Building Performance Simulation Association*, 2013.
- [83] Agnese Salvati and Maria Kolokotroni. Impact of urban albedo on microclimate and thermal comfort over a heat wave event in London. *Conference: Windsor 2020 Resilient Comfort ProceedingsAt: Windsor, Uk*, (May):566–578, 2020.
- [84] E.M.L. Scerri, M.G. Thomas, A. Manica, P. Gunz, J.T. Stock, C. Stringer, M. Grove, H.S. Groucutt, A. Timmermann, G.P. Rightmire, and F. D’Errico. Did Our Species Evolve in Subdivided Populations across Africa, and Why Does it Matter? *Trends in Ecology & Evolution*, 33(8):582–594, 2018.
- [85] P. J.C. Schrijvers, H. J.J. Jonker, S. R. de Roode, and S. Kenjereš. The effect of using a high-albedo material on the Universal Temperature Climate Index within a street canyon. *Urban Climate*, 17:284–303, 2016.
- [86] L. Shashua-Bar, I. Tsiros, and M. Hoffman. Passive cooling design options to ameliorate thermal comfort in urban streets of a Mediterranean climate (Athens) under hot summer conditions. *Building and Environment*, 57:110–119, 2012.
- [87] Avraham Shitzer. Wind-chill-equivalent temperatures: Regarding the impact due to the variability of the environmental convective heat transfer coefficient. *International Journal of Biometeorology*, 50(4):224–232, 2006.
- [88] W.G. Solheim. An earlier agricultural revolution. *Journal of Chemical Information and Modeling*, 226(4):34–41, 1972.
- [89] G. J. Steeneveld, S. Koopmans, B. G. Heusinkveld, L. W.A. Van Hove, and A. A.M. Holtslag. Quantifying urban heat island effects and human comfort for cities of variable size and urban morphology in the Netherlands. *Journal of Geophysical Research Atmospheres*, 116(20), 2011.
- [90] Adelia Ayu Sukma. Tool comparison for urban microclimate modelling. Technical report, 2020.
- [91] Mohammad Taleghani. Outdoor thermal comfort by different heat mitigation strategies- A review. *Renewable and Sustainable Energy Reviews*, 81(March 2017):2011–2018, 2018.

- [92] Mohammad Taleghani. The impact of increasing urban surface albedo on outdoor summer thermal comfort within a university campus. *Urban Climate*, 24(February):175–184, 2018.
- [93] Mohammad Taleghani and Umberto Berardi. The effect of pavement characteristics on pedestrians’ thermal comfort in Toronto. *Urban Climate*, 24:449–459, 2018.
- [94] Mohammad Taleghani, Laura Kleerekoper, Martin Tenpierik, and Andy Van Den Dobbelen. Outdoor thermal comfort within five different urban forms in the Netherlands. *Building and Environment*, 2015.
- [95] Natalie E. Theeuwes, Gert Jan Steeneveld, Reinder J. Ronda, and Albert A.M. Holtslag. A diagnostic equation for the daily maximum urban heat island effect for cities in northwestern Europe. *International Journal of Climatology*, 37(1):443–454, 2017.
- [96] Fazia Ali Toudert. Dependence of outdoor thermal comfort on street design in hot and dry climate. *Building and Environment*, (15), 2005.
- [97] UBC Physics & Astronomy Outreach. Heat Balance in the Human Body, 2019.
- [98] United Nations. The World ’s Cities in 2018 - Data Booklet. (*ST/ESA/SER.A/417*), 2018.
- [99] United Nations. *World Urbanization Prospects: The 2018 Revision (ST/ESA/SER.A/420)*. 2018.
- [100] United Nations. World population prospects 2019: Highlights. *ST/ESA/SER.A/423*, 2019.
- [101] U.S. Department of Energy. EnergyPlus Engineering Reference. Technical report, 2021.
- [102] U.S. Department of Energy. EnergyPlus Version 9.5.0 Documentation. Technical report, 2021.
- [103] U.S. Environmental Protection Agency. Urban Heat Island Basics. In *Reducing Urban Heat Islands: Compendium of Strategies*. 2008.
- [104] Frank van der Hoeven and Alexander Wandl. *Haagse Hitte*. 2018.
- [105] Frank Van Der Hoeven and Alexander Wandl. Hotterdam: Mapping the social, morphological, and land-use dimensions of the Rotterdam urban heat island. *Urbani Izziv*, 29(1):58–72, 2018.
- [106] L. W.A. Van Hove, C. M.J. Jacobs, B. G. Heusinkveld, J.A. Elbers, B. van Driel, and A. A.M. Holtslag. Temporal and spatial variability of urban heat island and thermal comfort within the Rotterdam agglomeration. *Building and Environment*, 83:91–103, 2015.
- [107] Ji Zhang, Chye Kiang Heng, Lai Choo Malone-Lee, Daniel Jun Chung Hii, Patrick Janssen, Kam Shing Leung, and Beng Kiang Tan. Evaluating environmental implications of density: A comparative case study on the relationship between density, urban block typology and sky exposure. *Automation in Construction*, 22:90–101, 2012.

- [108] Yanguo Zhang, Qinghai Li, and Hui Zhou. Theoretical Foundation and Basic Properties of Thermal Radiation. pages 1–43. 2016.